Cadmium Isotope Fractionation in Seawater

Driving Mechanisms and Palaeoceanographic Applications

Tristan J. Horner

A thesis submitted to The University of Oxford

for the degree of Doctor of Philosophy in Earth Sciences

Department of Earth Sciences & University College

Trinity Term 2012

Supervised by Prof. Gideon M. Henderson & Prof. Rosalind E.M. Rickaby

"An experiment is a question which science poses to Nature, and a measurement is the recording of Nature's answer."

–Max Planck

Cadmium Isotope Fractionation in Seawater

Driving Mechanisms and Palaeoceanographic Applications

Tristan J. Horner

A thesis submitted to the University of Oxford for the degree of Doctor of Philosophy in Earth Sciences

Department of Earth Sciences & University College

Trinity Term 2012

Abstract

THE global marine distributions of Cd and phosphate are closely correlated, which has led to Cd being considered as a marine micronutrient. Recent developments in Cd stable isotope mass spectrometry have revealed that Cd uptake by phytoplankton causes isotopic fractionation in the open ocean and in culture. The explanation for this nutrient-like behaviour is unknown as there is only one identified biochemical function for Cd, an unusual Cd/Zn carbonic anhydrase (CdCA1). This thesis investigates why Cd appears to act as an algal nutrient by performing subcellular analyses of microorganisms genetically-modified to express the CdCA1 gene. It was found that CdCA1 was not a significant contributor to whole-cell Cd isotope compositions. Instead, a large proportion of the internalized Cd is sequestered into cell membranes with a similar direction and magnitude of Cd isotopic fractionation as seen in surface seawater. This observation is explained if Cd is mistakenly imported with other divalent metals and subsequently managed by binding within the cell to avoid toxicity. This result implies that surface seawater Cd isotope compositions, if captured by an appropriate archive, may be invaluable for reconstructions of past marine productivity. The role of environmental factors in modulating the inorganic partitioning of Cd isotopes into calcite was investigated through a series of laboratory analogue experiments. In seawater, the light isotopes of Cd are always preferred in calcite. The magnitude of fractionation showed no response to temperature, ambient $[Mg^{2+}]$, or precipitation rate. To further identify suitable palaeaoceanographic archives, the Cd isotopic composition of a suite of modern deep-sea corals were investigated. It was found that the Cd/Ca and Cd isotope composition of coralline $CaCO_3$ followed the predicted trend for closed-system Rayleigh fractionation in the calcifying space. The lack of isotopic offsets between some corals and seawater will simplify the application of Cd isotopes in deep-sea corals – and potentially other marine calcifying organisms that vacuolize seawater prior to $CaCO_3$ precipitation – to palaeoceanography.

Cadmium Isotope Fractionation in Seawater

Driving Mechanisms and Palaeoceanographic Applications

Tristan J. Horner

A thesis submitted to the University of Oxford for the degree of Doctor of Philosophy in Earth Sciences

Department of Earth Sciences & University College

Trinity Term 2012

Extended Abstract

In addition to the macronutrients (nitrate, phosphate, silicate), phytoplankton require other vitamins, minerals, and metals to function correctly, typically in much smaller quantities than the major nutrients. These 'micronutrients' perform a wide range of functions in plankton. The transition metals are particularly important for the functioning of (metallo)enzymes, yet despite their importance to plankton, many of these metals are extremely scarce in surface seawater. The availability of micronutrient metals can limit oceanic primary productivity and dictate the partitioning of carbon between the surface ocean and atmosphere. Cadmium, element 48, is one such metal that is extremely scarce in surface seawater, and has a nutrient-like depth profile in the oceans, most similar to that of phosphate.

Recent isotopic analyses of dissolved Cd have shown that there are systematic variations, not only in the Cd concentration, but also in the Cd isotope composition of modern seawater. These studies have demonstrated that Cd isotopes display behavior similar to those of Si or N isotopes. As in these systems, Cd-depleted surface waters exhibit isotopically 'heavy' compositions, whereas deep waters have increasing Cd contents and isotopically 'lighter' signatures. This appears to reflect biological processes in the photic zone preferentially removing the lighter isotopes of Cd during metal uptake and regeneration of this signal at depth. This process has also been investigated for cultured phytoplankton, demonstrating that cultures were enriched in isotopically 'light' Cd due to biological uptake from the growth solution. Overall, the marine geochemistry of Cd is indicative of removal into phytoplankton, yet it is known to be toxic to life. The explanation for this nutrient-like behaviour is unknown as there is only one identified biochemical function for Cd, an unusual Cd/Zn carbonic anhydrase from the

marine diatom *Thalassiosira weissflogii*. Whilst ubiquitous in natural waters, CdCA1 is absent in numerous phytoplankton including coccolithophores, cyanobacteria, archaea, and several species of diatom and it is thus debatable whether the expression of this single enzyme can account for the nutrient-like distribution of Cd in the global ocean.

Using a systematic experimental approach, the general physiochemical pathways that fractionate Cd isotopes are identified by culturing genetically modified microorganisms. By introducing the CdCA1 metalloenzyme into a heterologous system (*Escherichia coli*; which otherwise has no biological function for Cd), the isotopic fractionation of Cd associated with metal insertion into CdCA1 was studied independently of other cellular processes. It was found that expression of CdCA1 made no difference to the Cd isotope composition of whole cells. Instead, a large proportion of the Cd is partitioned into cell membranes with a similar direction and magnitude of Cd isotopic fractionation as seen in surface seawater. This observation is well explained if Cd is mistakenly imported with other divalent metals and subsequently managed by binding within the cell to avoid toxicity (metal homeostasis). Since all organisms share a common ability to manage Cd, but do not share CdCA1, the proposed inadvertent uptake and homeostasis mechanism reconciles the rare genetic occurrence for CdCA1 with existing Cd isotopic and concentration data for cultured phytoplankton and the ubiquitous uptake and utilization of Cd seen in the global oceans. These experiments offer an alternative explanation as to the cause of the Cd-P association seen in the global ocean, and it is possible that this process may apply to other divalent metals whereby the accidental uptake and subsequent homeostasis may contribute to elemental distributions in seawater – even for elements commonly considered as micronutrients.

Extending the use of Cd isotopes into the past requires a suitable sedimentary archive with sufficiently high temporal and spatial resolution, as well as a high fidelity for the ambient seawater signal. It has been shown that the incorporation of Cd into foraminiferal tests occurs in proportion to the Cd concentration of the ambient seawater in which the test forms. Records of Cd/Ca are therefore assumed to reflect palaeo-Cd concentrations in seawater, once relevant corrections have been made for water-column depth (in benthic species) or temperature (for planktonic species). Foraminifera and other marine carbonates (e.g. corals, calcareous algae, etc.) are also likely to be good substrates to record past Cd isotope compositions, but before they can be used as such, it is necessary to assess whether environmental variables, such as temperature, control the fractionation of Cd isotopes during uptake into calcite. To this end,

inorganic $CaCO_3$ was precipitated in controlled experiments in artificial seawater solutions. Calcite was precipitated under different precipitation rates, temperatures, salinities, and ambient $[Mg^{2+}]$ to assess the variability in Cd isotopic partitioning. The isotopic fractionation factor for Cd into calcite in seawater is always less than one (i.e. light isotopes of Cd are preferred in calcite), and shows no response to temperature, $[Mg^{2+}]$, or precipitation rate across the range studied. The constancy of this fractionation in seawater suggests that biogenic marine calcites may provide a record of the local seawater composition, without the need to correct for effects due to environmental variables. No isotopic offset was observed between the growth solution and calcite when precipitates were grown in freshwater. Cadmium isotope fractionation during calcite growth can be explained by a kinetic isotope effect during the largely unidirectional incorporation of Cd at the mineral surface. The rate of Cd uptake and isotopic fractionation are modulated by increased ion blocking of crystal surface sites at high salinity. Despite the similar direction and magnitude of Cd isotope fractionation into $CaCO_3$ and that implicated for Cd removal from the surface ocean, flux calculations show that $CaCO_3$ precipitation is unlikely to play a significant role in setting the Cd isotope composition of seawater. (The dominant removal flux is Cd utilization in phytoplankton soft tissue.) Marine carbonates should record seawater Cd isotope chemistry – with potential as a palaeoceanographic proxy – rather than drive oceanic Cd isotope compositions.

The application of Cd isotopes, or any other tracer to palaeoceanography, first requires that a suitable carbonate archive be identified. A complication arises as the majority of these archives are biominerals and contain a physiological overprint which must be deconvolved from the environmental signal for it to be meaningful in a palaeoceanographic sense. Unlike surface-dwelling corals, deep-sea corals grow in near-constant environments and lack photosymbionts, thereby allowing for the independent study of biomineralization. The similar ionic radii of Cd^{2+} and Ca^{2+} and the high equilibrium partition coefficient of Cd relative to Ca into $CaCO_3$, render Cd a sensitive tracer of coral biomineralization. A suite of modern deep-sea coral specimens were analyzed for Cd/Ca and Cd isotope compositions. The deep-sea corals can be split into two populations: those which closely mimic assumed ambient seawater Cd/Ca and those which display high Cd/Ca that also varies systematically along the length of the coral septa. This grouping does not correlate with water column depth, $Cd/Ca_{water\ est.}$, or coral species. Whilst the corals which mimic seawater Cd/Ca have Cd isotopic compositions similar to seawater, the high Cd/Ca corals exhibit light Cd isotope compositions similar to those observed

during inorganic $CaCO_3$ precipitation. Together, the Cd/Ca and Cd isotope compositions of corraline $CaCO_3$ follow the predicted trend for closed-system Rayleigh fractionation in the calcifying space. These data demonstrate that Cd is highly sensitive to the balance between seawater exchange and $CaCO_3$ precipitation and supports the commonly used Rayleigh fractionation model for deep-sea coral biomineralization. The lack of isotopic offsets between some corals and seawater will facilitate the application of Cd isotopes in deep-sea corals to palaeoceanography. Deep-sea corals may be used to reconstruct deep-ocean Cd isotope chemistry without the need for any environmental corrections (e.g. coral species, water depth, etc.), so long as corals are screened for high Cd/Ca prior to isotopic analysis.

The overall aim of this thesis is to develop a new tool – Cd isotopes – in the context of applying it to study past and modern seawater chemistry, life, and biogeochemical cycling. Using an experimental and proxy approach, this work aims to elucidate the modern marine geochemistry of Cd and its isotopes, and set a framework in which to interpret measurements of past marine Cd isotope compositions to study the geological past.

Acknowledgements

THE work presented in this thesis would not have been possible without the support of my supervisors, Gideon Henderson and Ros Rickaby. Throughout these last four years of my D.Phil they both offered me guidance, expertise, patience, near-constant email support, dinners, BBQs, parties, walks in the countryside, and even opportunities to baby-sit. I really enjoyed working with you as well as between both of your research groups; the experience has put me in good stead for the future. Thank you to you both.

Renee, thanks for all your help and support back when we were working in the biology labs. Hopefully our many culturing disasters were offset by the free black-tie dinner at Univ in exchange for pretending to be my supervisor, and the free late-night sandwiches from the Plant Sciences café. I'm also indebted to Alex Thomas for many helpful discussions in the lab, as well as the tireless efforts of Andrew Mason and Phil Holdship in keeping the mass spectrometers running.

I'd also like to nod in the direction of Mark Rehkämper and Maria Schönbächler. You offered me the original opportunity to work on Cd isotopes when I was an undergraduate and I've been lucky enough to collaborate with you both since. Your continued encouragement (and not to mention references!) have helped me start a career.

Away from the lab, I'd like to thank my office mates for putting up with me over the years, playing our numerous office furniture-based games, and baking cakes: Clara Blättler, Dan Bassett, Johnny Armstrong Murtaugh, D. Paddy Devlin, Lilly Muller, Lara Kalnins, Holly Rouse-Sweeney, and Dan Frost. Of course, thanks also to FAT Tony Watts for hosting me in the Marine Geophysics Lab throughout this time.

When not in the lab or the office, thanks to all the friends I made in Oxford who made it fun to be here. Without wishing to single anyone out, special mention must go to Al White, who

braved the cold, the snow, and the raging torrent of beer to be at my Stag do. To everyone else (alphabetically) – Ros Armytage, Julia Barrott, Marcus Bell, Mark Bourne, Chris Day, Susie Ebmeier, John Elliott, Giovanni Fontana, Louise Gall, Laura Gregory, Alan Hsieh, Tom O'Toole, Helen Pillar, Yves Plancherel, Alex Robinson, Paul Savage, Rich Walters, Sam Weatherley, Jodi Young, and Xinyuan Zheng – cheers!

A list of friends wouldn't be complete without mentioning the 'BGC'. I'm glad that I was able to partake in this highly selective and academically rigorous weekly discussion forum. We certainly covered many important and topical geopolitical issues. To the BGC stalwarts – Maeve Eason-Hubbard, Katie Egan, Michaël Hermoso, Phil Renforth, and Emily Stevenson – thanks for the beers and for keeping me in the loop!

Then there's the extended 'family' of close friends outside of Oxford – Steven Gower, Ross Thomson, Marc Maringer, Jon Beetham, Ben Hosken, Mark Watkins, and Gary Martin – it never ceases to amaze me how little things have changed whenever we see one another.

To my family – my parents, my brother Adrian, and grandma Doreen – thank you for all the support, visits, and weekend breaks throughout my time in Oxford, and all the cups of coffee and dinners whenever I was back home (wherever that was!).

Last but certainly not least, Nicola. Whilst I'm sure you have enjoyed listening to me explain the many intricacies of a D.Phil (e.g. "the mass spec. isn't working", "some idiot stole my [insert object] in the lab", "I need to go into the department at 3 am today", etc.), being with you has reminded me that life is not just about column chemistry and partition coefficients. You have always been supportive, 'willing' to listen, kind, and helpful; I am thankful for that. We've had a few globe-trotting adventures together during our time in Oxford, and I'm glad to have you by my side as we *walk the miles*, leave Oxford, the UK, and start the next chapter of our lives.

And finally, to everybody mentioned above, and anybody else whom I've accidentally left out:

Thank you!

You all helped make this happen.

Contents

1 Introduction **1**

1.1 Motivation for study . . . 3

1.1.1 Sunlight, seawater, nutrients, life, and the carbon cycle . . . 3

1.1.2 A (very) brief history of element 48 . . . 4

1.1.3 Metals as nutrients . . . 5

1.1.4 Physiological status of Cd . . . 5

1.2 Cadmium in the oceans . . . 6

1.2.1 The Cd-PO_4^{3-} paradox . . . 6

1.2.2 Applying the Cd-PO_4^{3-} association to palaeoceanography . . . 8

1.3 Measurement of Cd isotopic compositions . . . 9

1.3.1 The first measurements . . . 9

1.3.2 A common isotopic reference material for Cd . . . 11

1.3.3 Cd isotope fractionation in seawater . . . 12

1.3.4 Records of past marine Cd isotope compositions . . . 16

1.4 Motivation for the work presented in this thesis . . . 19

2 Extended Methodology **21**

2.1 Measurement of trace metal isotopes in environmental samples . . . 23

2.2 Elemental purification . . . 23

2.3 Analytical considerations . . . 28

2.3.1 Choice of mass bias correction . . . 28

2.3.2 Characterization of instrumental mass fractionation for Cd . . . 31

2.4 Application of the double spike to mass bias correction . . . 36
2.4.1 Double spike optimization considerations . . . 37
2.4.2 Mixing and calibration of double spikes . . . 40
2.4.3 Data reduction . . . 44

3 Cellular uptake, homeostasis, and the marine Cd cycle 47

3.1 Introduction . . . 51
3.2 Methods . . . 54
3.2.1 Experimental design . . . 54
3.2.2 Preparation of transgenic *Escherichia coli* and over-expression of CdCA1 . 54
3.2.3 CdCA1 purification and cleavage of histidine tag . . . 56
3.2.4 Decomposition of cells and purification of elemental cadmium . . . 57
3.2.5 Isotopic analysis of cadmium . . . 59
3.2.6 Cell washing methodology . . . 59
3.3 Results . . . 60
3.3.1 Cell washing results . . . 60
3.3.2 Whole-cell isotopic results . . . 62
3.3.3 Intracellular isotopic results . . . 62
3.4 Discussion . . . 71
3.4.1 Intracellular mass balance for Cd . . . 71
3.4.2 Cellular Cd management . . . 71
3.4.3 Implications for the water column . . . 72
3.5 Conclusions . . . 74

4 Isotopic fractionation of cadmium into calcite **77**

4.1 Introduction . . . 81

4.2 Materials and Methods . . . 83

4.2.1 Experimental design . . . 83

4.2.2 Synthetic carbonate manufacture . . . 83

4.2.3 Sample processing and analysis . . . 88

4.3 Results . . . 90

4.3.1 Mineralogical data and elemental partitioning . . . 90

4.3.2 Cadmium isotopic partioning data . . . 92

4.4 Discussion . . . 99

4.4.1 Invariance of the fractionation factor in seawater . . . 99

4.4.2 The effect of salinity and the mechanism of Cd isotope fractionation . . . 99

4.4.3 Implications for the marine Cd cycle . . . 102

4.5 Conclusions . . . 103

5 Cd isotopes in deep-sea corals **107**

5.1 Introduction . . . 111

5.2 Methods . . . 114

5.2.1 Samples . . . 114

5.2.2 Deep-sea coral cleaning methods . . . 114

5.2.3 Purification and analysis of Cd . . . 116

5.3 Results . . . 118

5.3.1 Stepped cleaning results . . . 118

5.3.2 Cd/Ca and Cd isotopic results . . . 119

5.4 Discussion . . . 122

5.4.1 Elemental and isotopic partitioning of Cd . . . 122

5.4.2 Comparison with inorganic $CaCO_3$ precipitation . . . 125

5.4.3 Evidence of Rayleigh fractionation . . . 126

5.4.4 A possible mechanism and implications for palaeoceanography . . . 131

5.5 Conclusions . . . 132

6 Conclusions, outlook, and closing remarks **135**

6.1 Conclusions 137

6.2 Outlook 141

6.3 Closing remarks 143

References **145**

List of Figures

1.1 Depth profiles of dissolved phosphate and Cd from the North Pacific. 7

1.2 Global comparison of dissolved Cd and dissolved inorganic phosphorus concentrations. 7

1.3 Dissolved Cd concentrations and isotopic compositions for the two currently published seawater profiles. 13

1.4 Cd isotope and concentration variations in modern seawater. 15

1.5 Compilation of Cd isotope data for marine sediments and deep-ocean seawater. . 17

2.1 The Cd mass spectrum. 24

2.2 Column calibration for AG-1X8 resin. 26

2.3 Column calibrations for TRU resin. 27

2.4 Data from the linear mass fractionation assessment. 32

2.5 Data from the exponential mass fractionation assessment. 34

2.6 Comparison of Cd isotopic compositions for NIST SRM 3108 measured relative to BAM I012 Cd for various n. 35

2.7 Three dimensional geometric interpretation of the double spike. 37

2.8 Contribution of each isotope to the mass spectra (relative scale). 38

2.9 Optimization of a Cd double spike. 41

2.10 Spike calibration using spike-normal mixtures. 43

3.1 Cd isotope and concentration variations in modern seawater. 52

3.2 CdCA1 expression does not affect whole cell Cd isotopic compositions. 55

3.3 Cell isotope compositions do not depend on the digestion method. 58

3.4 The mass of bacterial pellets recovered depends on the cleaning strategy used. . 61

3.5 The Cd content of pellets strongly depends on the cleaning method used. 61

3.6 Subcellular mass balance for *E. coli* cells expressing CdCA1. 66

3.7 The isotopic composition of the cell membranes is sensitive to the cellular cleaning method. 67

3.8 The isotopic composition of whole cells is sensitive to the cellular cleaning method. 68

3.9 Proposed model for Cd isotopic fractionation in *E. coli*. 70

4.1 Growth-solution evolution during precipitation experiments in artificial seawater. 86

4.2 Relative abundances of inorganic aqueous Cd and Ca species in artificial seawater and freshwater experiments. 87

4.3 Secondary electron images of a selection of inorganic calcite precipitates from this study. 91

4.4 Summary of the seawater experiment data from this study. 95

4.5 Cd isotope data for all measurements from the seawater experiments plotted against fraction of dissolved Cd remaining in solution. 97

4.6 Cadmium isotope data for the two freshwater experiments plotted against fraction of dissolved Cd remaining in solution. 98

4.7 Schematic marine Cd cycling model. 104

5.1 Map of the deep-sea coral sample locations used in this study. 116

5.2 Deep-sea coral cleaning results. 119

5.3 Deep-sea coral Cd isotope and Cd/Ca results. 121

5.4 Deep-sea coral Cd elemental partitioning. 123

5.5 Comparison of deep-sea corals with inorganic $CaCO_3$ precipitates. 127

5.6 Closed-system Rayleigh fractionation during deep-sea coral biomineralization . 128

5.7 Sensitivity of the Rayleigh model to initial parameters 130

List of Tables

2.1 Cd separation chemistry for samples with 'unfavourable' Cd:matrix ratios. . . . 27

2.2 Second-stage Cd 'cleanup' chemistry or stand-alone separation protocol for samples with favorable Cd:matrix ratios. . . . 28

2.3 Detector configurations for Cd isotope analysis. . . . 30

3.1 BLAST results for the CdCA1 gene (from *T. weissflogii*) in various microorganisms for which the complete genome is available. . . . 53

3.2 Pellet recoveries and contaminant Cd for the cleaning agents tested. . . . 63

3.3 Isotopic data for whole cell washing experiments. . . . 64

3.4 Isotopic data for intracellular separates. . . . 65

4.1 Composition of artificial seawater solution used in this study. . . . 84

4.2 Summary of the results of this study. . . . 93

4.3 Summary of previously reported isotopic offsets between various substrates and dissolved Cd. . . . 96

5.1 Water column properties for the deep-sea coral samples analyzed in this study. . . . 115

5.2 Deep-sea coral cleaning procedure used in this study. . . . 117

5.3 Cd isotope and multi-element geochemical data for the deep-sea corals analyzed in this study. . . . 120

CHAPTER 1

Introduction

"All things are poison, and nothing is without poison; only the dose permits something not to be poisonous."

–Philippus Aureolus Theophrastus Bombastus von Hohenheim
Scientist, physician, alchemist, astrologer, occultist

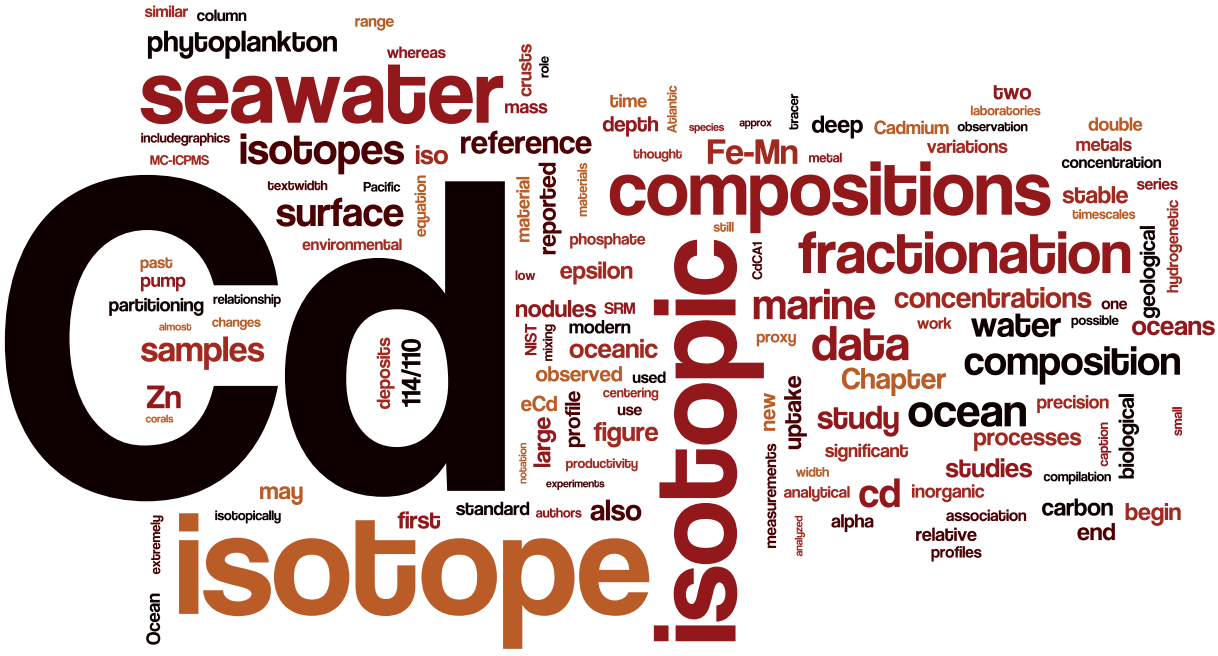

1.1 Motivation for study

1.1.1 Sunlight, seawater, nutrients, life, and the carbon cycle

MARINE phytoplankton account for about half of global annual primary productivity and consume ~ 80 Pg C yr^{-1} from surface seawater (*Field et al.*, 1998). Of this, around 13 Pg C yr^{-1} is exported to the deep ocean (*Jin et al.*, 2006), an amount roughly comparable with current anthropogenic carbon emissions ($8-9$ Pg C yr^{-1}; *Friedlingstein et al.*, 2010). This export is the sum of a number of processes collectively termed the 'biological pump', whereby organic carbon is fixed from inorganic carbon in surface seawater (which equilibrates, on decadal timescales with the atmosphere). This is then transferred to the abyssal ocean and seafloor, where $>$ 99 % is then converted back to inorganic carbon by respiration (*Hedges and Keil*, 1995). In this sense, the biological pump shifts the partitioning of inorganic carbon from the atmosphere and surface ocean to the deep ocean, leading to changes in atmospheric pCO_2 that may cause or amplify changes in global climate (*Sigman and Boyle*, 2000). The strength (or efficiency) of the pump is determined by the availability of light and nutrients in seawater (e.g. *Brand et al.*, 1983; *Mitchell et al.*, 1991; *Karl*, 2000), and is further modulated by physical transport and mixing of water masses (e.g. *Sarmiento and Toggweiler*, 1984; *Knox and McElroy*, 1984; *Martin*, 1990). Understanding how the biological pump relates to modern climate and pCO_2 on centennial to millennial timescales is best addressed by studying the modern oceans and by looking at the geological past using environmental proxy records.

The climatic link between the biological pump and pCO_2 is particularly important in the polar oceans. High-latitude oceans, principally the Southern Ocean, are inefficient regions of the biological pump; ocean upwelling releases deeply-sequestered carbon (as pCO_2) to the surface (*Stuiver et al.*, 1983; *Sigman et al.*, 2010) and delivers **h**igh concentrations of **n**utrients, but exhibits only modest productivity (**l**ow **c**hlorophyll, HNLC; *Pitchford and Brindley*, 1999). Changing the strength (or in the case of the Southern Ocean, the efficiency) of the biological pump strongly influences the partitioning of carbon between the atmosphere and the deep ocean.

Increasing the degree of nutrient consumption (i.e. efficiency) in HNLC regions is one of a number of possible mechanisms thought to play a key role in determining pCO_2 on glacial-interglacial timescales and is still a subject of debate (e.g. *Sigman et al.*, 2010). Existing environmental proxy records of this region have proven to be contradictory (e.g. *De La Rocha*, 2006), suggesting that either our knowledge of the underlying processes that control the proxies is incomplete, or the nature of the ecosystem changed significantly.

The development of new environmental proxies – once calibrated and validated – often complements existing proxies and informs our understanding of the underlying physical processes that operate in nature. New tools are needed if we are to elucidate the processes that act in the modern ocean, how they may have acted in the past, and how they may have changed through time. This thesis describes the development of one such tool, Cd isotopes, by examining the processes that are thought to control its distribution and isotopic fractionation in the modern ocean, and how we can apply these results to study and interpret the geological past.

1.1.2 A (very) brief history of element 48

Cadmium, a (post-) transition metal first discovered by Friedrich Stomeyer in 1817, is typically associated as an impurity with Zn (*Lockemann and Oesper*, 1953). The name derives from *cadmea*, the name given by Pliny the Elder in his *Natural History* to the white residue found in furnaces or chimneys that had been used for smelting (probably 'Calamine', Zn carbonate or Zn silicate). Whilst Pliny thought that *cadmea* had certain medicinal properties (most notably for healing wounds), Cd bioaccumulates, is highly toxic and carcinogenic in humans and animals. As such, human applications of Cd greatly declined throughout the latter half of the 20^{th} century, with almost all current industrial Cd use restricted to the manufacture of Ni-Cd rechargeable batteries. (Following the 2006 European Union 'Battery Directive', this is set to further decrease.) A small amount of Cd is still used for colouring bright, light-fast paint pigments (e.g. Cadmium Yellow).

1.1.3 Metals as nutrients

In addition to the macronutrients (nitrate, phosphate, silicate), phytoplankton require other vitamins, minerals, and metals to function correctly, typically in much smaller quantities than the macronutrients (e.g. *Karl*, 2000). These 'micronutrients' perform a wide range of functions, ranging from maintaining intracellular pH (K^+, Na^+, or Ca^{2+}–$2H^+$-coupled transport; e.g. *Eilam et al.*, 1985) to protein folding or enzyme cofactors (e.g. *Waldron et al.*, 2009). The latter set of functions is performed almost exclusively by the transition metals, yet despite their importance to plankton, many of these metals are extremely scarce in seawater (*Morel and Price*, 2003). The availability of micronutrient metals can limit oceanic primary productivity and dictate the partitioning of carbon between the surface ocean and atmosphere (*Martin*, 1990; *Morel et al.*, 1994). As metal availability has changed through geological time, marine microorganisms have evolved to (sometimes extensively) substitute one metal for another (*Saito et al.*, 2003), much more so than with other macronutrients (*Quigg et al.*, 2003). Studying the marine distributions of the transition metals and their isotopes, both in the modern ocean and through sedimentary or proxy archives, is currently of great interest to biological and chemical oceanographers, climatologists, ecologists, and palaeoceanographers; it is also a key scientific objective of the international GEOTRACES consortium (*GEOTRACES Planning Group*, 2006).

1.1.4 Physiological status of Cd

Despite being toxic to humans, phytoplankton grown in culture will consume and internalize small quantities of Cd (equivalent to 1 Cd for every $\sim 5,000$ P; *Ho et al.*, 2003). This observation led biochemists to theorize that Cd possessed a biochemical function in certain phytoplankton. A series of studies have shown that Cd (and Co) can replace some of the Zn requirements of *Thalassiosira weissflogii* (a centric coastal diatom; *Price and Morel*, 1990; *Lee et al.*, 1995), with later macroscopic culturing experiments demonstrating that lower $[CO_2]_{(aq.)}$ and/or [Zn] in the culture medium increased Cd uptake, suggesting that Cd was associated with the CCM (carbon

concentrating mechanism; *Cullen et al.*, 1999). Later x-ray structural studies confirmed this, identifying a cambialistic Cd/Zn carbonic anhydrase (hereafter CdCA1) in *T. weissflogii* (*Lane et al.*, 2005; *Xu et al.*, 2008). This adaptation to use a previously toxic metal likely reflects an evolutionary response to the extremely nutrient-impoverished nature of the Phanerozoic surface ocean (e.g. *Xu et al.*, 2008; *Waldron et al.*, 2009). The genetic coding that allows *T. weissflogii* to interchangeably use Cd or Zn is absent in many lineages of phytoplankton (e.g. *Park et al.*, 2007; Chapter 3), and so the degree to which CdCA1 can account for Cd uptake in the oceans is unclear. It is this question that forms the rationale for the experiments described in Chapter 3.

1.2 Cadmium in the oceans

1.2.1 The Cd-PO_4^{3-} paradox

The marine distributions of PO_4^{3-} (phosphate) and Cd are similar (Fig. 1.1; *Boyle et al.*, 1976), despite the fact that PO_4^{3-} is the *"staff of life"* (*Karl*, 2000), whereas Cd is toxic to it. The explanation(s) for this association are still debated and include passive scavenging of Cd by sinking organic matter (*Collier and Edmond*, 1984), physiological utilization of Cd (*Cullen et al.*, 1999; *Xu et al.*, 2008), to the inadvertent uptake of Cd by phytoplankton during their search for other essential metals (*Boyle*, 1988; Chapter 3). Irrespective of the mechanism, the Cd-PO_4^{3-} association is observed throughout the global oceans (Fig. 1.2), with a linear slope of $\sim 3,300$ mol P per mol Cd that is similar to the extended elemental stoichiometry of phytoplankton ($\sim 5,000$; *Ho et al.*, 2003). The systematic increase in PO_4^{3-} concentrations between ocean basins is also reflected in [Cd], implying a similar mechanism of uptake and transport.

Several processes have been identified that can modulate the Cd-P relationship in seawater (Fig. 1.2). Changes in phytoplankton assemblages with different Cd:P requirements, altered ocean circulation, or changes in surface ocean productivity can all affect oceanic Cd:P (*Frew and Hunter*, 1992). The role of the Southern Ocean in modulating oceanic Cd:P has also received

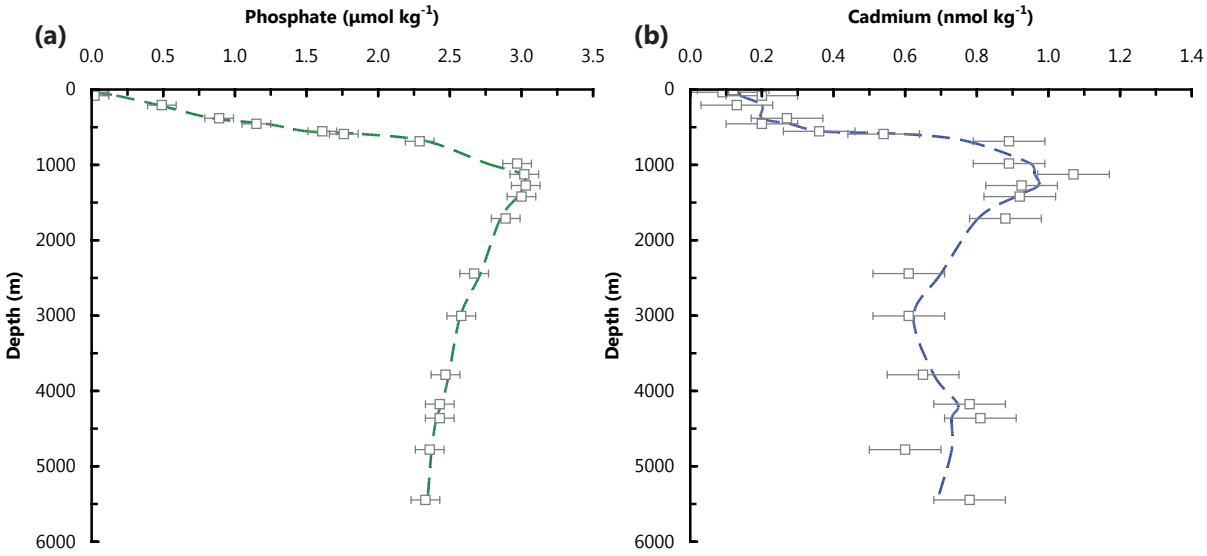

Figure 1.1: Depth profiles of dissolved (a) phosphate and (b) Cd from the North Pacific. Data are from Station 226; (*Boyle et al.*, 1976). Despite the large uncertainties on the Cd concentration measurements, it was noted that Cd and phosphate both had concentrations that were close to zero in the surface mixed layer, remineralized at the same shallow depth ($\sim$ 1 km), and showed a decrease in concentration at depth because of lateral outflow (*Boyle et al.*, 1976).

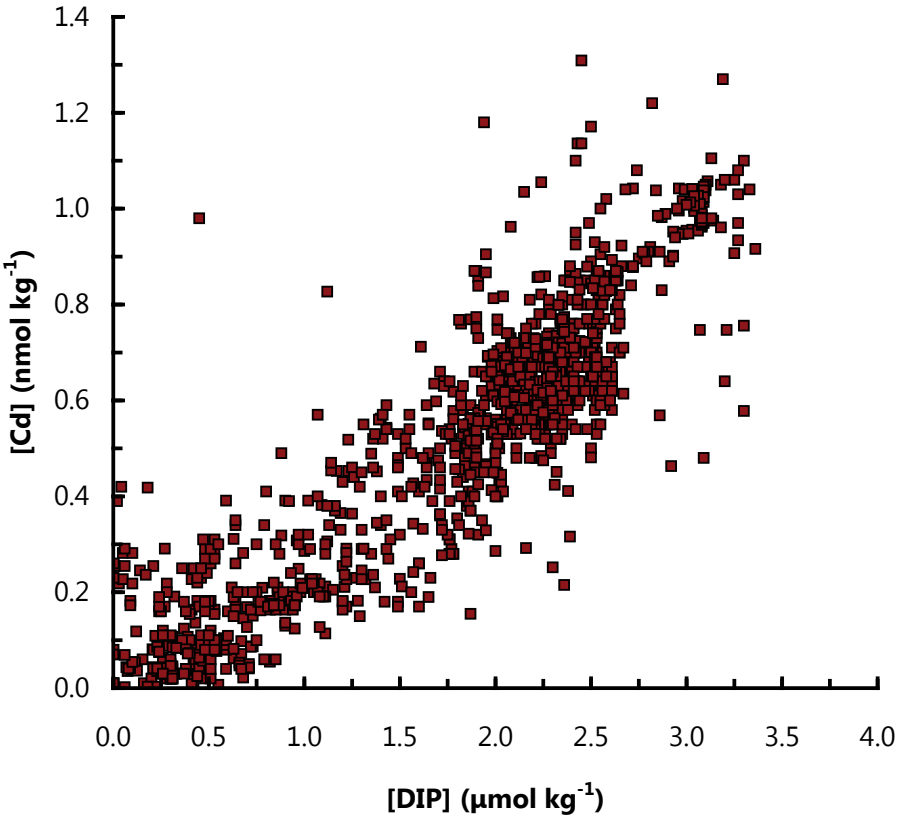

Figure 1.2: Global comparison of dissolved Cd and DIP concentrations. (DIP, dissolved inorganic phosphorus; plotted using the same data and data sources as *Rehkämper et al.* 2011). The large amount of data scatter and the slight non-linearity of the relationship are readily apparent. The causes of, as well as the mathematical description of the Cd-P association has been the subject of extensive research, and in particular, the supposed 'kink' at $\approx$ 1.3 μmol kg^{-1} DIP (e.g. *Frew and Hunter*, 1992; *de Baar et al.*, 1994; *Elderfield and Rickaby*, 2000; *Cullen*, 2006).

particular attention, because the high-latitude oceans play an important role in controlling primary productivity and glacial/interglacial climate shifts (e.g. *Sigman and Boyle*, 2000; *Sarmiento et al.*, 2004; *Sigman et al.*, 2010). Preferential removal of Cd relative to P by particles in the surface Southern Ocean has been suggested as the dominant process in this regard (*Elderfield and Rickaby*, 2000), and a number of physiological explanations have been suggested to account for the elevated Cd/P of South Ocean biomass (e.g. *Cullen and Sherrell*, 2005; *Cullen*, 2006; *Lane et al.*, 2008, 2009).

1.2.2 Applying the Cd-PO_4^{3-} association to palaeoceanography

The close association of Cd and P has led to significant interest in marine [Cd] reconstructions by palaeoceanographers for over 35 years. Past PO_4^{3-} concentrations are not easily reconstructed, as there are few – if any – adequate sediment [PO_4^{3-}] records (*Henderson*, 2002). Given the ubiquity of $CaCO_3$ in the oceans, and the inorganic substitution of Cd for Ca into $CaCO_3$ lattice sites (i.e. solid solution partitioning between Ca and Cd; *Tesoriero and Pankow*, 1996), past [PO_4^{3-}] can be reconstructed with Cd.

Core-top and live-catch studies have demonstrated that the Cd content of calcareous foraminifera is directly proportional to the Cd content of the ambient seawater (*Boyle*, 1981; *Ripperger et al.*, 2008; when normalized to [Ca], which is assumed to be invariant on < 1 Myear-timescales). Empirical calibrations have been devised to correct for both water-column depth (in benthic species; e.g. *Boyle*, 1988) and temperature (for planktonic species, e.g. *Rickaby and Elderfield*, 1999). Using these corrections, palaeoceanographers have made temporal reconstructions of deep ocean circulation (e.g. *Boyle*, 1988, 1992) and surface-ocean nutrient concentrations (e.g. *Rickaby and Elderfield*, 1999; *Robinson et al.*, 2005) to address questions relating to Earth's climate history.

1.3 Measurement of Cd isotopic compositions

1.3.1 The first measurements

There is a long history of Cd isotope analyses, starting with the study of *Rosman and De Laeter* (1975). That earliest, and subsequent studies utilized TIMS (thermal ionization mass spectrometry) in conjunction with double spiking (see Chapter 2 for a full discussion of the analytical aspects of Cd isotope measurement) to hunt for both mass-dependent and mass-independent Cd isotope variation in geological materials. It was thought that mass-dependent Cd isotope anomalies could originate from (de)sorption/diffusion reactions in the solar nebula (*Rosman and De Laeter*, 1976), whereas mass-independent Cd isotope fractionation could result from thermal n (neutron) capture:

$$^{113}\mathrm{Cd} + \mathrm{n} \rightarrow {}^{114}\mathrm{Cd} + \gamma \tag{1.3.1}$$

The isotope ^{113}Cd is particularly sensitive to this reaction as it has a large neutron capture cross-section ($\approx 20 \times 10^{-25}$ m^2, or 20 kilobarn). The earliest study (*Rosman and De Laeter*, 1975) found no variation in terrestrial samples, but their subsequent work found significant Cd isotope variability in some meteorites (up to $\pm$1.5 % AMU^{-1}; atomic mass unit; e.g. *Rosman and De Laeter*, 1976, 1978; *Rosman et al.*, 1980). These large variations were attributed to both mass-dependent and mass-independent processes; similarly large variations were later observed for lunar soils (*Sands, Rosman, and De Laeter*, 2001; *Schediwy, Rosman, and De Laeter*, 2006). Both the mass-dependent and mass-independent variations observed by *Rosman and De Laeter* (1976) and subsequent co-workers have recently been confirmed by the improved analytical techniques described below. Large mass-dependent variations have been documented in ordinary, enstatite, and Rumuruti chondrites ($\pm$0.5 % AMU^{-1}; e.g. *Wombacher et al.*, 2003, 2008), as well as comparitively smaller variations in carbonaceous chondrites ($\pm$0.1 % AMU^{-1}; *Baker et al.*, 2010). Mass-independent Cd isotope variation caused by thermal neutron capture

was also confirmed by *Wombacher et al.* (2008). Considering the extremely large range of Cd isotope compositions observed in meteorites and other solar system samples, analytical precision was not a limiting concern, with external precision for the earliest double spike TIMS method reported as ± 0.5 ‰ AMU^{-1}, equivalent to ~ 500 ppm AMU^{-1}.

The first study to measure Cd isotopes by MC-ICPMS (multiple collector inductively-coupled plasma mass spectrometry) was *Wombacher et al.* (2003). In that study, the authors investigated Cd isotope fractionation in a wide range of geological materials, as well as during Cd purification from samples with low Cd contents, and within the mass spectrometer itself. For the first time, small variations in the Cd isotope composition of terrestrial materials were observed owing to improvements in analytical precision that reduced analytical uncertainty to ± 110 ppm AMU^{-1} (achieved by external normalization to admixed Sb or Ag; see Sec. 2.3.2). Given the limited range in stable Cd isotope compositions observed in terrestrial materials and the increased precision of the MC-ICPMS method, a new notation – referred to herein as the epsilon-notation (*Wombacher and Rehkämper*, 2004) – was devised:

$$\epsilon^{114/110}\text{Cd} = \left(\frac{^{114}\text{Cd}/^{110}\text{Cd}_{spl}}{^{114}\text{Cd}/^{110}\text{Cd}_{std}} - 1 \right) \times 10,000 \tag{1.3.2}$$

In this notation, Cd isotope compositions are reported with a 4 AMU spacing in parts per 10,000, relative to a given reference standard (this issue is discussed below in Sec. 1.3.2). This notation has now been widely adopted by most laboratories measuring Cd stable isotope compositions and can be easily converted to isotopic fractionation factors, α, between two phases, A and B, by:

$$\frac{\epsilon^{114/110}\text{Cd}_\text{A} + 10,000}{\epsilon^{114/110}\text{Cd}_\text{B} + 10,000} = \frac{^{114/110}\text{Cd}_\text{A}}{^{114/110}\text{Cd}_\text{B}} \equiv \alpha_{\text{A}-\text{B}} \tag{1.3.3}$$

The MC-ICPMS protocol for measuring Cd isotopes was further refined by the study of *Ripperger and Rehkämper* (2007). In that paper, the authors describe the development of a Cd

double spike technique for measuring the isotopic composition of ng quantities of Cd extracted from seawater. The double spike MC-ICPMS technique is now the most widely used amongst the Cd stable isotope community, and a modified version of their method is used in this thesis. Cadmium double spike MC-ICPMS can routinely achieve an external precision of ± 25 ppm AMU^{-1} for as little as 10 ng Cd isolated from representative geological matrices (e.g. corals, seawater, etc.), although one group have developed a double spike TIMS method that can achieve an external precision of as low as ± 10 ppm AMU^{-1} (*Schmitt et al.*, 2009a; *Abouchami et al.*, 2011).

1.3.2 A common isotopic reference material for Cd

A significant obstacle to the intercomparison of isotopic data generated by different laboratories, for any isotope system, is the reference standard. This is because stable isotope compositions are almost exclusively reported relative to a given standard composition rather than as an absolute value. For the 'traditional' isotope systems, these reference standards are well-established (e.g. Vienna Standard Mean Ocean Water or Standard Light Antarctic Precipitation for O and H, the Pee Dee Belemnite for C, atmospheric nitrogen for N, and the Canyon Diablo Troilite meteorite for S; *Slater et al.*, 2001), with mechanisms in place to ensure their distribution amongst interested research groups.

In the case of Cd, no such standard or distribution system exists, with most laboratories reporting Cd isotopic data relative to their own 'in-house' isotopic reference material (usually an ICPMS Cd concentration standard). A recent study by *Pritzkow et al.* (2007) advocated the use of BAM-I012 as a reference material for Cd (prepared by the Bundesanstalt für Materialforschung und -prüfung; the Federal Institute for Materials Research and Testing). Isotopic analysis of BAM-I012 Cd revealed that it possesses an extremely fractionated composition $\epsilon^{114/110}\text{Cd} \approx -13$ relative to the BSE (Bulk Silicate Earth; *Schmitt et al.*, 2009b), whereas most 'zero-delta' standards in other isotope systems are much closer in composition to the substrates

with which they are frequently compared.

To address these issues, a round-robin intercalibration was undertaken by seven laboratories to identify a suitable isotopic reference material for Cd (MPI Mainz, Universität zu Köln, Imperial College London, The University of Manchester, The University of Oxford, University of Otago, and The University of British Columbia). The intercalibration effort involved characterization of multiple 'in-house' reference standards against one another for the purposes of checking consistency between laboratories and also the suitability of various solutions as the primary reference standard. The main result of the intercalibration was the adoption of NIST SRM 3108 Cd (prepared by the National Institute of Standards and Technology) as the new 'zero delta' reference material for Cd isotopes by the Cd stable isotope community (*Abouchami, Galer, Horner, Rehkämper, Wombacher, Xue, Lambelet, Gault-Ringold, Stirling, Schönbächler, Shiel, Weis, and Holdship*, 2012). Although NIST SRM 3108 Cd was originally intended as an ICPMS concentration standard, its Cd isotopic composition is within 1 $\epsilon^{114/110}$Cd unit of the best estimate for the BSE (*Abouchami et al.*, 2012), thus rendering it a suitable and easily-obtained isotopic reference material.

The contribution, *A Common Reference Material for Cadmium Isotope Studies – NIST SRM 3108 Cd*, is dedicated to John de Laeter (1933 – 2010) and Kevin Rosman (1943 – 2009) in recognition of their pioneering work into cadmium isotope fractionation.

1.3.3 Cd isotope fractionation in seawater

The first indications of Cd isotope fractionation in seawater were reported by *Lacan et al.* (2006). The authors cultured and analyzed two species of freshwater phytoplankton for Cd isotopic compositions (*Chlorella* sp. and *Chlamydomonas reinhardtii*). It was reported that both species of algae internalized isotopically light Cd relative to the growth medium, with an isotopic fractionation factor, $\alpha_{\text{cells}-\text{Cd}_{(\text{aq.})}} \approx 0.9986 \pm 0.0006$. *Lacan et al.* (2006) also analyzed two depth profiles of Cd isotopic compositions from the Mediterranean Sea and the northwest Pacific.

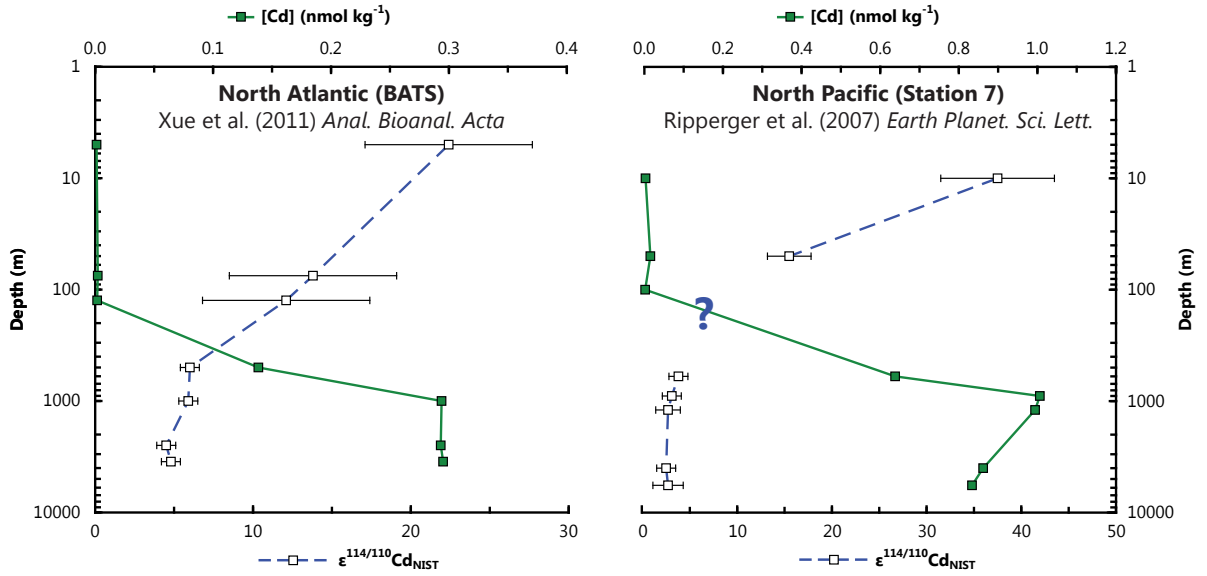

Figure 1.3: Dissolved Cd concentrations and isotopic compositions for the two currently published seawater profiles. The Atlantic profile is from *Xue et al.* (2011); the Pacific profile from *Ripperger et al.* (2007). The data have been replotted on a logarithmic scale to highlight the variation in Cd isotopic compositions in the uppermost water column. Cd concentrations (solid line) return to background concentrations at both stations by $\sim 1,000$ m, whereas isotopic compositions are 'reset' in the upper few 100 m. The different 'reset' depths are controlled by isotopic mixing; isotopic fractionation in the surface is assumed to follow closed-system Rayleigh fractionation (i.e. an exponential relationship), whereas end-member isotopic mixing follows a hyperbolic relationship (e.g. Fig 1.4). The large '?' denotes isotopic data of spurious quality that has been omitted from the Figure. Unlike the Atlantic profile, the Pacific profile shows the characteristic decrease in Cd concentrations at depths below 1,000 m; in both cases, the Cd isotopic compositions of the abyss remains constant and similar between the two ocean basins (within uncertainty).

Unfortunately, the measurement precision was insufficient to identify any Cd isotopic variability (outside of analytical uncertainty), with one of the conclusions of the work being that future studies should employ double spiking in conjunction with an improved Cd separation protocol. Sure enough, the next study to report measurement of Cd isotopic compositions in seawater did indeed employ double spiking and an improved separation protocol (*Ripperger and Rehkämper*, 2007). These authors identified small, but well-resolved variations in three seawater samples (total range in isotopic compositions was between $3-6\ \epsilon^{114/110}$Cd-units, relative to the JMC Münster reference, between the abyssal Pacific and surface Atlantic), and even larger variations of up to 0.1 % AMU^{-1} in a follow-up study (*Ripperger et al.*, 2007).

The study by *Ripperger, Rehkämper, Porcelli, and Halliday* (2007) is also notable for reporting the first depth profile of Cd isotope compositions (Fig. 1.3). The $\epsilon^{114/110}$Cd depth profile demonstrated that Cd isotope compositions can vary by up to almost 40 $\epsilon^{114/110}$Cd-units in the water

column, with the most Cd-depleted samples exhibiting the isotopically 'heaviest' compositions, and the Cd-rich ocean interior displaying isotopically uniform compositions. This pattern is thought to reflect the near-quantitative removal of Cd from surface seawater by marine phytoplankton – with a slight preference for the lighter isotopes of Cd (*Lacan et al.*, 2006) – and the subsequent remineralization and regeneration of this biological material at depth. The uptake and isotopic fractionation of Cd from surface seawater, as a first order approximation, follows closed-system Rayleigh fractionation (*Ripperger et al.*, 2007; Fig. 1.4). As reported by the authors, coupled [Cd]-$\epsilon^{114/110}$Cd measurements reveal additional information about water column processes that are not readily apparent from [Cd] measurements alone. By using a concentration and isotopic tracer, it is possible to calculate isotopic fractionation factors for Cd removal from seawater ($\alpha_{\text{removal}-\text{Cd}_{\text{aq.}}}$; Fig. 1.4). Paired seawater measurements of [Cd]-$\epsilon^{114/110}$Cd enables the distinction between Cd uptake and utilization by plankton to be distinguished from water mass mixing, thus making Cd isotopes a powerful new tracer in chemical oceanography (*Ripperger et al.*, 2007; Fig. 1.4).

Since the first water column profile of *Ripperger et al.* (2007), several recent studies have expanded the database of seawater Cd isotope measurements (*Abouchami et al.*, 2011; *Xue et al.*, 2011; *Gault-Ringold et al.*, 2012; Fig. 1.4). A second full water column profile has been measured (North Atlantic; Fig. 1.3; *Xue et al.*, 2011), confirming the water column Cd isotope structure of *Ripperger et al.* (2007). The work presented by *Xue et al.* (2011) also outlines a new $Al(OH)_3$-Cd co-precipitation (pre-concentration) technique for large volumes of seawater (up to 20 L), allowing the examination of extremely low [Cd] seawater (as low as 1 pmol L^{-1}). These studies are both interesting and important because they reveal the structure of the oceans for a new isotopic tracer, whilst simultaneously investigating the applicability of [Cd] and Cd isotopes as a proxy of Cd uptake and utilization of Cd (and by association with PO_4^{3-}, key oceanic macronutrients).

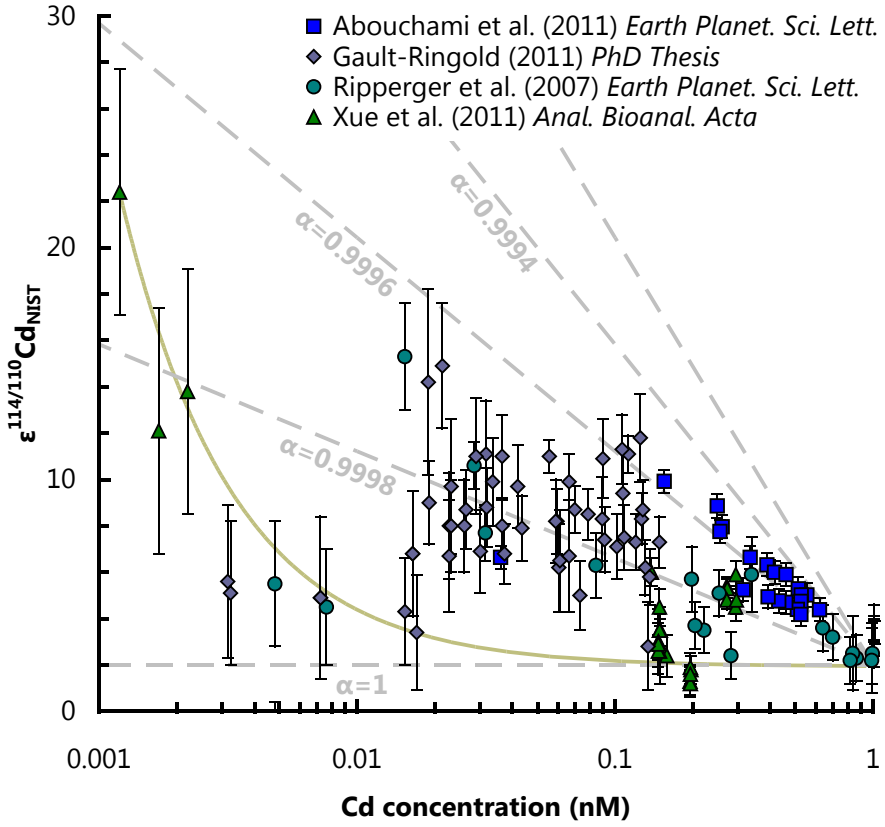

Figure 1.4: Cd isotope and concentration variations in modern seawater. Comparison of dissolved Cd isotope compositions and Cd concentrations for all published analyses of seawater. All data have been renormalized to NIST SRM 3108 (*Abouchami et al.*, 2012). Dashed tie lines are shown for uptake that follows closed-system Rayleigh fractionation (as various α values) assuming an isotopically light removal phase, $\alpha_{\text{removal-Cd(aq.)}}$ (*Ripperger et al.*, 2007; *Abouchami et al.*, 2011; *Xue et al.*, 2011; *Gault-Ringold et al.*, 2012). The large scatter in the data is thought to be largely a consequence of water mass mixing of isotopically distinct water masses. To illustrate the hyperbolic mixing relationship between $\epsilon^{114/110}$Cd and [Cd], a hypothetical mixing line is shown in yellow. This mixing line joins a Cd-depleted and highly-fractionated water mass with a Cd-replete and 'unfractionated' sample from the deep ocean interior.

1.3.4 Records of past marine Cd isotope compositions

A similar version of this section was published as **Cadmium Isotopes in Marine Sediments** in: *Rehkämper, Wombacher, Horner, and Xue* (2011) Natural and anthropogenic Cd isotope variations, in *Handbook of Environmental Isotope Geochemistry, Adv. Isot. Geochem.*, vol. 1, edited by M. M. Baskaran, 1st ed., pp. 125–154, Springer Berlin Heidelberg, Heidelberg, doi:10.1007/978-3-642-10637-8_8 (Section 8.4.4.3).

Applying Cd isotopes to palaeoceanography requires sedimentary archives with sufficient spatial and temporal resolution, and a high fidelity for capture of the ambient seawater signal. At present, only a limited number of marine deposits have been analyzed for Cd isotope compositions, with a database that encompasses ten samples related to sub-seafloor hydrothermal activity at spreading centers and 50 hydrogenetic ferromanganese nodules and crusts (the hydrothermal data are omitted from this thesis, but are discussed in detail elsewhere; *Schmitt et al.*, 2009b; *Rehkämper et al.*, 2011). All data in Fig. 1.5 have been renormalized to NIST SRM 3108 (see Sec. 1.3.2).

Investigations of hydrogenetic Fe-Mn deposits are of particular interest and such samples hence dominate the current Cd isotope database for marine sediments (Fig. 1.5). This interest is based on the observation that the surface layers of hydrogenetic Fe-Mn crusts and nodules faithfully record the isotopic composition of seawater for numerous trace metals. Consequently, time series data obtained for older deposits have been used in paleoceanographic studies, to interrogate temporal changes in the radiogenic (e.g., Nd, Pb) and stable (e.g., Tl, Mo, Fe) isotope composition of seawater (*Frank*, 2002; *Levasseur et al.*, 2004; *Rehkämper et al.*, 2002, 2004; *Siebert et al.*, 2003).

The compendium of recently available Cd isotope data encompasses 15 Fe-Mn crusts (*Horner et al.*, 2010) and 37 Fe-Mn nodules (*Schmitt et al.*, 2009b). These two types of deposits differ in that Fe-Mn crusts form on basaltic substrates whereas nodules are precipitated on pelagic sediments. Despite this difference, crusts and nodules were observed to display similar Cd contents (of about $1 - 20$ μg g^{-1}) and isotope compositions, with $\epsilon^{114/110}$Cd values of between about 0 and $+5.5$ (Fig. 1.5). In particular, essentially all hydrogenetic Fe-Mn deposits are characterized by Cd isotope composition that are similar to the oceanic deep water average reported

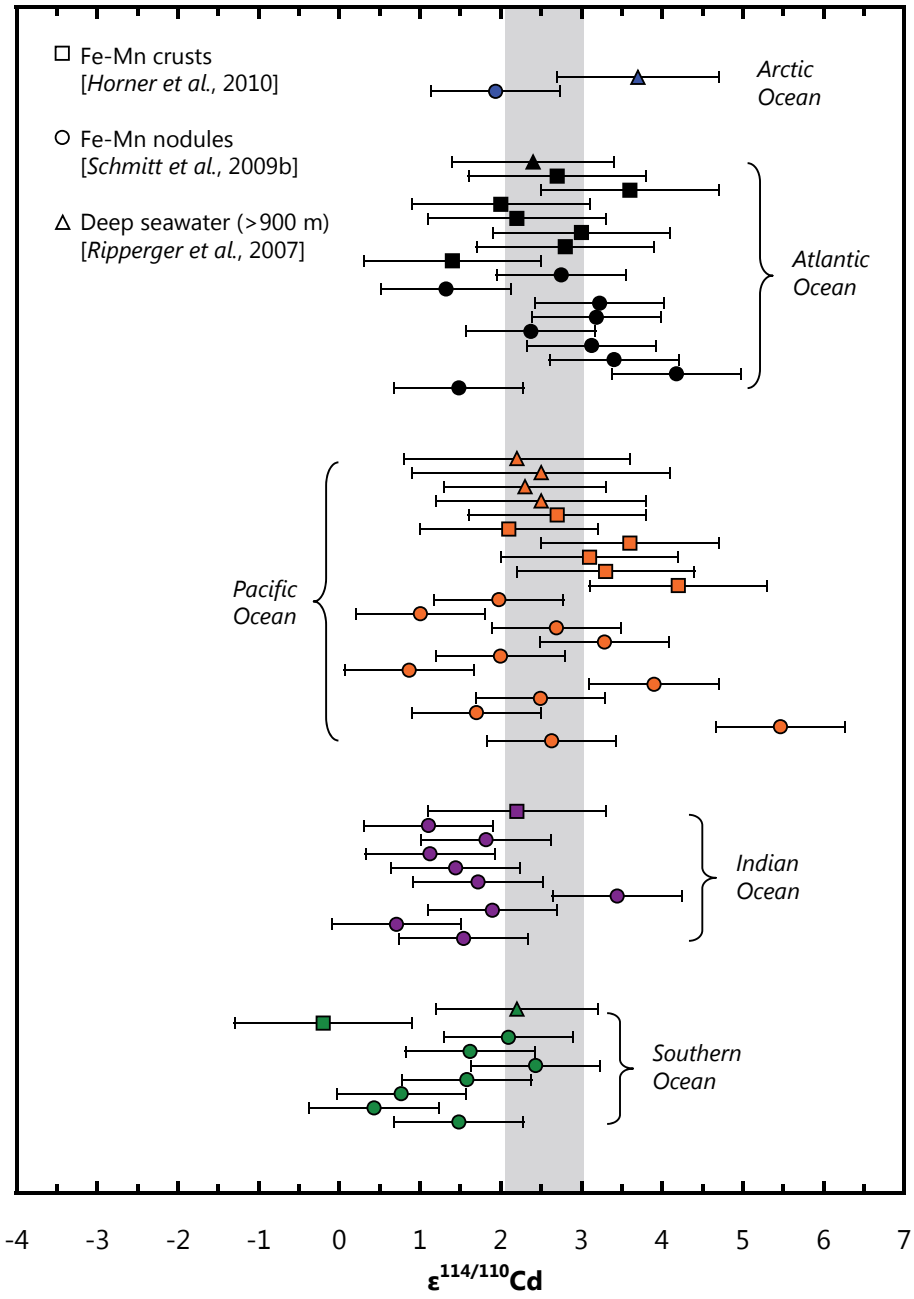

Figure 1.5: Compilation of Cd isotope data for marine sediments and deep-ocean seawater. Data from *Schmitt et al.* (2009b), *Horner et al.* (2010), and *Ripperger et al.* (2007). Sample isotope compositions have been converted to $\epsilon^{114/110}$Cd and are reported relative to NIST SRM 3108 Cd. The samples are grouped by location and type. The mean Cd isotopic composition of oceanic deep waters of $\epsilon^{114/110}\text{Cd} = +2.5 \pm 0.5$ (1 SD), is denoted by the grey band (*Ripperger et al.*, 2007). The uncertainties (2 SD) are shown as reported in the original publications.

by *Ripperger et al.* (2007) of $\epsilon^{114/110}\text{Cd} = +2.5 \pm 1.0$ (2 SD). This result is significant because it implies that Fe-Mn crusts and nodules record the Cd isotope composition of seawater without significant isotopic fractionation (*Schmitt et al.*, 2009b; *Horner et al.*, 2010). This observation is surprising because it contrasts with the behavior of Zn, an element that generally exhibits similar marine biogeochemical characteristics to Cd. The Zn isotope composition of deep ocean seawater (*Bermin et al.*, 2006) appears to be offset from isotopically heavier Zn in Fe-Mn nodules (*Maréchal et al.*, 2000) by about 5 ϵ for $^{66}\text{Zn}/^{64}\text{Zn}$. This fractionation has been corroborated by laboratory studies, which have shown that 'heavy' Zn isotopes are preferentially scavenged from solutions by (oxy)hydroxide precipitates (*Pokrovsky et al.*, 2005; *Balistrieri et al.*, 2008; *Juillot et al.*, 2008). Offsets in stable isotope compositions between seawater and hydrogenetic Fe-Mn deposits are also common for other elements, including Mo (*Barling et al.*, 2001) and Tl (*Rehkämper et al.*, 2002, 2004), although the mechanisms of isotopic fractionation are still the subject of ongoing research and may be different for each element.

The absence of isotopic effects during the incorporation of Cd into hydrogenetic Fe-Mn crusts and nodules is a promising result because this simplifies the interpretation of Cd isotope time series data that are obtained for such samples. Based on this finding, it may be possible to interpret temporal variations in $\epsilon^{114/110}\text{Cd}$ that are identified for Fe-Mn deposits, as reflecting changes in the Cd isotope composition of seawater, rather than differences in the isotopic fractionation between seawater and the Fe-Mn minerals. Preliminary time-resolved Cd isotope data were obtained for a Fe-Mn nodule from the Atlantic Ocean by *Schmitt et al.* (2009b). Six samples with ages of between 0 and 8 Ma were analyzed and no significant change in $\epsilon^{114/110}\text{Cd}$ was detected. This suggests that the Cd isotope composition of oceanic deep water is relatively stable through geological time (*Schmitt et al.*, 2009b), assuming that the Cd stable isotope systematics of this nodule were not altered by diagenetic processes, such as isotopic equilibration with Cd from pore fluids (e.g. *Rehkämper et al.* 2002).

The time series data for the nodules also do not preclude short-term fluctuations in the Cd isotope composition of the deep oceans and these may be best recorded in marine carbonates. This

conclusion follows from the observation that abyssal carbonate records of Cd/Ca (e.g. *Boyle and Keigwin*, 1982; *Boyle*, 1992) and other trace metal isotope systems (e.g. *Lea*, 2006; *Lynch-Stieglitz*, 2006) can show significant variability on glacial/interglacial timescales. One possible source of Cd isotope variation may arise from the sensitivity of the oceanic Cd inventory to the areal extent of suboxic sediments, which may change over glacial/interglacial timescales (*van Geen et al.*, 1995; *Rosenthal et al.*, 1995). Cadmium isotope data on carbonates – with the exception of a single synthetic aragonite – have not been reported prior to this thesis (e.g. Chapter 5). This lack of data reflects the challenging nature of the analyses, which are rendered particularly difficult by the low Cd contents of such materials (e.g. foraminiferal tests; *Rickaby et al.*, 2000). This necessitate that large samples (typically > 1 g) are processed for analysis, because at least $1 - 10$ ng of Cd are required for a reasonably precise isotopic measurement.

1.4 Motivation for the work presented in this thesis

With the development of any environmental proxy there are a series of challenges, both technical (i.e. analytical) and in the application to a question of environmental significance. The technical aspects of measuring Cd isotopes in geological samples are discussed in Chapter 2. The sections above outline the current understanding of Cd isotopes in the marine realm, suggesting that [Cd] and Cd isotopes may become useful oceanic tracers of nutrient utilization. However, there are still several outstanding questions that are fundamental to the use of Cd isotopes as a new tracer, namely: *why* does Cd behave like an algal nutrient and *how* can this be applied to palaeoceanography? This thesis is divided into two parts; the first describes the *why* (Chapter 3) and the second describes the *how* (Chapters 4, 5).

To investigate the *why* (Chapter 3), a novel combination of molecular and isotopic techniques were used to examine the role of CdCA1 in determining cellular (and by inference, oceanic) Cd isotope compositions. This was achieved by expressing the genetic coding for CdCA1 in a heterologous system, allowing the observation of isotopic fractionation on length scales as

small as a few Å. The results of this study reconcile the rare genetic occurrence of the CdCA1 enzyme in marine phytoplankton with the ubiquitous uptake and fractionation of Cd isotopes observed in seawater.

The *how* is addressed in two ways (Chapters 4, 5). As discussed above, extending the use of Cd isotopes into the past requires the Cd isotope signal to be captured and faithfully preserved in a suitable sedimentary archive. As a starting point, the role of environmental factors (e.g. temperature, growth rate, ambient [Mg^{2+}]) in controlling the inorganic partitioning of Cd isotopes into calcite was investigated (Chapter 4). Through a series of laboratory analogue experiments, the dominant control (salinity) was elucidated, as well as a tentative mechanism to explain the observed Cd isotopic fractionation during incorporation into this geologically-ubiquitous mineral.

Using the inorganic partitioning experiments as the conceptual basis for further study, a suite of modern deep-sea corals were investigated for their suitability to record past seawater Cd isotope compositions (Chapter 5). By applying a new isotopic tracer to deep-sea corals, it was also possible to test the nature of elemental and isotopic partitioning during skeletal biomineralization. Chapter 5 posits a Rayleigh fractionation model to explain Cd/Ca and Cd isotope compositions during deep-sea coral skeletogenesis and from this the potential application(s) of these samples to palaeoceanography.

CHAPTER 2

Extended Methodology

"...for cadmium is so complex an element and its lines so near the limit of resolution that without the enhanced resolving power given by the peculiar properties of the schumannized plates it is doubtful if any reliable interpretation could have been made."

–*Aston* (1925)

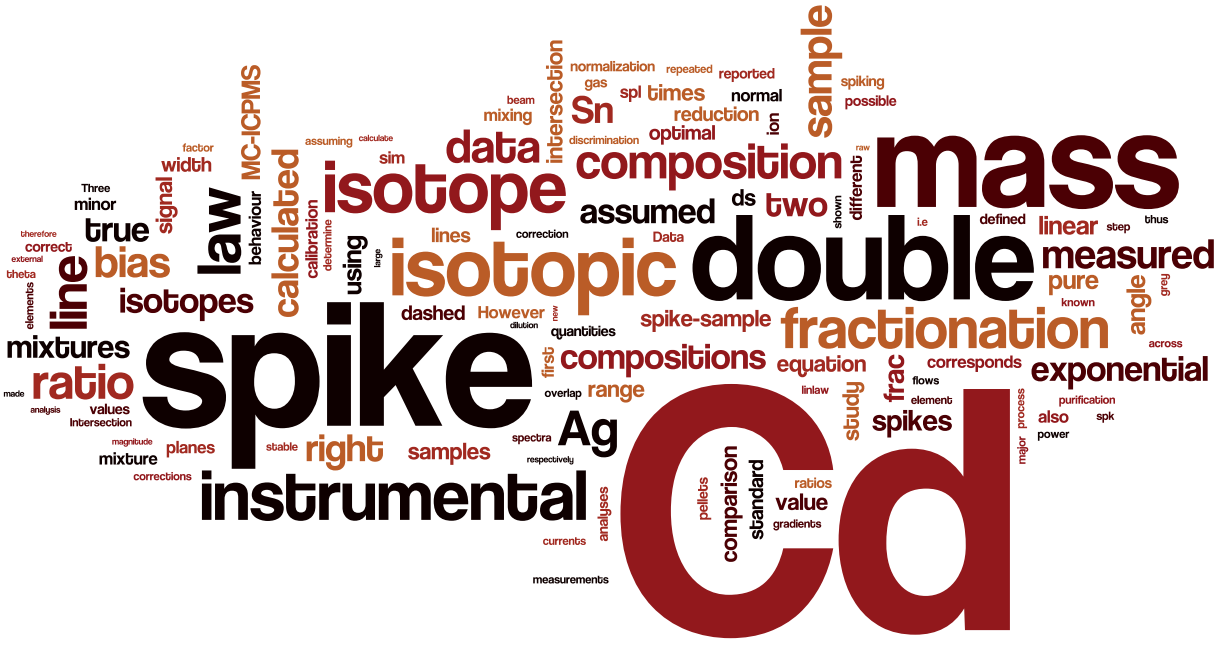

2.1 Measurement of trace metal isotopes in environmental samples

TRACE metals – by their very nature – are scarce and their analysis relies on sensitive measurement techniques. In the case of Cd, the average upper crustal concentration is about 100 ng g^{-1} (*Wedepohl*, 1995), and as such the amount of Cd generally observed in non-polluted environmental samples is also extremely low. Measurement of Cd isotope compositions requires that the utmost care is taken in the preparation of environmental samples so as not to contaminate prior to analysis. The analysis itself also requires careful consideration as there are a number of factors that can affect the precision and accuracy of measured Cd isotope ratios.

This chapter outlines the analytical considerations for the measurement of Cd stable isotope ratios in environmental samples. There are two prior steps that must be undertaken before arriving at the analysis stage: the initial selection of samples and their preparation. Whilst it is important to select the correct samples, this issue is not discussed in detail in this chapter (see instead Chapters 3, 4, or 5). The steps required to avoid contamination in the laboratory are briefly discussed, as well as other sample preparatory steps (e.g. chemical separation; Sec. 2.2). The main focus of this chapter is the methodological steps specific to the precise and accurate determination of Cd isotope ratios by MC-ICPMS. In particular, this chapter concentrates on the application of the double spike protocol to correct for instrumental mass bias. Many of these considerations are not specific to Cd but also apply to the analysis of other elements.

2.2 Elemental purification

To apply Cd isotope ratio measurements to geological samples, an elemental purification scheme is required to separate Cd from the sample matrix. The high ionization capability of plasma-source mass spectrometers ensures that nearly all elements are ionized during sample introduction. Elemental purification thus becomes doubly necessary to remove any elements with isobaric or molecular overlap with Cd (e.g. Sn, In, MoO, ZrAr, etc.; Fig. 2.1), as well as to

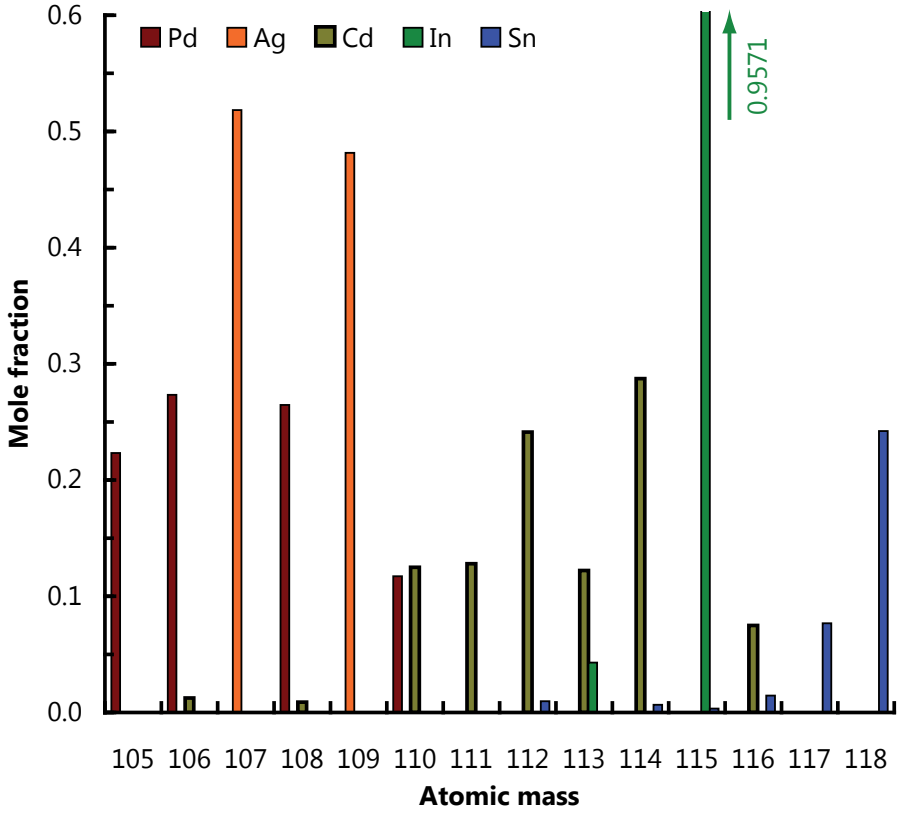

Figure 2.1: The Cd mass spectrum. The relative proportions of other elements in the Cd mass range are also shown; Cd is displayed in bold. Isobaric overlap with Cd occurs for Pd (masses 106, 108, and 110), In (mass 113), and Sn (masses 112, 114, and 116). Only ^{111}Cd is free of isobaric overlap. Relative elemental abundances from *De Laeter et al.* (2003).

ensure that major elements without overlap (e.g. Na, Ca, Mg, etc.) do not alter the instrumental mass bias (e.g. *Halliday et al.*, 1995; *Rehkämper et al.*, 2001; Sec 2.3.2).

Cadmium suffers from numerous isobaric interferences across its mass range (Fig. 2.1). In addition to isobaric Pd, In, and Sn, a range of molecular interferences can also affect Cd isotope measurement (e.g. *Abouchami et al.*, 2012). The relevant molecular interferences, considering the range of substrates analyzed in this thesis (organic matter, Chapter 3; $CaCO_3$, Chapters 4 and 5), are ZnAr, MoO, and SrO. Elemental purification schemes, such as the one outlined below, must also also account for these elements as they are not easily monitored during Cd stable isotope measurements. Such purification should also aim to achieve quantitative yields, as incomplete elution can cause Cd isotopic fractionation during anion exchange (*Wombacher et al.*, 2003; *Schmitt et al.*, 2009a), although if double spiking is employed, this becomes less of a concern (Sec 2.4). The low quantities of Cd that generally occur in natural samples also

necessitates that yields be kept as high as possible for optimum sensitivity. A review of relevant separation protocols can be found in *Rehkämper, Wombacher, Horner, and Xue* (2011).

Before any such separation can be utilized, it must first be calibrated for optimal separation. This was achieved by separating Cd from samples with representative matrices for each resin or column combination. The first stage separation utilized the AG-1X8 resin (*Strelow*, 1978). For calibration in the large columns (1.6 mL AG-1X8), $\sim$ 1 g of assorted shell material was used, doped with 1 μg of OxCad (large Cd concentrations were used as Cd elution was monitored by collecting multiple, sequential 'cuts'). For the small columns (200 μL AG-1X8), a single gastropod shell ($\sim$ 50 mg) was used, again doped with 1 μg of OxCad. The results of the separation are shown in Fig. 2.2. For both columns, the major elements (e.g. Ca, Sr, Mg, K, etc.) are initially eluted in HCl, before Zn is eluted in a mixture of HBr and HNO_3 (Fig. 2.2). As can be seen, minor quantities of Sn elute with Cd for both columns, necessitating a second/third pass through TrisKem (formerly Eichrom) TRU resin (Table 2.2; Fig. 2.3). The TRU resins were calibrated by mixing 1 μg of Sn, Mo, and Cd and passing through columns (Fig. 2.3). Both Sn and Mo are retained by the resin (*Yi et al.*, 1995), and no breakthrough occurs during the first 4 mL of elution, whereas Cd is completely eluted within 3 mL. Following separation, the resin is discarded.

In this thesis, a two-stage column chemistry was used to isolate Cd from sample matrix. This protocol uses a modified version of the protocol first outlined by *Wombacher et al.* (2003) and used for the isolation of Cd from seawater by *Ripperger and Rehkämper* (2007). Sample preparation was carried out in Class 10 laminar flow workstations at all times to minimize Cd contamination. All mineral acids had been purified prior to use by sub-boiling distillation in quartz glass stills, or in the case of HBr, was purchased at 'Optima'-grade from Fisher Scientific. For samples with 'unfavourable' Cd:matrix ratios (i.e. [Cd] $<$ 1 ppm dry mass), a double pass through AG 1-X8 resin was needed (Table 2.1, 2.2; Fig. 2.2). If samples had more favourable Cd:matrix ratios ([Cd] $>$ 1 ppm dry mass), only a single pass was through AG 1-X8 was needed before removal of Sn through the TRU resin (Table 2.2).

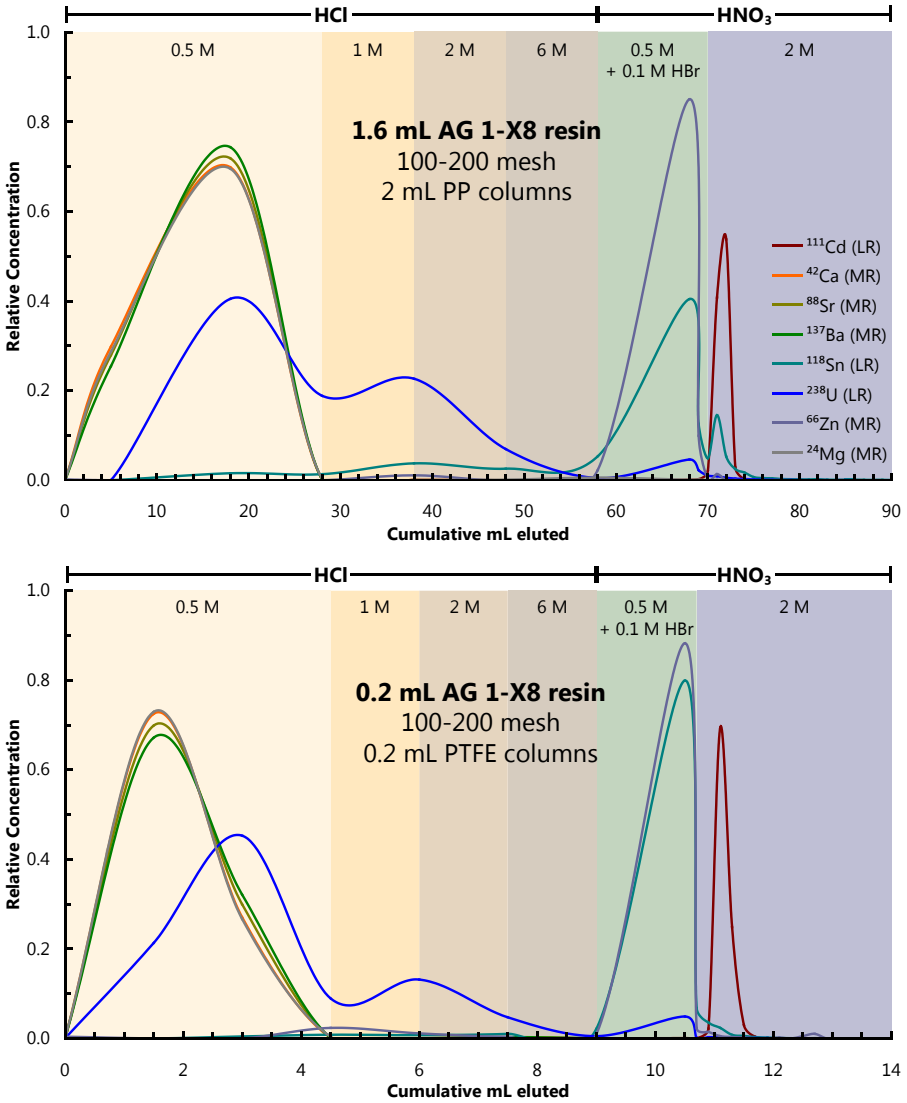

Figure 2.2: Column calibration for AG-1X8 resin. The upper panel illustrates elemental separation for 1.6 mL of resin (i.e. samples with 'unfavourable' Cd:matrix ratios), the lower panel for the 0.2 mL columns. For the large columns, cuts were collected and measured, on average, for every 10 mL eluted until the eluent was switched to HNO_3, when cuts were collected for analysis every 1 mL. (For the small columns, cuts were collected for every 1.5 mL and 0.2 mL eluted, respectively.)

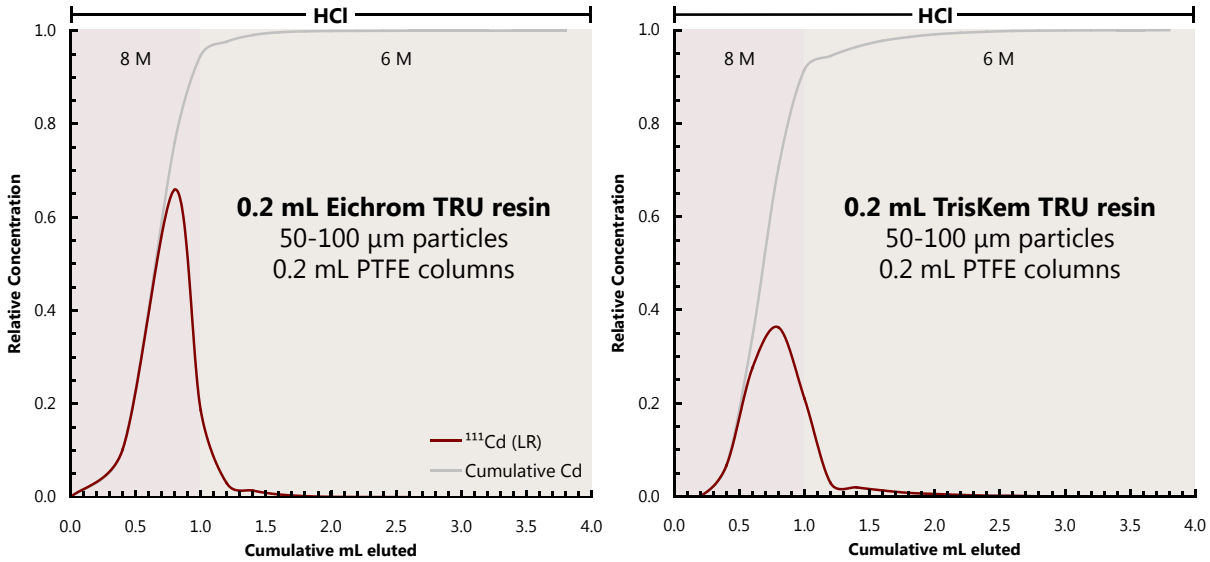

Figure 2.3: Column calibrations for TRU resin. Two calibrations were performed as the resin supplier changed during the course of this work; this did not appear to affect the calibration. A smaller 'cut' size was used when testing elution with TrisKem TRU resin compared to Eichrom TRU resin (200 μL compared with 400 μL, respectively), causing the elution peak to appear smaller; the cumulative elution curve remained unchanged.

Table 2.1: Cd separation chemistry for samples with 'unfavourable' Cd:matrix ratios. Protocol adapted from *Wombacher et al.* (2003).

1.6 mL Biorad AG 1-X8 anion exchange resin (dry mesh: 100 – 200)		
Eluent	Quantity (mL)	Purpose
2 M HNO_3	11	Resin cleaning
18.2 MΩ H_2O	0.5	Rinse
6 M HCl	16	Resin cleaning
0.5 M HCl	11	Resin conditioning
1 M HCl Sample Solution	Variable	Elute Matrix
0.5 M HCl	23	Elute Matrix
1 M HCl	10	Elute Matrix
2 M HCl	10	Elute Matrix
6 M HCl	10	Elute Matrix (Ag)
0.5 M HNO_3 + 0.1 M HBr mixture	10	Elute Matrix (Zn)
2 M HNO_3	1.5	Ready Beakers
2 M HNO_3	8	Elute Cd

Table 2.2: Second-stage Cd 'cleanup' chemistry or stand-alone separation protocol for samples with favorable Cd:matrix ratios. This protocol is adapted from *Horner et al.* (2010).

200 μL Biorad AG 1-X8 anion exchange resin (dry mesh: 100 − 200)		
Eluent	Quantity (μL)	Purpose
2 M HNO_3	1,500	Resin cleaning
18.2 MΩ H_2O	100	Rinse
6 M HCl	2,100	Resin cleaning
0.5 M HCl	1,100	Resin conditioning
1 M HCl Sample Solution	Variable	Elute Matrix
0.5 M HCl	4,500	Elute Matrix
1 M HCl	1,500	Elute Matrix
2 M HCl	1,500	Elute Matrix
6 M HCl	1,500	Elute Matrix (Ag)
0.5 M HNO_3 + 0.1 M HBr mixture	1,500	Elute Matrix (Zn)
2 M HNO_3	200	Ready Beakers
2 M HNO_3	1,500	Elute Cd
200 μL TrisKem TRU resin (50 − 100 μm particles)		
6 M HCl	10,000	Resin Condition
8 M HCl Sample Solution	400	Elute Cd
8 M HCl	400	Elute Cd
6 M HCl	3,000	Elute Cd

Following ion-exchange chemistry, samples were taken up in an appropriate volume of 2 % HNO_3 for mass spectrometry. A 100 μL sub-sample would also be taken to check concentrations and spike/sample ratios. Any other sample-specific preparatory steps are outlined in the latter chapters of this thesis (e.g. digestion of bacterial pellets in Chapter 3, preparation of artificial seawater in Chapter 4, cleaning of $CaCO_3$ in Chapter 5).

2.3 Analytical considerations

2.3.1 Choice of mass bias correction

The advent of plasma-source mass spectrometry brought with it the possibility of analyzing new elements with unprecedented precision. Elements with particularly high ionization potentials (e.g. Zn, Cd, Hf, W, Hg) became significantly easier to analyze and, when coupled with the ability to run samples directly from dilute solutions, it was widely thought that sample throughput would dramatically increase. As with TIMS, plasma-source instruments demon-

strate significant mass bias (> 1 %; *Belshaw et al.*, 1998), which may be attributable to so-called 'space-charge' effects (e.g. *Olivares and Houk*, 1985; *Tanner*, 1992; *Montaser*, 1998). Unlike TIMS, this mass bias is much more stable over short time periods (minutes to hours), and can be characterized and therefore corrected.

Three approaches have previously been developed to correct for instrumental mass fractionation during isotope ratio analysis by MC-ICPMS (for any element): internal/external normalization (*Rehkämper and Halliday*, 1998; *Belshaw et al.*, 1998), standard-sample bracketing (*Zhu et al.*, 2000), and double spiking (*Siebert et al.*, 2001):

- Internal normalization corrects for any mass discrimination by normalizing against an internal reference or invariant isotope ratio within the sample being analyzed. This method cannot normally be applied to the measurement of stable isotope compositions because the correction would 'reset' any stable isotope effects. The correction must therefore be made to a second element (hence, external normalization) that is added for the analyses (e.g. Mg for Si, *Cardinal et al.*, 2003; Tl for Pb and vice versa, *Rehkämper and Halliday*, 1998; Zn for Cu and vice versa, *Archer and Vance*, 2004; Ag or Sb for Cd, *Wombacher et al.*, 2003).

- Standard-sample bracketing techniques require samples to be 'bracketed' (i.e. preceded and followed) by measurements of a standard. The instrumental mass bias is then interpolated between the two standard measurements and used to correct the sample.

- Double spiking – first described by *Dodson* (1963) at the Department of Geology and Mineralogy (now Earth Sciences), University of Oxford – is essentially another form of internal normalization. It requires that the element of interest possesses at least four isotopes. Following dissolution, samples are doped with a combination of two (or more) isotopes of that element with a known isotopic ratio. The benefit of this approach is that the instrumental mass fractionation can be calculated directly from the analysis of the element of interest, rather than being inferred from a dopant or interpolated from a standard.

Table 2.3: Detector configurations for Cd isotope analysis. The ion current for a given mass and the corresponding DVM (digital voltmeter) assigned to that mass is shown for the different configurations used in this thesis. Focusing limitations and the presence of ion counters (ICx) do not permit every collector to be occupied by an ion beam. The principal ion currents (i.e. used for data reduction) in each configuration are shown in **bold**.

Meter	DVM0	DVM1	DVM2	DVM3	DVM4	DVM5	DVM6	DVM7	DVM8	IC1	DVM9	IC2	DVM10	IC3	DVM11
Normal data acquisition configuration															
Step 0	**117**	116	**115**	–	**114**	–	**113**	–	**112**	–	**111**	–	110	–	109
Spike calibration configuration															
Step 0	117	116	115	–	**114**	–	**113**	–	**112**	–	**111**	–	110	–	109
Step 1	112	111	110	–	**109**	–	108	–	**107**	–	106	–	105	–	104
Mass fractionation assessment configuration															
Step 0	117	116	115	–	**114**	–	**113**	–	**112**	–	111	–	110	–	109
Step 1	115	114	113	–	**112**	–	**111**	–	**110**	–	109	–	108	–	107

Double spiking has the additional benefit of increasing the signal to noise ratio of analyses, as the measured mixtures contain both sample- and spike-derived analyte.

2.3.2 Characterization of instrumental mass fractionation for Cd

Use of a double spike, or any of the aforementioned corrections, to correct for instrumental mass bias first requires the general fractionation behaviour of the instrument to be known. To this end, a series of tests were performed to determine the mass bias of Nu Plasma 010 over the course of two months (December 2008 – January 2009). This was achieved by optimizing the signal intensity for a solution standard, 'OxCad' (*Horner et al.*, 2011) and measuring isotopic compositions in two batches of 15×10 s integrations (collector configuration are given in Table 2.3). The instrumental mass bias is particularly sensitive to the gas flows surrounding the plasma (and also to numerous external factors, e.g. temperature, extraction efficiency, etc.). Membrane gas flows were adjusted on the desolvator (referred to as 'sweep gas' on Aridus systems), the peak shape re-optimized and the measurements repeated. This whole process was repeated eight times across a wide range of membrane gas flows ($\sim 1 - 4$ L min Ar), leading to a ~ 1 % AMU^{-1} variation in measured Cd isotope compositions and a range of signal intensities (Fig. 2.4).

Several empirical 'laws' have been developed to characterize instrumental mass fractionation on MC-ICPMS; the linear law (e.g. *Galer*, 1999):

$$R = \frac{r}{(1 + f\,(m_2 - m_1))} \tag{2.3.1}$$

the power law (e.g. *Halliday et al.*, 1995):

$$R = r\,(1 + f)^{m_2 - m_1} \tag{2.3.2}$$

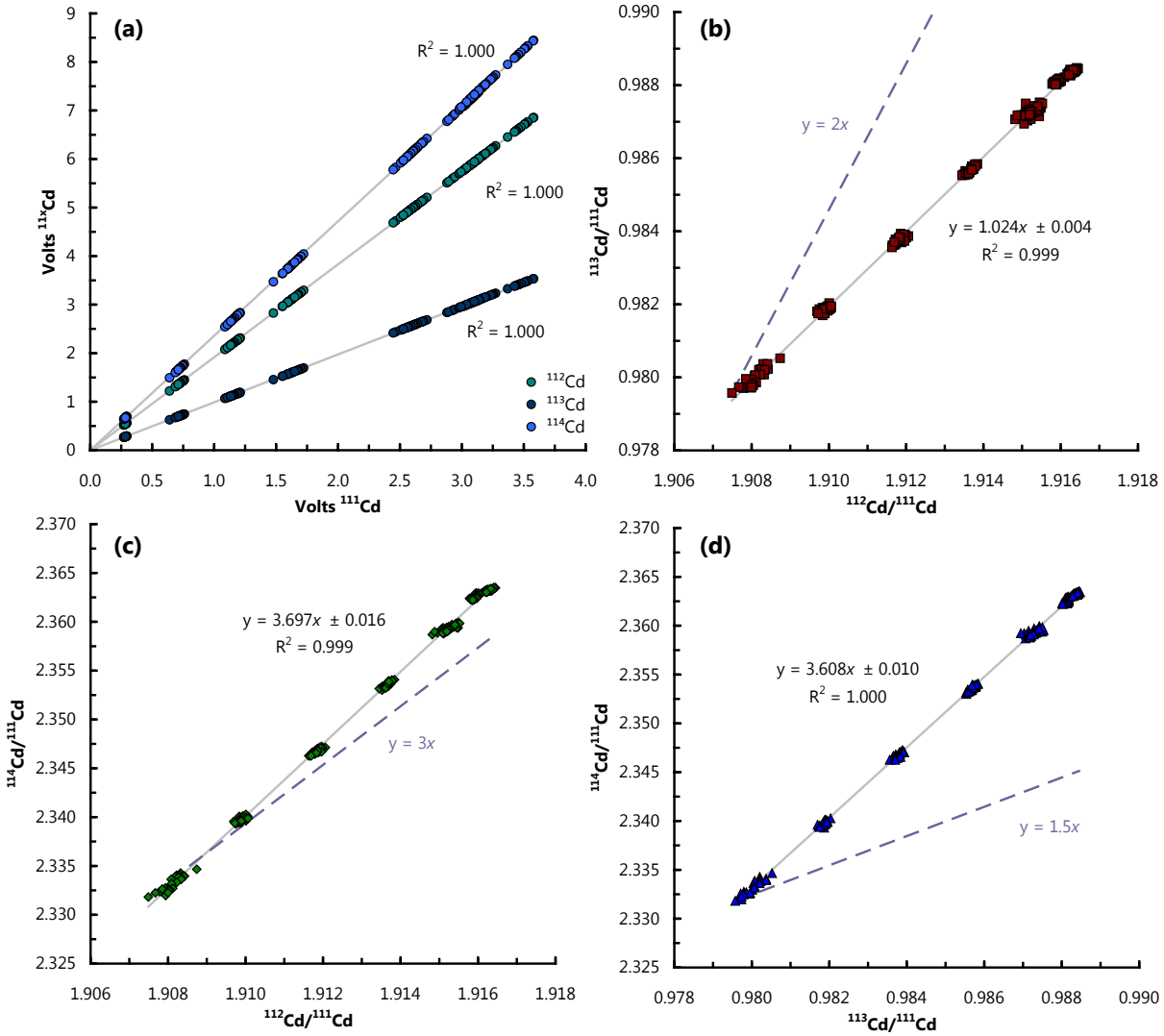

Figure 2.4: Data from the linear mass fractionation assessment. (a) Voltages of the major Cd ion beams used in the calculations plotted against signal intensity on ^{111}Cd. (b)–(d) Three isotope plots showing the raw data, measured gradients (grey lines) and predicted (dashed purple lines) for linear law instrumental mass bias. No 'true' Cd isotopic compositions are assumed (i.e. the position of the linear law line is arbitrarily drawn).

and the exponential law (e.g. *Belshaw et al.*, 1998):

$$R = r\left(\frac{m_2}{m_1}\right)^f \tag{2.3.3}$$

where R is the 'true' ratio, corrected for instrumental mass bias; r is the measured (uncorrected) ratio; f is the fractionation factor; and m_i is the mass of isotope i.

The data in Fig. 2.4b–d demonstrate that the linear law is inadequate at describing the mass fractionation for Cd associated with MC-ICPMS. This is illustrated by the large deviations from the predicted slope of the linear law and the measured gradients. In Fig. 2.5a–c, the same data are plotted again assuming exponential law behaviour; measured gradients are much closer to the theoretical behaviour. However, there are still subtle deviations from pure exponential law behaviour, as has been observed for Nd (*Vance and Thirlwall*, 2002).

The power law has been described in detail by *Maréchal et al.* (1999). Briefly, the generalized form (Eq. 2.3.4), unlike the exponential law, has an explicit parameterization of the the mass dependence of the instrumental mass discrimination, n. By changing the exponent n, it is possible to modify the GPL (generalized power law) to describe different fractionation behaviors (and by inference, instrumental setups):

$$R = rf^{(m_2^n - m_1^n)} \tag{2.3.4}$$

If assuming a 'true' Cd isotope composition (e.g. *De Laeter et al.*, 2003), an instrumental fractionation factor, f, can be calculated for any single measurement:

$$f = \left(\frac{R}{r}\right)^{\frac{1}{(m_2^n - m_1^n)}} \tag{2.3.5}$$

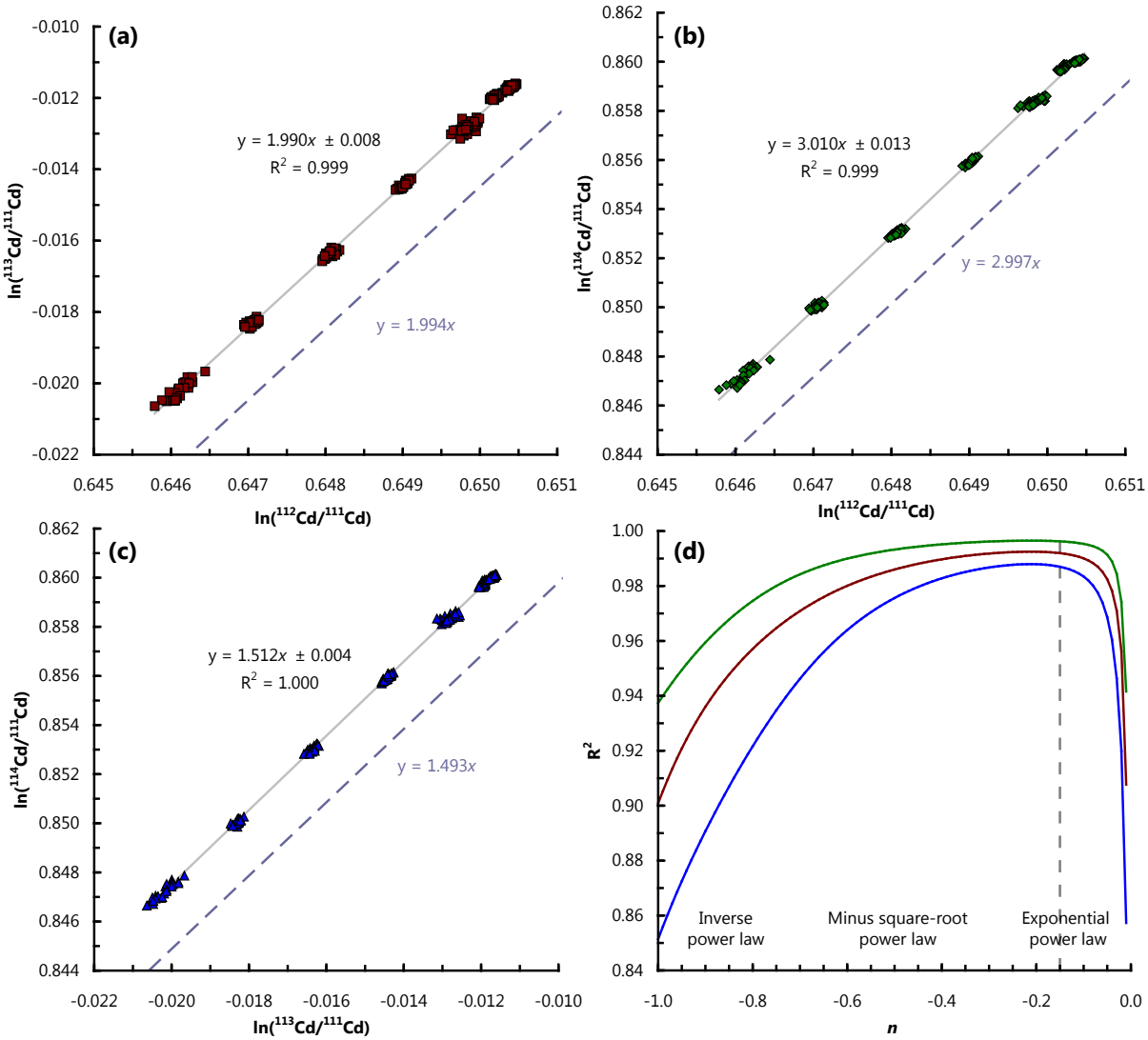

Figure 2.5: Data from the exponential mass fractionation assessment. (a)–(c) Three isotope plots in log-log space showing the raw data, measured gradients (grey lines) and predicted (dashed purple lines) for exponential law instrumental mass bias. No 'true' Cd isotopic compositions are assumed (i.e. the position of the exponential law line is arbitrarily drawn). (d) Mass fractionation factor correlation coefficients against n (see text for details). The dashed grey line corresponds to $n = -0.15$, the value used in this study. The red, green, and blue lines correspond to panels (a), (b), and (c), respectively.

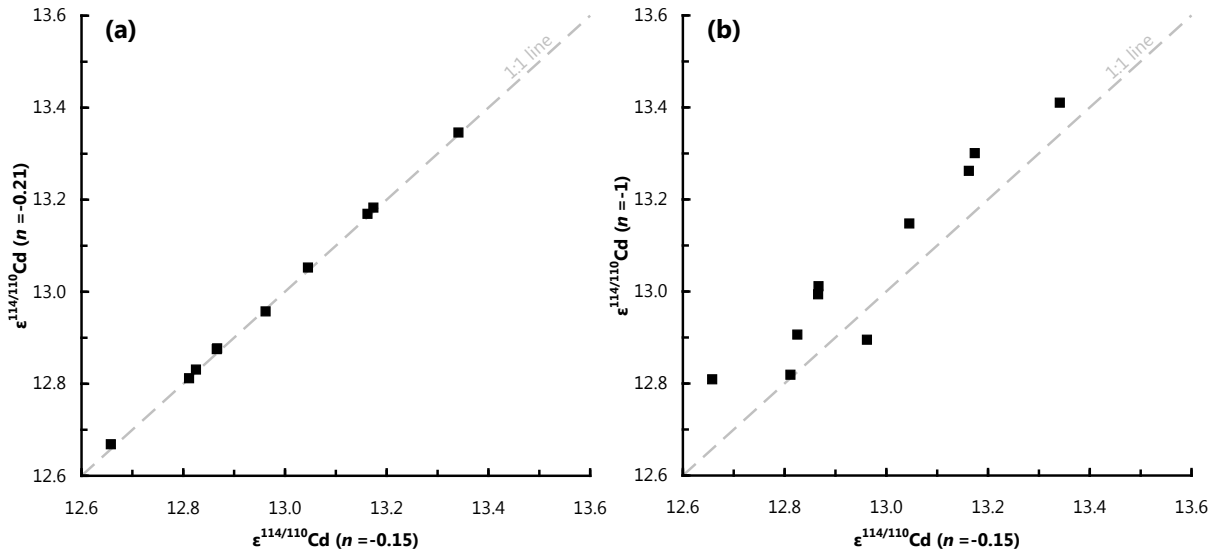

Figure 2.6: Comparison of Cd isotopic compositions for NIST SRM 3108 measured relative to BAM I012 Cd for various n. Analyses were performed at Oxford and are the same as those reported in *Abouchami et al.* (2012). (a) $\epsilon^{114/110}$Cd for $n = -0.21$ against $\epsilon^{114/110}$Cd for $n = -0.15$. (b) $\epsilon^{114/110}$Cd for $n = -1.00$ against $\epsilon^{114/110}$Cd for $n = -0.15$. The reprocessing of the Cd stable isotope data for different n demonstrates that over the range of optimal n (where $R^2 > 0.985$; approximately -0.10 to -0.35; Fig 2.5), Cd isotope compositions are essentially identical to within < 0.01 $\epsilon^{114/110}$Cd -units, whereas $n = -1.00$ generates minor random offsets.

Using the GPL and a 'true' Cd isotopic composition, values of f were computed for each isotope ratio pair (i.e. ^{11x}Cd/^{111}Cd) in each of the 236 analyses shown in Figs. 2.4 & 2.5. The mass dependence of f was then investigated by systematically varying the value of n from from pure exponential behaviour ($n \rightarrow 0$) to pure inverse power law behaviour ($n \rightarrow -1$). If the mass fractionation behaviour of the mass spectrometer is perfectly described by the mass fractionation law being used, the calculated values of f should be identical when calculated from any isotope ratio pair (i.e. ^{11x}Cd/^{111}Cd; for any single measurement). In reality, these values do not perfectly agree; the disparity in f values depends on n. To quantify the effect of varying n on f, values of f are calculated for each of the isotope ratio pairs (i.e. ^{112}Cd/, ^{113}Cd/, or ^{114}Cd/^{111}Cd) and compared against one another for each n. The agreement between calculated values of f is expressed as the coefficient of determination, R^2 (Fig. 2.5d). Large values of R^2 for a given n indicate that there is good agreement across isotope ratio pairs in the estimates of f.

It is clear that the best-fit instrumental mass fractionation law deviates from pure exponential mass fractionation. Instead, a mixture of minus square-root and exponential laws characterizes mass discrimination for Cd on Nu Plasma 010. The best fit to the data occurs for $n = -0.21$,

although values in the range of -0.10 to -0.35 lead to good agreement in f between isotope ratio pairs ($R^2 > 0.985$; Fig. 2.5d). Non-systematic (albeit minor) isotopic offsets occur when Cd isotope ratios are reprocessed for different values of n (Fig. 2.6), suggesting inadequate mass bias correction. The detailed study of *Wombacher and Rehkämper* (2003) notes that variations in the torch position, cone geometries, gas flows, and accelerating potentials (i.e. "routine operations") can lead to variations in the optimal n from -0.2 to -0.4 (for Nd). Rather than optimize n for each analysis session, a constant value of $n = -0.15$ was used throughout this thesis. Whilst this value is slightly away from the optimal value calculated for the mass fractionation assessment described above, the optimal value of n is likely to vary day-to-day, and small variations in n have only a minor effect on measured Cd isotope ratios (Fig. 2.6). The value of $n = -0.15$ has been successfully used in previous Cd isotope studies (e.g. *Wombacher et al.*, 2004; *Ripperger and Rehkämper*, 2007; *Ripperger et al.*, 2007; *Horner et al.*, 2010).

2.4 Application of the double spike to mass bias correction

Several groups now routinely use double spike methods for stable isotopic analyses of Cd, as spiking has been shown to provide superior precision and accuracy over conventional instrumental mass bias corrections (e.g. *Galer*, 1999; *Rudge et al.*, 2009). An interesting development is that most research groups have opted for different combinations of spike isotopes. For example, the first reported use of a Cd double spike (*Rosman and De Laeter*, 1975) opted for a ^{106}Cd-^{111}Cd mixture in conjunction with TIMS (a more recent study by *Schediwy et al.* 2006 also opted for this combination of spike isotopes using MC-ICPMS). Other reported combinations include ^{110}Cd-^{111}Cd on MC-ICPMS (*Ripperger and Rehkämper*, 2007; *Ripperger et al.*, 2007; *Gault-Ringold and Stirling*, 2012), ^{106}Cd-^{108}Cd on TIMS (*Schmitt et al.*, 2009b,a), ^{111}Cd-^{113}Cd on MC-ICPMS (*Horner et al.*, 2010; *Xue et al.*, 2011; Chapters 3 and 5), and ^{111}Cd-^{112}Cd on MC-ICPMS (*Horner et al.*, 2011; Chapter 4). The issues underlying these diverse choices of spike isotopes are discussed in the next section.

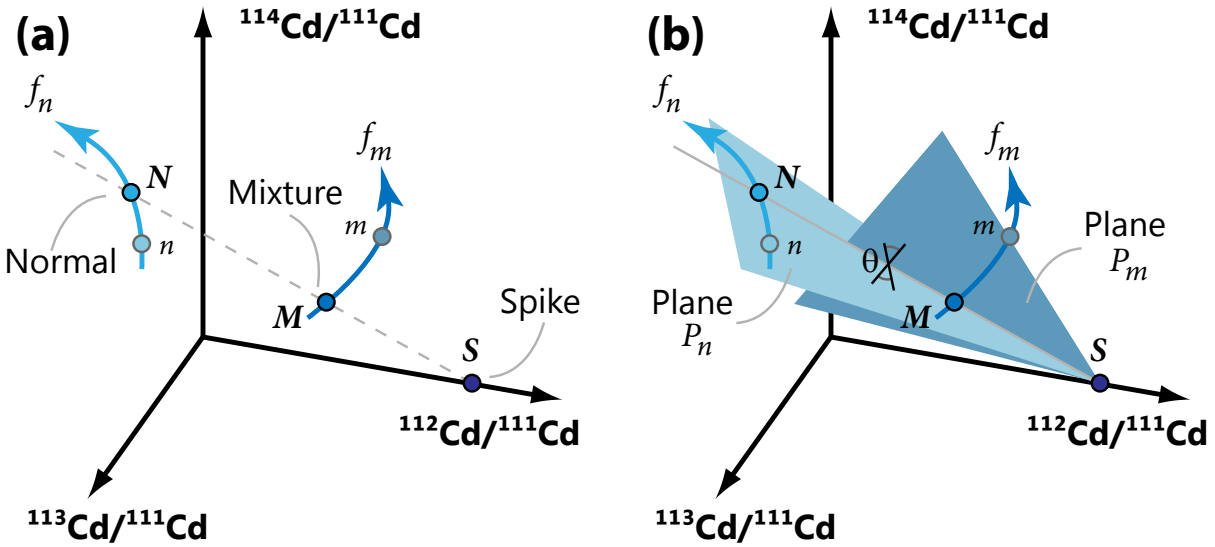

Figure 2.7: Three dimensional geometric interpretation of the double spike. This interpretation is similar to the one described for Pb isotopes in *Galer* (1999). (a) N refers to the true sample isotope composition and n to the standard composition. M is the composition of the true spike-sample mixture, m the value measured by mass spectrometry. (S is the spike, either ^{111}Cd-^{112}Cd or ^{111}Cd-^{113}Cd.) The vectors joining N to n (f_n) and M to m (f_m), pass through every allowable Cd isotope composition. The vectors are curved as mass-dependent isotopic fractionation is assumed to follow the exponential (f_n) and generalized power laws (f_m). As such, true Cd isotopic compositions (N and M) can be defined by scalar vector multiplication (from points n and m). (b) Panel (a) redrawn with two planes that contain S, N, n, and S, M, m (P_n and P_m, respectively). The intersection of the two planes defines the linear mixing line N-M-S at an angle of θ.

2.4.1 Double spike optimization considerations

The double spike calculation has a three-dimensional geometric interpretation (*Galer*, 1999; Fig. 2.7). In this interpretation, each axis corresponds to an isotope ratio pair; this requires that the element being measured possesses at least four stable isotopes. Before double spiking can be applied to measure isotope ratios, there are numerous optimization considerations. It is important to consider any isobaric interferences (e.g. Fig. 2.1), the ability to measure the isotopes of interest synchronously (e.g. Table. 2.3), the magnitude of the ion currents of the relevant beams, the availability and purity of the spike isotopes themselves, and any error propagation associated with the spike selection (parameterized as θ; see below).

Measurement optimization

For Cd, with its eight stable isotopes, there are 420 possible combinations of double spikes across the numerous isotope ratio pairs. In Fig. 2.7, each axis has ^{111}Cd as the denominator iso-

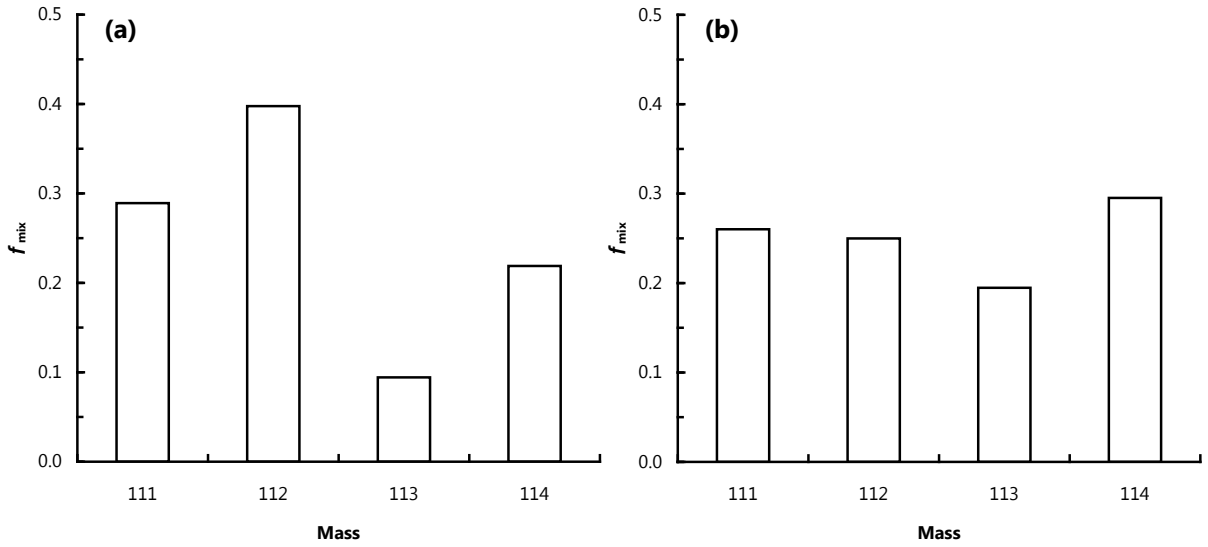

Figure 2.8: Contribution of each isotope to the mass spectra (relative scale). Idealized spectra are shown on a relative scale (f_{mix}) for optimal spike-sample mixtures (grey lines from Fig.2.9) for (a) the ^{111}Cd-^{112}Cd double spike and (b) the ^{111}Cd-^{113}Cd double spike.

tope, and ^{112}Cd, ^{113}Cd, and ^{114}Cd the numerator isotopes on the x-, y-, and z-axes, respectively. (For a given set of four isotopes, the choice of numerator and denominator isotope should have no effect the calculated Cd isotope ratios *Rudge et al.*, 2009.) These isotopes were chosen as together they constitute ≈ 78 % of the Cd mass spectrum and avoid isobaric overlap with Pd (but not Sn; Fig. 2.1). Although Pd was unlikely to be present in any significant quantity in the samples analyzed in this thesis (e.g. corals), it was detected in trace amounts for seawater samples and required an interference correction (e.g. *Ripperger and Rehkämper*, 2007). Given the focusing constraints of the MC-ICPMS (Table 2.3), it is not possible to monitor ^{105}Pd and ^{117}Sn – the only major isotopes of these elements that are free isobaric interferences themselves – in the same analysis step as the major isotopes of Cd (^{110}Cd to ^{114}Cd). This requires that a second analysis step be used, when measuring samples, to monitor ^{105}Pd. By using ^{111}Cd, ^{112}Cd, ^{113}Cd, and ^{114}Cd as the four isotopes in the double spike data reduction, it was possible to monitor Cd, In, and Sn in the same analysis step (Table 2.3). Choosing these four isotopes reduces the number of possible double spike combinations to six: ^{111}Cd−^{112}Cd, ^{111}Cd−^{113}Cd, ^{111}Cd−^{114}Cd, ^{112}Cd−^{113}Cd, ^{112}Cd−^{114}Cd, and ^{113}Cd−^{114}Cd.

It is also necessary to consider the size of the Cd ion currents during measurement optimiza-

tion. Since most of the samples analyzed here have Cd contents in the sub μg g^{-1} range, the main limitation on analytical precision is beam size. Use of a double spike increases the signal-to-noise ratio of analyses, as the measured mixtures contain both sample- and spike-derived analyte. This effect is enhanced if the double spike is applied on the minor isotope beams of Cd (i.e. ^{111}Cd and ^{113}Cd). During the course of this thesis, two different double spikes were used. In Chapter 4, a ^{111}Cd-^{112}Cd double spike was used. In subsequent chapters, a ^{111}Cd-^{113}Cd double spike was used, similar to the spike choice (and composition) of *Horner et al.* (2010) and *Xue et al.* (2011). The new ^{111}Cd-^{113}Cd spike was preferred to the existing ^{111}Cd-^{112}Cd spike, as it dramatically increased the beam size, and hence overall signal to noise ratio, for ^{113}Cd (Fig. 2.8). This change enabled more than a two-fold reduction in the amount of Cd required for the most precise isotopic analyses (25 reduced to 10 ng).

Spike optimization

The treatment of spikes thus far has considered pure (mono-isotopic), and therefore idealized, components. In reality, whilst spike isotopes are enriched in the target isotope, they also contain minor quantities (up to several %) of the adjacent mass isotopes. The spikes used in this study were obtained from JV Isoflex, Moscow (^{113}Cd, 93.35 %) and Oak Ridge National Laboratory, Tennessee (^{111}Cd, 96.44 %; ^{112}Cd, 98.23 %). Different suppliers were used for the various spikes so as to obtain the highest possible enrichment of the target isotope.

It is further necessary to optimize the isotopic composition of the double spike based on the actual purity of the spike isotopes. Full details of the compositional optimization algorithm are given in *Galer* (1999). In the subsequent discussion, the measure of spike efficacy is given as the intersection angle, θ, of the two planes P_n and P_m (these are the two planes containing the spike-sample-standard and spike-mixture-measured mixture compositions, respectively; Fig. 2.7b). The intersection angle is a useful, but crude metric in this regard, as it does not account for beam size (e.g. *Rudge et al.*, 2009). In the isotope ratio space shown in Fig. 2.7, the

mixing line between the spike (S), mixture (M), and sample (N) is a straight line, defined by the intersection of the two planes P_n and P_m. The intersection angle of the two planes is θ; this angle has a maximum at 90° (planes are perpendicular), to a minimum at 0° (planes are parallel and hence no mixing line can be defined). If no mixing line can be defined, it is not possible to determine the isotopic composition of a sample. Thus, 'good' spikes ensure that the angles of intersection $\sim 90°$ across a wide range of spike-sample ratios. Assuming constant instrumental mass fractionation and relatively minor natural mass fractionation, the intersection angle, θ, can be calculated for different spike compositions and spike/sample mixtures (Fig. 2.9).

Based on the optimization shown in Fig. 2.9, the optimal $^{112}Cd/^{111}Cd$ was ≈ 1.1 for the ^{111}Cd-^{112}Cd double spike, and $^{113}Cd/^{111}Cd$ was ≈ 0.7 for the ^{111}Cd-^{113}Cd double spike. These values were set as the compositional targets for the respective double spikes during preparation (Sec. 2.4.2). Based on these values, idealized spike-sample mass spectra have been calculated for each of the double spikes used in this thesis (Fig. 2.8). This figure highlights the problem that the magnitude of the ^{113}Cd beam is a major factor that limits analytical precision for the ^{111}Cd-^{112}Cd double spike. Further, if samples are 'overspiked' (i.e. $Q >> 0.7$; Fig. 2.9), the magnitude of the ^{112}Cd beam can become so large that samples require significant dilution before they can be analyzed, further suppressing the ^{113}Cd signal. This highlights the problem that for Cd, the errors associated with spike 'unmixing' for small values of θ are insignificant compared to the uncertainties associated with counting statistics (i.e. the magnitude of the ion beams; see above discussion).

2.4.2 Mixing and calibration of double spikes

The presence of minor quantities of the adjacent mass isotopes in the double spike requires precise quantification. The metal flakes (or oxide powder) of each enriched isotope were weighed and dissolved separately in $\sim$ 125 mL of 2 M HNO_3. Mixtures of the two spikes were then prepared such that the double spike would have the optimal $^{11x}Cd/^{111}Cd$ ratio (to within 1 %)

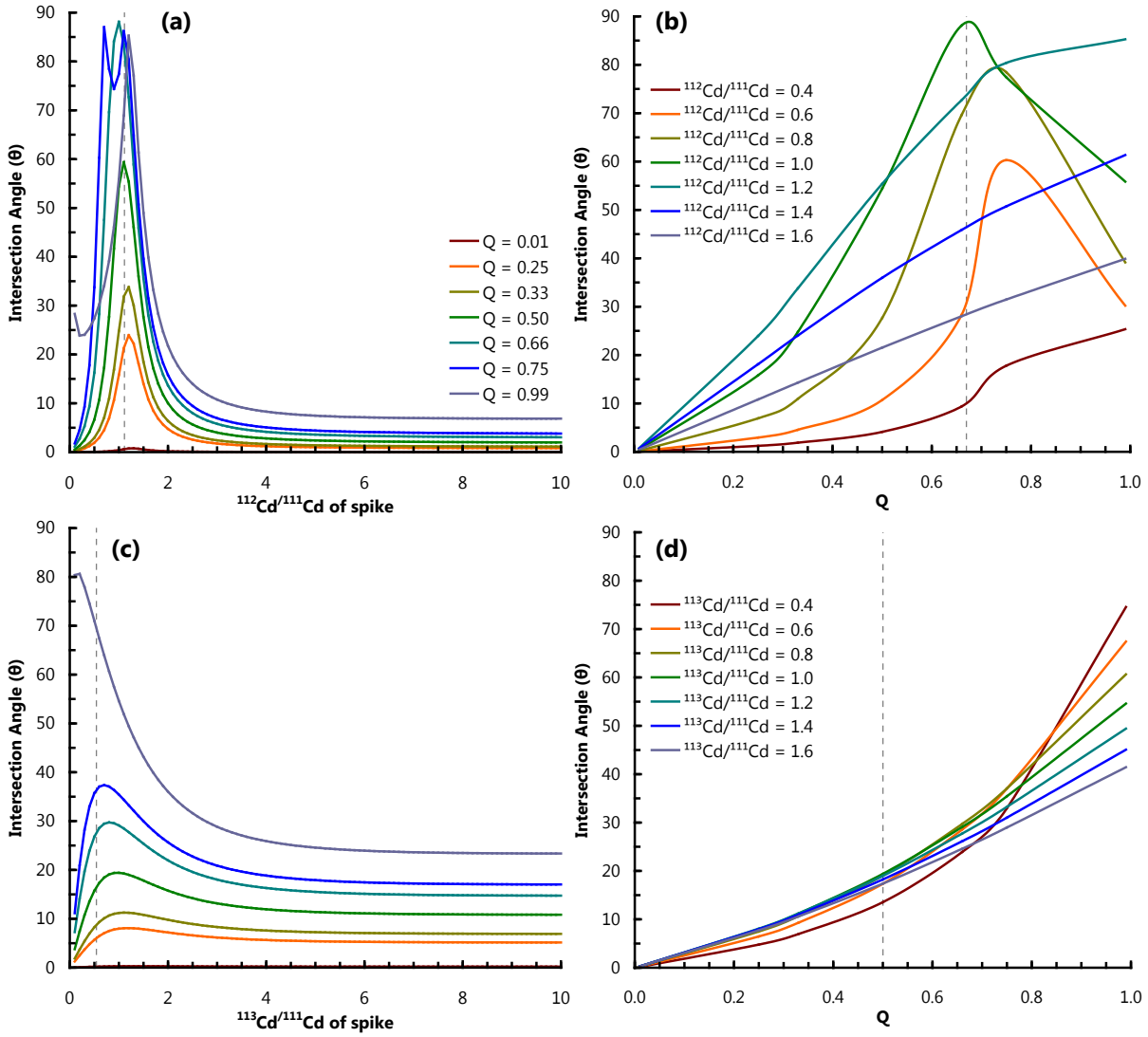

Figure 2.9: Optimization of a Cd double spike. (a) Intersection angle against $^{112}Cd/^{111}Cd$ of double spike for a range of spike-sample mixtures (Q). The dashed line corresponds to the optimal spike composition of $\approx$ 1.1. (b) Intersection angle against Q for the spikes shown in panel (a). The dashed line corresponds to the optimal spike/sample ratio of $\approx$ 0.67 (*Horner et al.*, 2011). (c) Intersection angle against $^{113}Cd/^{111}Cd$ of double spike for a range of spike-sample mixtures. The dashed line corresponds to the optimal spike composition of $\approx$ 0.5 (*Rudge et al.*, 2009). (d) Intersection angle against Q for the spikes shown in panel (c). The dashed line corresponds to the optimal spike/sample ratio of $\approx$ 1 (*Rudge et al.*, 2009).

before calibration by MC-ICPMS (Section 2.4.2). Spike calibration was performed by correcting for the instrumental mass bias with admixed Ag (Table 2.3). As discussed in Sec. 2.3.2, external normalization is commonly used for correcting instrumental mass bias, as the discrimination is almost entirely dependent on mass (*Rehkämper et al.*, 2001). However, rather than internally normalizing to an assumed Cd isotopic ratio in a standard, as has been reported previously (e.g. *Wombacher et al.*, 2004; *Ripperger and Rehkämper*, 2007), no Cd isotope ratios are assumed. Instead, a 'true' Ag isotopic ratio is assumed ($^{107}Ag/^{109}Ag = 1.076369$; *De Laeter et al.*, 2003), and instrumental mass bias is calculated by comparing the measured $^{107}Ag/^{109}Ag$ with the 'true' value. The decision to use a 'true' Ag isotope reference value (instead of Cd) was made based on the observation that there exists significant variation in Cd isotope compositions between various in-house ICPMS standards (e.g. *Abouchami et al.*, 2012). Since these variations appear to be much smaller for Ag isotope standards (e.g. *Woodland et al.*, 2005), by rearranging Eq. 2.3.4 and substituting in for Ag, instrumental mass bias can be calculated from Ag to correct Cd isotopic ratios:

$$f = \left(\frac{^{107}Ag/^{109}Ag_{true}}{^{107}Ag/^{109}Ag_{measured}} \right)^{\frac{1}{m^n_{^{107}Ag} - m^n_{^{109}Ag}}} \tag{2.4.1}$$

Data were collected dynamically by using a two step analysis template (Table 2.3). In the first step, the ion currents of Ag were measured for 5×10 s integrations before the Cd ion currents were measured in the second step for 10×10 s; this pattern was repeated four times for each sample to account for any variability in f within-run. This process was used to calculate a Cd isotopic composition for the 'normal' to be used in data reduction (Fig. 2.7; Sec. 2.4.3) as well as the double spike itself.

The ion currents of the minor isotopes in the spike are particularly small for mixtures of Ag and pure double spike. This problem leads to a large uncertainty for the isotopic composition of the minor isotopes in the double spike. This was overcome by mixing variable quantities of NIST SRM 3108 Cd (*Abouchami et al.*, 2012) with the spike and calculating the mixing line

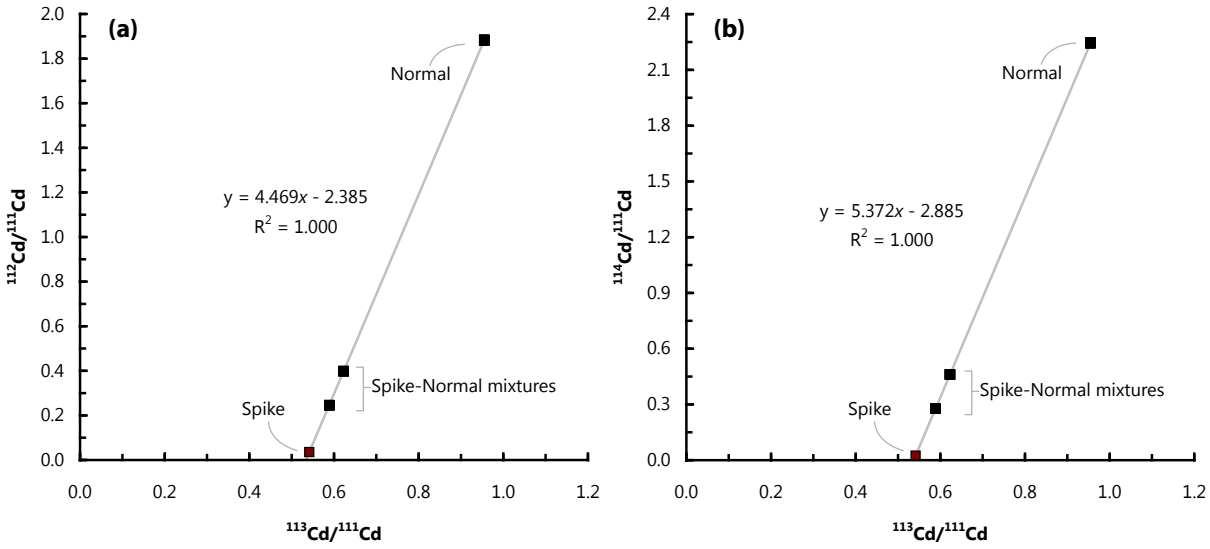

Figure 2.10: Spike calibration using spike-normal mixtures. Calibration of the ^{111}Cd-^{113}Cd double spike is shown as an example. In each panel, the black dots represent the data cloud associated for each mixture, and the red dot the calculated spike composition. (a) Calibration of the ^{112}Cd/^{111}Cd ratio. (b) Calibration of the ^{114}Cd/^{111}Cd ratio. The spike composition does not intersect the x-axis because of the presence of minor impurities in the spike.

between the spike and the normal (Fig. 2.10). For this purpose, measurements of the minor isotopes are omitted from the regression for mixtures of pure double spike and Ag (i.e. ^{113}Cd & ^{114}Cd, or ^{112}Cd & ^{114}Cd) but are included when measuring double spike-normal mixtures. The composition of the spike is determined by calculating the intersection of the mixing line with the isotopic composition of the major isotopes of the double spike (^{112}Cd/^{111}Cd or ^{113}Cd/^{111}Cd, depending on the spike used; Fig. 2.10; *Rudge et al.*, 2009).

Deviations from optimal spike:sample ratios can cause anomalous isotopic shifts, most likely because of improper calibration of the minor isotopes in the double spike (e.g. *Xue et al.*, 2011). In the event of significant deviations optimal spike:sample, additional standards were prepared for analysis alongside samples, and the $\epsilon^{114/110}$Cd of the samples would be calculated relative to the mean of the standards with similar spike:sample and Cd concentrations. This has previously shown to yield reliable results (*Ripperger and Rehkämper*, 2007).

The final step of spike calibration was the determination of the Cd concentration. For this purpose, a gravimetrically-prepared Cd solution was made from Puratronic-grade (99.9999 % pure) Cd metal pellets (Alfa Aesar, lot #11351). Prior to dissolution, pellets were leached in 2 % HNO_3 to remove oxide coatings and rinsed in ethanol. The pellets were taken out of

ethanol and immediately transferred to FEP (fluorinated ethylene propylene) for weighing and dissolution in 2 M HNO_3 (after exposure to air for more than a few seconds the pellets begin to visibly corrode). Mixtures of the spike and dissolved metal pellets were weighed and analyzed by MC-ICPMS using reverse isotopic dilution to determine Cd concentrations:

$$\frac{spk}{spl} = \frac{\left(\frac{111}{114} \times f^{114}\mathrm{Cd}_{spl}\right) - f^{111}\mathrm{Cd}_{spl}}{f^{111}\mathrm{Cd}_{spk} - \left(\frac{111}{114} \times f^{114}\mathrm{Cd}_{spk}\right)} \tag{2.4.2}$$

where $\frac{111}{114}$ refers to the instrumental mass bias-corrected isotope ratio in the spike-sample mixture and f^x refers to the proportion of isotope x in the pure end-member $_{spl}$ or $_{spk}$. Average values of $f^x\mathrm{Cd}_{spl}$ were used (i.e. a constant Cd isotope composition was assumed in nature; *De Laeter et al.*, 2003) because small natural variations make no significant difference to the calculation result.

2.4.3 Data reduction

The raw isotopic data collected for spike-sample mixtures require 'unmixing' to be meaningful. For radiogenic isotope systems, a spiked (m on Fig. 2.7) and an unspiked (n) measurement are required to calculate true sample isotopic compositions. When using a double spike to calculate stable isotopic compositions (first outlined for MC-ICPMS by *Siebert et al.*, 2001), only a single measurement is needed (m), as sample isotopic compositions are assumed to fall on a continuum (f_n) that is defined by the exponential law. In this case, the system is solved for N, by 'unmixing' along the line N-M-S (the mixing line between the spike, S, mixture, M, and sample N; the complete set of equations is given in *Siebert et al.*, 2001).

Isobaric corrections were applied to the Cd isotope data following standard protocols (e.g. *Halliday et al.*, 1995). During Cd isotopic analysis, the ion currents on masses 115 (^{115}In, ^{115}Sn) and 117 (^{117}Sn) are also monitored (Table 2.3). It is assumed that the value of instrumental mass bias calculated for Cd, f, is applicable to elements with similar masses (as for Ag during

spike calibration; Sec. 2.4.2; *Rehkämper et al.*, 2001). Fractionation-corrected Sn interference ratios ($^{117}Sn/^{112}Sn$, $^{117}Sn/^{114}Sn$, $^{117}Sn/^{115}Sn$; assuming solar abundances; *De Laeter et al.*, 2003) were subsequently used to modify the ^{112}Cd, ^{114}Cd, and ^{115}In signal intensities. Following Sn correction, ^{115}In was used to correct for ^{113}In on ^{113}Cd (again assuming solar abundances). The magnitude of the Sn interference was rarely observed to be larger than $\sim$ 100 ppm, and the In correction would only be employed when the In signal was $>$ 10 ppm of the ion current on mass 113.

Following data reduction, the calculated value of f was used to 'tweak' the mass fractionation for the isobaric corrections, and the whole process was iterated (in MATLAB) – along with all other calculation steps described in *Siebert et al.* (2001) – until $\epsilon^{114/110}Cd$ values converged. High-precision concentration data (from isotope dilution) are a by-product of this calculation. Data were subsequently converted from the calculated x, y, and z coordinates to Cd isotope compositions using the ϵ-notation of *Wombacher and Rehkämper* (2004) relative to the isotopic reference standard in question:

$$\epsilon^{114/110}\mathrm{Cd} = \left(\frac{^{114}\mathrm{Cd}/^{110}\mathrm{Cd}_{spl}}{^{114}\mathrm{Cd}/^{110}\mathrm{Cd}_{std}} - 1 \right) \times 10,000 \tag{2.4.3}$$

Whilst ^{110}Cd is not used in the data reduction, Cd isotope ratios are reported as deviations in parts per 10,000 in the $^{114}Cd/^{110}Cd$ ratio. Since natural Cd isotope fractionation is assumed to be mass dependent and follow the exponential law (equivalent to $n \rightarrow 0$ when calculated using the GPL), any of the isotope ratios calculated in the double spike data reduction (i.e. $^{11x}Cd/^{111}Cd$) can be converted to a $^{114}Cd/^{110}Cd$ ratio by multiplying through by a correctional factor, β:

$$\beta = \frac{(m_1^n - m_2^n)}{(m_1^n - m_3^n)} \tag{2.4.4}$$

where m_i is the mass of isotope i.

Based on these methodological steps, Cd stable isotope measurements cam be applied to environmental samples. These applications are discussed in the following chapters.

CHAPTER 3

Non-specific uptake and homeostasis drive the oceanic cadmium cycle

A modified version of this chapter is under consideration for publication as: Horner, Lee, Henderson, and Rickaby (subm.) Non-specific uptake and homeostasis drive the oceanic cadmium cycle.

"It is plausible that organisms inadvertently remove Cd from seawater in their quest for chemically similar essential micronutrients such as zinc and have evolved pathways for sequestering toxic or unnecessary elements into sites where they do not damage the organism."

–*Boyle* (1988)

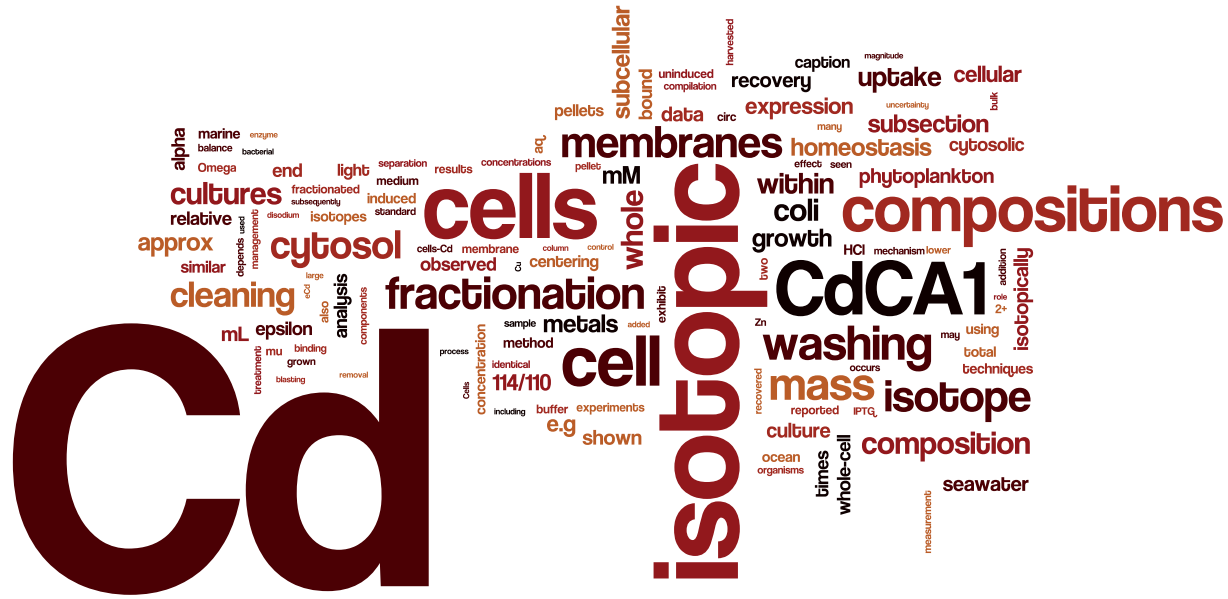

Abstract

The global marine distributions of Cd and phosphate are closely correlated, which has led to Cd being considered as a marine micronutrient, despite its toxicity to life. The explanation for this nutrient-like behaviour is unknown as there is only one identified biochemical function for Cd, an unusual Cd/Zn carbonic anhydrase. Recent developments in Cd isotope mass spectrometry have revealed that Cd uptake by phytoplankton causes isotopic fractionation in the open ocean and in culture. Here we investigate the physiochemical pathways that fractionate Cd isotopes by performing subcellular Cd isotope analysis on genetically modified microorganisms. We find that expression of the Cd/Zn carbonic anhydrase makes no difference to the Cd isotope composition of whole cells. Instead, a large proportion of the Cd is partitioned into cell membranes with a similar direction and magnitude of Cd isotopic fractionation as seen in surface seawater. This observation is well explained if Cd is mistakenly imported with other divalent metals and subsequently managed by binding within the cell to avoid toxicity. This process may apply to other divalent metals whereby the accidental uptake and subsequent homeostasis may contribute to elemental distributions in seawater, even for elements commonly considered as micronutrients.

3.1 Introduction

IN addition to the macronutrients nitrate, phosphate, and silicate, marine phytoplankton require many essential metals to function correctly (*Morel and Price*, 2003). The uptake and utilization of these 'micronutrients' results in large vertical isotopic and concentration gradients for many transition metals in seawater (*Bruland*, 1980). In the open ocean, Cd concentrations are as low as a few pmol kg^{-1} (*Boyle et al.*, 1976; *Bruland*, 1980), with associated highly fractionated Cd isotopic compositions of up to several permil (Fig. 3.1; *Ripperger et al.*, 2007). In culture, phytoplankton consume small quantities of Cd (*Ho et al.*, 2003; *Price and Morel*, 1990; *Xu et al.*, 2007), and exhibit light Cd isotope compositions (*Lacan et al.*, 2006). Taken together, the available data suggest that the marine geochemistry of Cd is dominated by nutrient-like processes (i.e. required uptake). However, only one biochemical function for Cd is known: CdCA1, a Cd/Zn carbonic anhydrase from the marine diatom *Thalassiosira weissflogii* (*Lane et al.*, 2005; *Xu et al.*, 2008). Whilst ubiquitous in natural waters (*Park et al.*, 2007), CdCA1 is absent in numerous phytoplankton including coccolithophores, cyanobacteria, archaea, and several species of diatom (e.g. *Park et al.*, 2007; Table 3.1) and it is thus debatable whether the expression of this single enzyme can account for the nutrient-like distribution of Cd in the global ocean. Here we examine the isotopic fractionation of Cd associated with CdCA1 that has been expressed, in vivo, by the model microorganism, *Escherichia coli*. Because *E. coli* has no inherent use for Cd, our experimental design permits comparison of cultures both overexpressing and not expressing CdCA1, in otherwise identical organisms. Using a systematic experimental approach, we are able to identify the general physiochemical pathways that fractionate Cd isotopes.

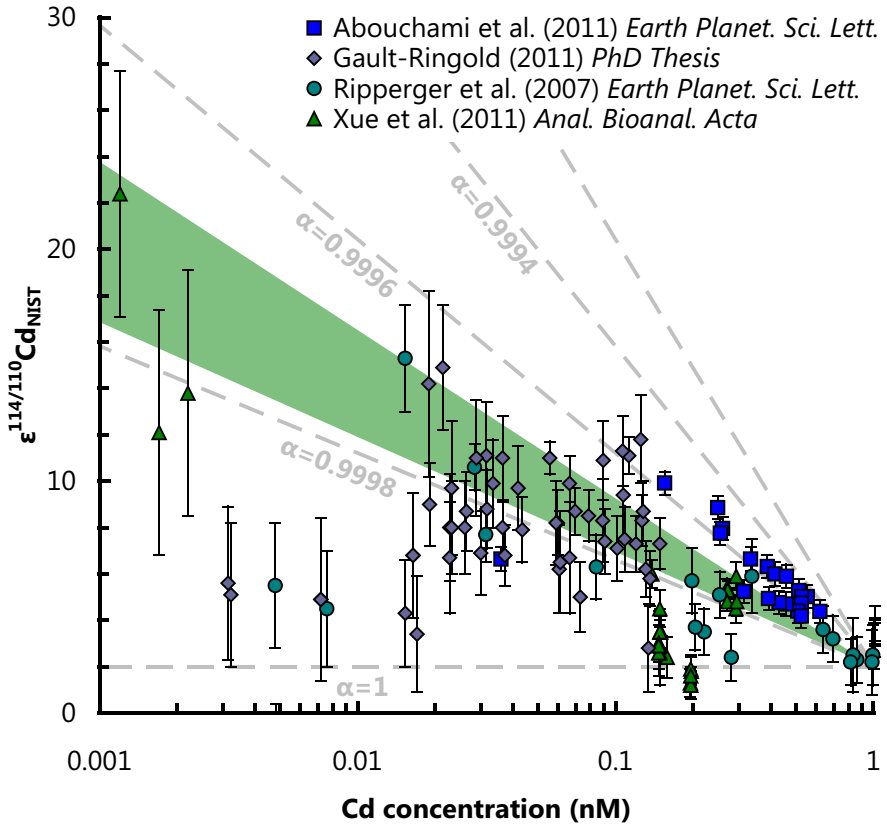

Figure 3.1: Cd isotope and concentration variations in modern seawater. Comparison of dissolved Cd isotope compositions and Cd concentrations for all published analyses of seawater. All data have been renormalized to NIST SRM 3108 (*Abouchami et al.*, 2012). Dashed tie lines are shown for uptake that follows closed-system Rayleigh fractionation (as various α values) assuming an isotopically light removal phase, where $\alpha_{\text{removal}-\text{Cd(aq.)}} = (^{114}\text{Cd}/^{114}\text{Cd})_{\text{removal}}/(^{114}\text{Cd}/^{114}\text{Cd})_{\text{Cd(aq.)}}$. The fractionation factor observed for membrane storage (homeostasis, $\alpha_{\text{homeo.}} = 0.99974 \pm 0.00005$, green shaded region), is consistent with the direction and magnitude of Cd isotope fractionation observed in modern seawater (*Ripperger et al.*, 2007; *Abouchami et al.*, 2011; *Xue et al.*, 2011; *Gault-Ringold et al.*, 2012). The large scatter in the data is largely a consequence of water mass mixing of isotopically distinct water masses.

Table 3.1: BLAST results for the CdCA1 gene (from *T. weissflogii*) in various microorganisms for which the complete genome is available.
*Expected values (number of hits that may occur by chance within a given genome) $> 10^{-3}$ are omitted for clarity unless there is > 10 % sequence overlap.
†Using NCBI (National Center for Biotechnology Information) annotation.

Lineage	*Genus species*	E-value*	Sequence Overlap	First hit†	Accession #
Chlorophyte	*Chlorella* sp. NC64A	-	-	-	-
	Chlamydomonas reinhardtii	-	-	-	-
	Coccomyxa sp. C-169	-	-	-	-
	Volvox carteri f. nagariensis	-	-	-	-
	Micromonas pusilla CCMP1545	$\sim 10^{-79}$	100 %	Predicted protein	XP_003063214
	Ostreococcus RCC809	-	-	-	-
	Ostreococcus tauri	-	-	-	-
	Ostreococcus lucimarinus	-	-	-	-
Heterokont	*Fragilariopsis cylindrus*	-	-	-	-
	Phaeodactylum tricornutum CCAP1055	-	-	-	-
	Thalassiosira pseudonana CCMP1335	$\sim 10^{-121}$	99 %	Predicted protein	XP_002295227
	Phaeodactylum tricornutum UTEX	Detected by nested PCR		Cadmium-specific CA	See *Park et al.* (2007)
	Thalassiosira weissflogii	$\equiv 0$	100 %	Cadmium-specific CA	AAX08632
Cyanobacteria	No matches				
Archaea	*Vulcanisaeta distributa* DSM14429	$\sim 10^{0}$	14 %	50S ribosomal protein L15	YP_003901354
	No other matches				
Bacteria	*Plesiocystis pacifica* SIR-1	$\sim 10^{-49}$	99 %	Hypothetical protein PPSIR1_39640	ZP_01905628
	Nitrosomonas sp. AL212	$\sim 10^{0}$	22 %	CA, cadmium-binding protein	YP_004295035
	Hoeflea phototrophica	$\sim 10^{0}$	82 %	Iron-regulated protein FrpC	ZP_02165618
	No other matches				

3.2 Methods

3.2.1 Experimental design

The role of CdCA1 expression in determining whole-cell isotopic compositions was investigated by introducing the CdCA1 coding sequence from *T. weissflogii* into the competent *E. coli* strain BL21(DE3). (Details of transformation are given below in Sec. 3.2.2.) Seven replicate experiments were performed that differed only in the final cell washing step (Sec. 3.2.6). In each experiment, the culture suspension was divided into two parallel cultures which were grown with and without the addition of IPTG (isopropyl-β-D-thiogalactopyranoside; a chemical inducer) to promote overexpression of CdCA1 (Fig. 3.2). By adding IPTG to only seven of the 14 cultures, we were able to independently study the role of CdCA1 expression in determining whole-cell Cd isotopic compositions without complications arising from differing physiologies. The 14 cultures were grown for up to four hours and harvested during the exponential growth stage.

3.2.2 Preparation of transgenic *Escherichia coli* and over-expression of CdCA1

The pET15b-CdCA1 construct was obtained from *Xu, Feng, Jeffrey, Shi, and Morel* (2008). Briefly, the CdCA1 coding sequence for this construct was amplified from *T. weissflogii* cDNA. The PCR product was subsequently cloned into a pET15b expression vector (Novagen). This construct was transformed into a competent *E. coli* strain BL21(DE3). Positive transformants were selected on LB plates with ampicillin (10 μg mL^{-1}). The recombinants were also screened by PCR using the T7 Promoter and T7 Terminator Primer. Positive clones were further sequenced with the same primer pair.

Cells were initially grown until the exponential stage of growth in Cd-free starter cultures at 37 °C to an optical density of 0.5 to 0.8 at 600 nm. Cd was subsequently added to a Cd^{2+} concentration of $\sim$ 60 μM (0.5 mM total, or analytical [Cd], added as $CdCl_2$), and the culture

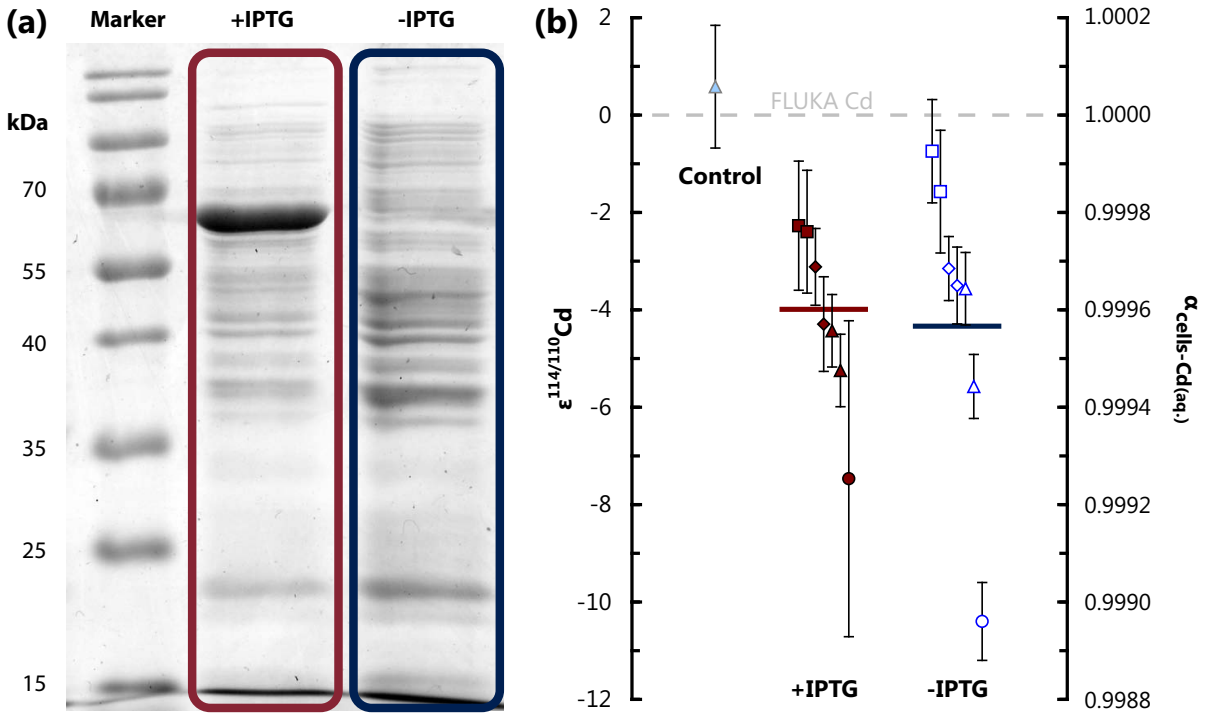

Figure 3.2: CdCA1 expression does not affect whole cell Cd isotopic compositions. (a) SDS-PAGE gel separation of proteins (stained with Coomassie brilliant blue R-250). CdCA1 (with histidine tag) expression is seen in the induced cultures (+IPTG) at 67.5 kDa (*Xu et al.*, 2008) but not in the uninduced (no IPTG). (b) Whole cell isotopic compositions for the control, induced, and uninduced cultures (with the means of the induced and uninduced cultures, weighted by 1/uncertainty, shown as the red and blue horizontal bars, respectively). Isotopic data are reported relative to the Cd in the growth solution and as fractionation factors: $\alpha_{\text{cells}-\text{Cd(aq.)}}$. The control refers to cells that were harvested after $\approx$ 10 s exposure to Cd^{2+}. The spread in Cd isotopic compositions relates primarily to the cell washing tests; when cells treated with the same treatment are compared (same symbols) +IPTG and -IPTG cultures are isotopically indistinguishable (see Sec. 3.3.1; Fig. 3.8).

split into two. At Cd^{2+} concentrations $<<$ 60 μM, the Zn form of CdCA1 is produced (*Xu et al.*, 2008). CdCA1 overexpression was induced in seven of the 14 cultures by addition of 1.0 mM isopropyl-β-D-thiogalactopyranoside (IPTG) so as to study the effect of CdCA1 expression on whole-cell isotopic compositions. Cells continued to grow in the exponential stage (determined by optical density) until they were harvested, typically after 4 h. Cells were harvested by centrifugation ($5,000 \times g$ for 15 min at 4 °C), rinsed with 18.2 MΩ H_2O and the pellets frozen at -80 °C until needed for further analysis.

3.2.3 CdCA1 purification and cleavage of histidine tag

Nickel columns were prepared by packing the His·Bind Resin, Ni-charged, into chromatography columns (Novagen Chromatography Columns, Novagen) according to the manufacturer's protocol. Frozen bacterial pellets were defrosted and resuspended in 20 mL extraction buffer (20 mM Tris-Cl, pH 8.0, 100 mM Na_2SO_4), with 1 protease inhibitor tablets (Complete Protease Inhibitor Cocktail Tablet, EDTA-free, Roche Diagnostics Ltd., Burgess Hill, West Sussex, UK) and sonicated at 4 to 6 A for 30 s bursts (on ice) with an interval of 1 minute between sonications. The lysate was centrifuged and the supernatant was filtered through a 0.45 μm filter. The resulting filtrate was loaded onto an equilibrated column at a flow rate of no faster than 1 to 2 mL per minute; the pellet, composed mostly of cell membranes (and some other cellular debris), was stored for [Cd] and isotopic analysis. Non-specifically bound proteins were removed and collected by washing with 40 ml wash buffer (20 mM Tris-Cl, pH 8.0, 100 mM Na_2SO_4) through the Ni columns. On-column cleavage of the target protein from the histidine tag was carried out by loading 20 mL elution buffer (20 mM Tris-Cl, pH 8.0, 100 mM Na_2SO_4, 20 mM imidazole) into the column. After the buffer had flowed through, the column was capped and cleavage was allowed to occur overnight in the presence of 2 ml elution buffer with thrombin. The target protein was eluted the following day by adding 5 mL elution buffer and collecting the first 4 mL of the flow-through. Purified proteins were further concentrated by passing the extract through an Ultracel-30 membrane (Amicon Ultra-4 Centrifugal Filter Unit; 30 kDa cut-

off; Millipore (UK) Ltd., Watford, UK). Both the purified protein and the residue (denatured CdCA1) were stored for analysis.

Proteins were separated on 12 % (V V^{-1}) SDS-PAGE (sodium dodecyl sulphate-polyacrylamide gel electrophoresis) using the Laemmli method (*Laemmli*, 1970; *Sambrook and Russell*, 2001), gels were subsequently stained with Coomassie brilliant blue R-250. Protein concentration of each sample was determined using the Bradford method (*Bradford*, 1976).

3.2.4 Decomposition of cells and purification of elemental cadmium

Whole cells and subcellular fractions were taken to dryness and weighed before acid digestion. Typically, 1 mL conc. aqua regia was added per 15 mg (dry mass) of cells up to a maximum of 10 mL and refluxed at 80 °C for 24 hours before evaporating to dryness at 120 °C and re-sampling in 2 % HNO_3 for analysis by ICPMS. This process was repeated until no meniscus (caused by latent organic compounds) was observed in the suspension. To check for congruent dissolution, four bacterial isolates were sub-sampled and digested using a microwave treatment similar to the one described by *Larner et al.* (2011) allowing direct comparison with the hotplate method. Cells were suspended in a mixture of 5 mL conc. HNO3 and 3 mL 30 % H_2O_2 and heated to 240 °C at 60 atm. for 90 minutes. The measured Cd isotopic compositions from the two methods, following ion exchange chromatography are within $< 0.3\ \epsilon^{114/110}$Cd of the alternative decomposition treatment (1:1 line $R^2 > 0.9$; Fig. 3.3), suggesting that the hotplate method was robust in ensuring congruent dissolution and liberation of Cd from cell organic matter.

Decomposed samples were spiked with a suitable amount of Cd double spike (^{111}Cd-^{113}Cd) and Cd was purified using a two-stage purification chemistry in 200 μL shrink-fit polytetrafluoroethylene columns (*Wombacher et al.*, 2003; *Ripperger and Rehkämper*, 2007). The total analytical blank was negligible in all cases at 8 ± 6 pg Cd (SD, $n = 7$), equivalent to < 0.1 % of the Cd present on any single isotopic measurement.

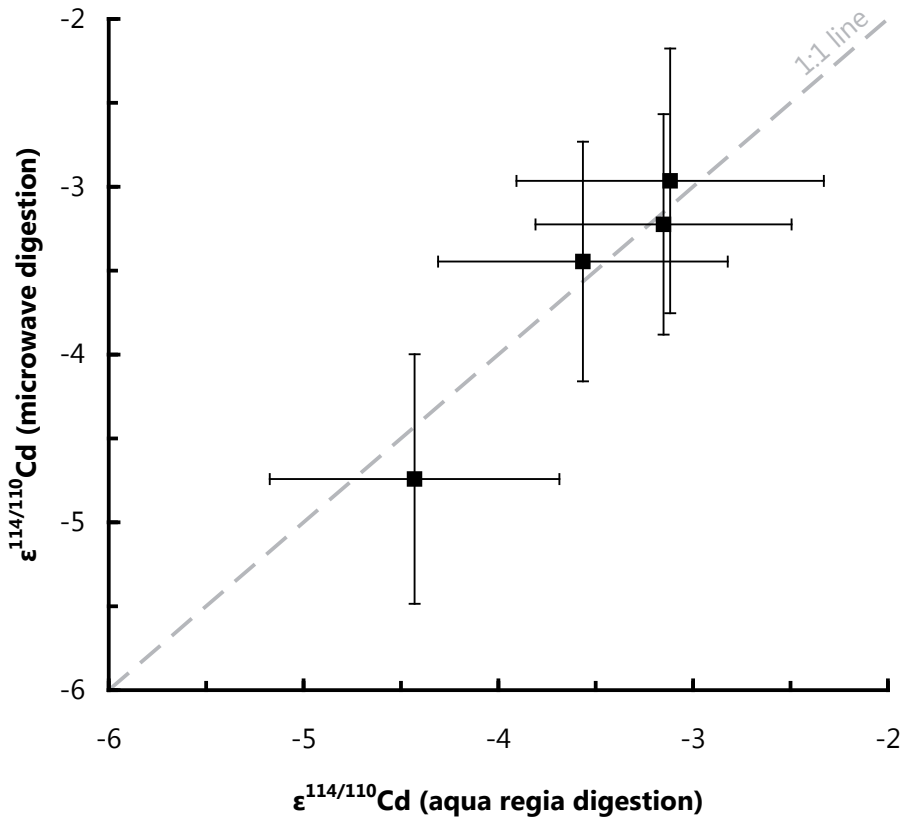

Figure 3.3: Cell isotope compositions do not depend on the digestion method. Comparison of Cd isotope compositions for cells digested using the microwave treatment compared with those digested in aqua regia. The similarity of isotopic compositions indicates that the aqua regia digestion was sufficiently aggressive to ensure congruent dissolution of cellular organic matter. Cd isotope notation shown in Eq. 3.2.1.

3.2.5 Isotopic analysis of cadmium

Isotopic methods have been reported in detail previously (*Horner et al.*, 2011). Briefly, samples were introduced into a Nu Instruments DSN-100 desolvation system (at 120 μL min^{-1}) with an Elemental Scientific PFA MicroFlow Nebulizer. The desolvated sample was introduced into a Nu Instruments Nu Plasma MC-ICPMS. All ion currents from 110 AMU (^{110}Cd, ^{110}Pd) – 117 AMU (^{117}Sn) were measured simultaneously in 40 $\times$ 10 s integrations, using a MATLAB-based script to iteratively deconvolve sample isotopic compositions from the spike-sample mixture and isobaric interferences (^{112}Sn on ^{112}Cd, ^{113}In on ^{113}Cd, ^{114}Sn on ^{114}Cd). Final isotopic compositions are reported relative to FLUKA Cd (Sigma-Aldrich $CdCl_2$, batch #20899), using the $\epsilon^{114/110}$Cd notation (*Wombacher and Rehkämper*, 2004):

$$\epsilon^{114/110}\mathrm{Cd} = \left(\frac{^{114/110}\mathrm{Cd}_{\mathrm{sample}}}{^{114/110}\mathrm{Cd}_{\mathrm{standard}}} - 1 \right) \times 10,000 \tag{3.2.1}$$

Since all Cd isotope compositions are reported relative to the Cd in the growth solution, the choice of reference standard was unimportant. Where possible, uncertainties are quoted as two times the standard deviation of sample replicates (when $n > 5$). When there was insufficient Cd to repeat the isotopic analyses > 5 times, measurement uncertainties were derived from standard replicates, with similar Cd concentrations and spike/sample ratios that were run in the same analysis session, as this is generally a good approximation of the measurement uncertainty (*Ripperger and Rehkämper*, 2007). The uncertainty reported is always the larger of the two. The Cd isotopic composition of FLUKA, relative to our in-house ICPMS standard 'OxCad' (*Horner et al.*, 2011) was determined as $\epsilon^{114/110}\mathrm{Cd} = +7.5 \pm 1.0$ (2 SD, $n = 13$).

3.2.6 Cell washing methodology

To determine the validity of the cellular Cd isotope compositions, a series of tests examining the effect of cell washing were carried out. The purpose of cell washing is to remove Cd from

cells that is not metabolically assimilated (e.g. passive adsorption to cell exterior; *Tang and Morel*, 2006). A series of cleaning agents were prepared and tested: 0.05 M trisodium citrate–0.075 M disodium EDTA, 0.85 % NaCl–5 mM disodium EDTA, 100 mM disodium oxalate–50 mM disodium EDTA, 0.1 M HCl, 0.1 M EDTA, 0.42 M NaCl, and 18.2 MΩ H_2O. To test the various cleaning agents, a Cd-free starter culture of *E. coli* was grown (as described above), then transferred to a 1 L container. Immediately ($\approx$ 10 sec) following the addition of Cd, 50 mL aliquots of the culture were transferred to centrifuge vials and the cultures harvested (as outlined above). The pellets were resuspended in a cleaning agent and the suspension was gently agitated for $\sim$ 1 min. Following this, the cells were centrifuged again, 18.2 MΩ H_2O added, centrifuged again, then the final pellet was dried for weighing.

3.3 Results

3.3.1 Cell washing results

The dry mass of recovered pellets for each cleaning agent is shown in Fig. 3.4 and Table 3.2. We find that all treatments lead to similar levels of recovery except for the citrate-EDTA treatment ($\sim$ 3.5$\times$ less than the others). However, when the Cd content of each pellet is normalized by recovery mass (Fig. 3.5, Table 3.2), we find that all treatments have essentially identical amounts of Cd present, except for the HCl treatment.

Collectively, the washing data suggest that the rapid uptake of Cd by the cells was not reversible adsorption, but instead reflects some sort of biologically-mediated binding of Cd to the cell surface (e.g. *Kenney and Fein*, 2011), as has been reported for Cu (*Navarrete et al.*, 2011). Unlike Cu however, this does not lead to Cd isotopic fractionation (Fig.3.2), in accord with the (limited) dataset of adsorbed Cd isotopic compositions (*Schmitt et al.*, 2009b; *Horner et al.*, 2010). Since cleaning with 18.2 MΩ H_2O yielded similar Cd contents as the various cleaning agents tested (Fig. 3.5) but did not demonstrably attack the cells (e.g. HCl or citrate-EDTA mixtures;

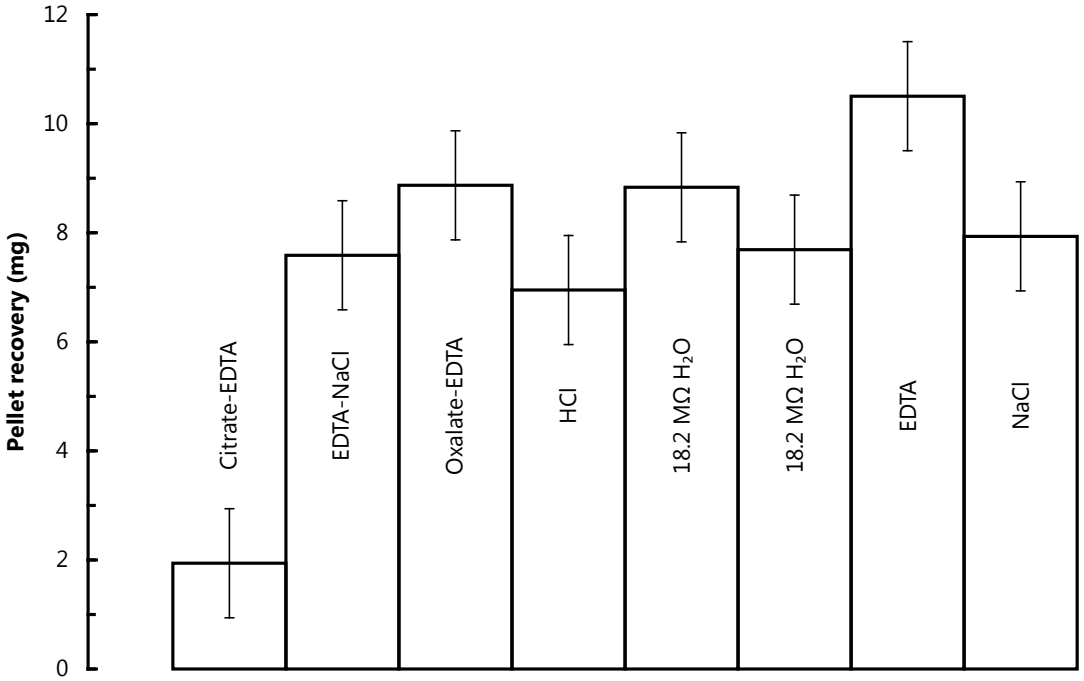

Figure 3.4: The mass of bacterial pellets recovered depends on the cleaning strategy used. Dry mass of pellets recovered for a range of different cell washing solutions. All techniques yielded similar recovery masses, except for the citrate-EDTA solution, which was significantly lower.

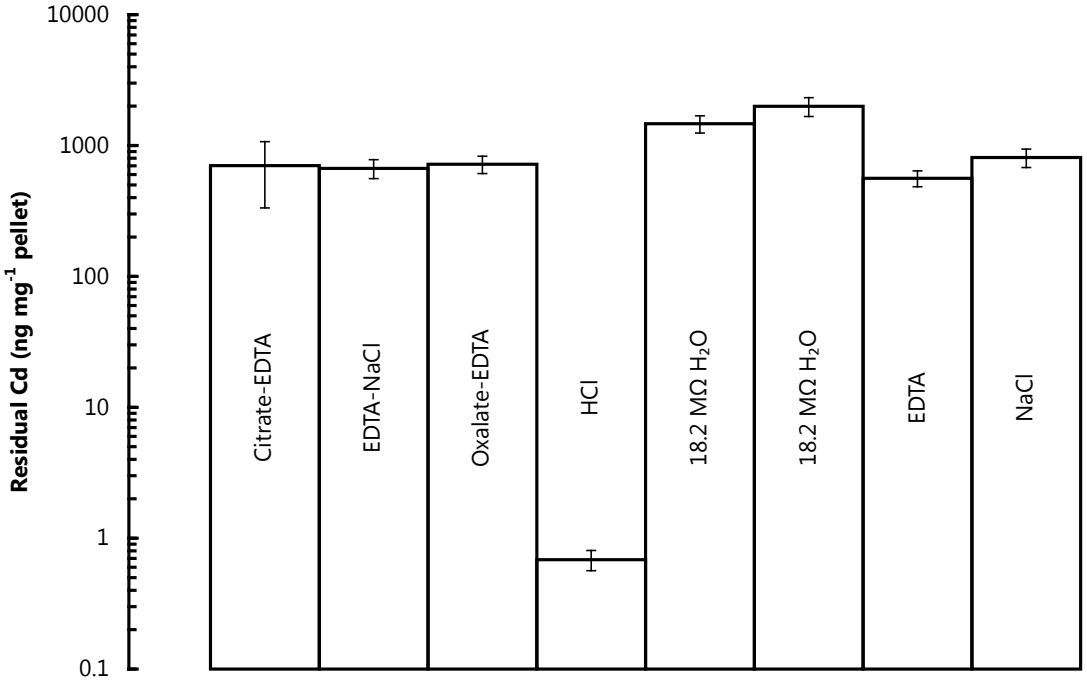

Figure 3.5: The Cd content of pellets strongly depends on the cleaning method used. Total Cd (ng) per mg (dry mass) of bacterial pellets for the same cleaning techniques outlined in Fig. 3.4. All cleaning techniques yielded similar Cd contents, except for the HCl rinse ($\sim$ 3 orders of magnitude lower Cd content than the other cleaning techniques).

Fig. 3.4) we consider the H_2O cleaning to be the most robust in assessing the true Cd isotopic composition of cells studied here.

3.3.2 Whole-cell isotopic results

The whole-cell Cd isotope compositions in the 14 cultures from this study are lighter than the growth medium in experiments both with and without the expression of CdCA1. The weighted means of the two sets of cultures are $\alpha_{\text{cells}-\text{Cd(aq.)}} = 0.99960$ and $\alpha_{\text{cells}-\text{Cd(aq.)}} = 0.99957$ for induced and uninduced cultures, respectively (Fig. 3.2, Table 3.3). The mean offset $\alpha_{\text{cells}-\text{Cd(aq.)}} \approx 0.9996$) is in accord with the existing, albeit limited (and lower precision) Cd isotope dataset for cultured freshwater phytoplankton $\alpha_{\text{cells}-\text{Cd(aq.)}} = 0.9986 \pm 0.0006$; *Lacan et al.*, 2006) and the growing literature for other biologically-active transition metals, whereby microorganisms exhibit a general preference for the light isotopes of a given element, e.g. Mo (*Wasylenki et al.*, 2007), Cu (*Navarrete et al.*, 2011), Zn (*John et al.*, 2007), Fe (*Beard et al.*, 1999), Ni (*Cameron et al.*, 2009). We rule out adsorption as the cause of the light isotopic fractionation observed for Cd in cultured cells, as a subset of cells plunged into the growth medium for a short time ($\approx$ 10 s) resulted in no fractionation of Cd isotopes (Fig. 3.2 'control'; Sec. 3.3.1).

3.3.3 Intracellular isotopic results

To probe the processes responsible for Cd isotopic fractionation, we dissected the *E. coli* cells into key subcellular components. The cells were first mechanically separated, by sonication and centrifugation, into cell membranes and the bulk cytosol. The cytosolic components were further separated by chromatography into the non-specifically bound Cd (termed Cd ligand, 'CdL'), Cd bound in CdCA1, and denatured CdCA1 (Fig. 3.6).

The subcellular separates exhibited a wide range of Cd isotope compositions (Table 3.4). The Cd bound in the cell membranes exhibited isotopic compositions negatively fractionated by

Table 3.2: Pellet recoveries and contaminant Cd for the cleaning agents tested (data plotted in Figs. 3.4, 3.5).
Weighing uncertainty ±1 mg.
†Measurement uncertainty ±0.1 ng mg^{-1} pellet.

Cleaning agent	Dry mass of pellet recovered (mg)*	Residual Cd (ng Cd per mg pellet)
0.05 M trisodium citrate–0.075 M disodium EDTA	2	702 ± 369
0.85 % NaCl–5 mM disodium EDTA	8	669 ± 111
100 mM disodium oxalate–50 mM disodium EDTA	9	720 ± 108
0.1 M HCl	7	$1 \pm 0^{\dagger}$
0.1 M EDTA	11	562 ± 78
0.42 M NaCl	8	809 ± 130
18.2 MΩ H_2O [i]	9	1467 ± 222
18.2 MΩ H_2O [ii]	8	1994 ± 327

Table 3.3: Isotopic data for whole cell washing experiments.
Uncertainties reported as 2× the standard deviation of sample replicates (when $n > 5$) or reproducibility of solution standards within the same analysis session, whichever is the larger of the two.
†Number of independent isotopic measurements.
‡Adsorption only experiment (cells were harvested after ≈ 10 s).

Experiment #	IPTG (+/−)	Washing	[Cd] (ng Cd per mg dry pellet)	$\epsilon^{114/110}$Cd	±2 SD*	$n^{\dagger}$
CdCA03	+	3× DI H_2O	> 2,000 (above calibration)	−2.3	1.3	5
	−		> 2,000 (above calibration)	−0.7	1.1	4
CdCA04	−‡	3× DI H_2O	1,842	+0.6	1.3	5
	−		2,366	−1.6	1.3	6
	+		2,957	−2.4	1.3	7
CdCA05	+	2× HCl	2	−7.5	3.2	1
	+		< 1	-	-	-
	−		< 1	-	-	-
	−		18	−10.4	0.9	1
CdCA06a	+	1× HCl	44	−4.3	1	5
	+		326	−3.1	0.8	5
	−		180	−3.2	0.7	5
	−		129	−3.5	0.8	5
CdCA06b	+	1× HCl + extra rinse	193	−4.4	0.7	5
	+		161	−5.2	0.7	5
	−		74	−5.6	0.7	5
	−		260	−3.6	0.7	5

Table 3.4: Isotopic data for intracellular separates.
*Percentage of total cellular Cd and †cytosolic Cd.
‡CdL refers to non-specifically bound Cd in the cytosol (i.e. eluted from the His·Bind column before tag cleavage).
§Other isolates (e.g. CdCA1) from the cells washed in HCl contained negligible Cd, that is, non-specifically bound Cd was essentially the only component present in acid-cleaned cells.

Experiment #	IPTG (+/−)	Washing	Cellular separate	$\epsilon^{114/110}$Cd	±2 SD	n	% cellular Cd*	% cytosolic Cd†
CdCA05	+	1× DI H_2O	CdCA1	−6.7	0.7	8	-	-
CdCA06a	+	1× DI H_2O	Membranes	−2.6	0.5	5	68 ± 13	-
			Cytosol	−0.3	0.7	5	32 ± 13	-
			CdL‡	−0.9	0.6	5	-	98.7 ± 0.2
			CdCA1	−5.9	0.7	5	-	1.1 ± 0.3
			Denatured CdCA1	+1.7	0.5	2	-	0.13 ± 0.03
CdCA06b	+	1 × 0.1 M HCl	Membranes	−4.9	0.6	5	89.2 ± 1.7	-
			Cytosol	+0.1	0.6	2	10.6 ± 1.9	-
			CdL‡	+2.3	1.7	3	-	≈ 100§

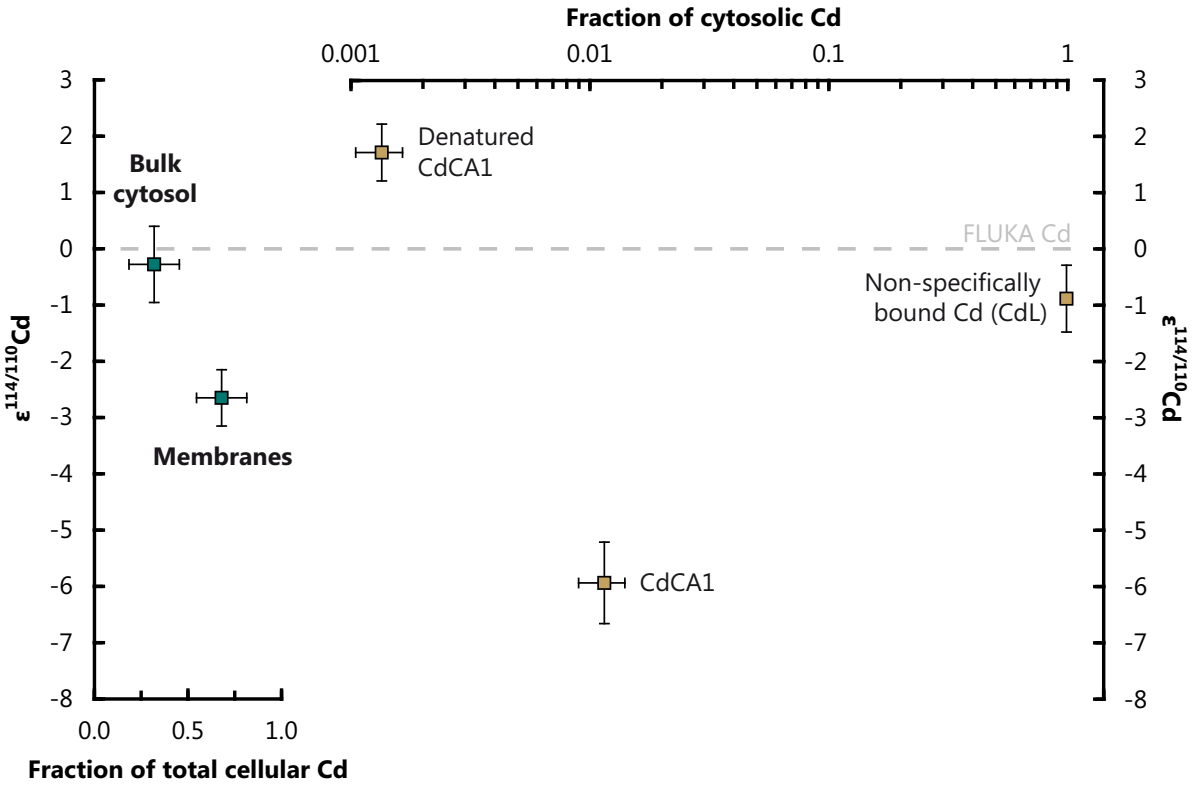

Figure 3.6: Subcellular mass balance for *E. coli* cells expressing CdCA1. The isotopic composition of the cytosol (pre separation) and cell membranes are shown in the left panel, demonstrating that the membranes dominate whole-cell isotopic compositions. The isotopic composition of the cytosolic components (post chromatographic separation) are shown in the right panel; note the log scale. Non-specifically bound Cd within the cytosol is isotopically identical to the bulk Cd isotopic composition of the cytosol and accounts for nearly all cytosolic Cd ($\approx$ 99 %). CdCA1 is isotopically light by around $-6\,\epsilon^{114/110}$Cd-units, equivalent to $\alpha_{\mathrm{CdCA1-cytosol}} = 0.9994 \pm 0.0001$, whereas denatured CdCA1 exhibits the only positively fractionated Cd within the cell.

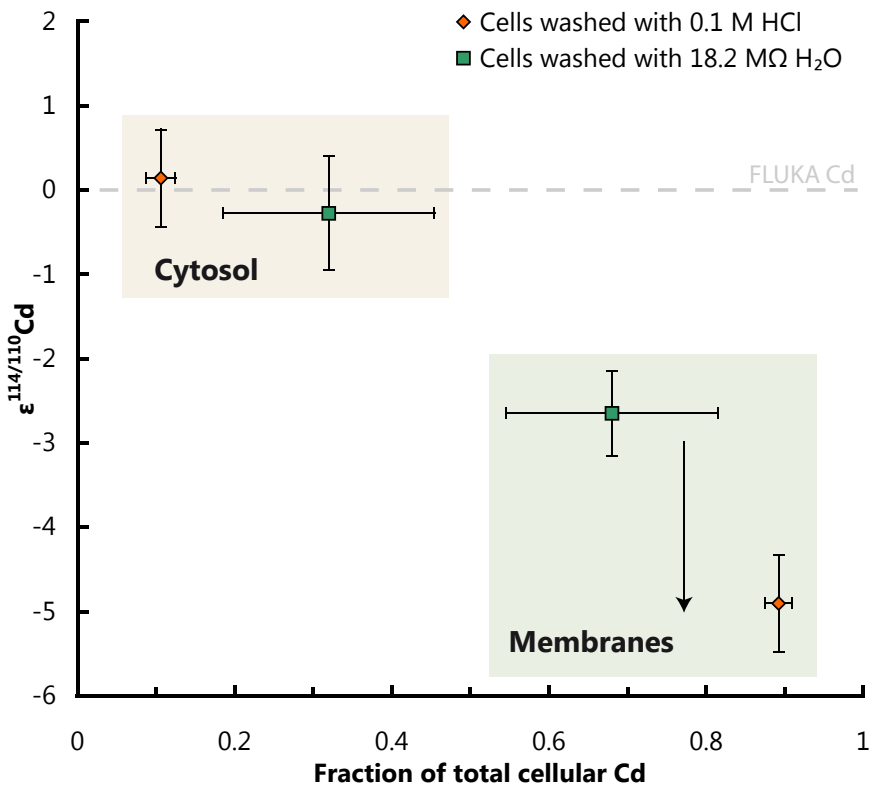

Figure 3.7: The isotopic composition of the cell membranes is sensitive to the cellular cleaning method. Cd isotopic composition vs. fraction of total cellular Cd for cells cleaned in 18.2 MΩ H_2O and 0.1 M HCl. The total Cd recovered from cells cleaned with HCl was ≈ 34 times lower than those cleaned with H_2O, despite all other experimental conditions remaining the same. Further, cleaning with HCl was found to shift the observed partitioning of Cd within cells from the cytosol to the membranes and change the isotopic composition of the membranes (denoted by the arrow), although but not the cytosol.

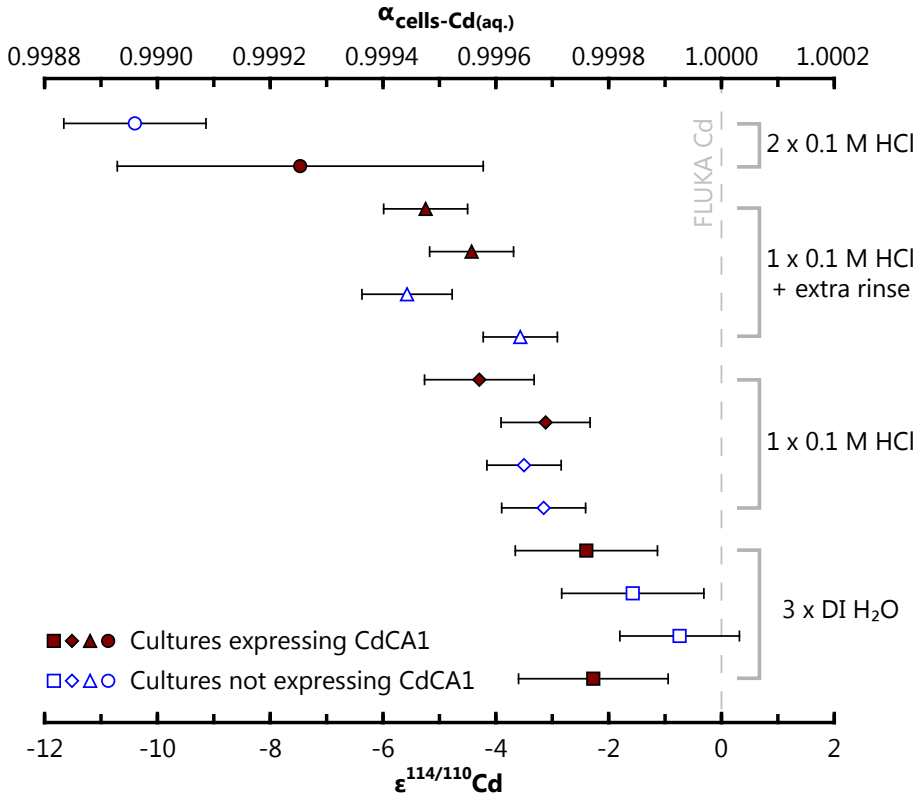

Figure 3.8: The isotopic composition of whole cells is sensitive to the cellular cleaning method. Range of cleaning techniques (relative scale) against whole cell isotopic compositions for induced and uninduced cultures (filled and open symbols, respectively). The relative ferocity of the cell washing leads to increasingly fractionated Cd isotopic compositions. Similar washing treatments are grouped by symbol. In each case, the induced and uninduced cells cleaned with the same agents exhibit isotopic compositions that are indistinguishable (within uncertainty).

$\epsilon^{114/110}Cd_{membranes} = -2.6 \pm 0.5$ compared to the growth medium ($\epsilon^{114/110}Cd_{membranes} \equiv 0$) and accounted for $\approx$ 68 % of the total cellular burden. Cytosolic Cd ($\epsilon^{114/110}Cd_{cytosol} = -0.3 \pm 0.7$) is isotopically indistinguishable from the growth medium and contained the residual $\approx$ 32 % of the cellular Cd (Fig. 3.6). The unfractionated Cd isotopic compositions of the cytosol implies that metal acquisition by *E. coli* either does not fractionate Cd isotopes or that Cd isotopic equilibration across the membrane occurs quickly.

Further separation of the cytosolic components reveals similarly large $\epsilon^{114/110}Cd$ variations within the cytosol (Figs. 3.6, 3.9; Table 3.4). The largest pool of Cd in the cytosol was the non-specifically bound Cd (CdL $\approx$ 99 % of cytosolic Cd), with an isotope composition of $\epsilon^{114/110}Cd_{CdL} = -0.9 \pm 0.6$ (i.e. within uncertainty of the bulk cytosol isotopic measurement). Insertion of Cd into CdCA1, which occurs *in vivo* within the cytosol, was observed to cause the largest isotopic fractionation within the cell ($\epsilon^{114/110}Cd_{CdCA1} = -5.9 \pm 0.7$ relative to the growth medium), but accounts for only $\approx$ 1 % of the cytosolic Cd. In a full replicate culture, and subsequent multistep insertion and extraction of Cd into CdCA1, we obtained a statistically identical value of $\epsilon^{114/110}Cd = -6.7 \pm 0.7$ (relative to the growth medium) for Cd bound in CdCA1. Denatured CdCA1 exhibited positive Cd isotope compositions ($\epsilon^{114/110}Cd_{denat.\ CdCA1} = +1.7 \pm 0.5$), but is insignificant in terms of the cytosolic mass balance, accounting for $\approx$ 0.1 % of cytosolic Cd. Whilst there is potential for Cd isotopic fractionation during protein extraction and purification chromatography, the subdivision of cells into membranes and bulk cytosol is a mechanical process, thus the observation that the membranes dominate the whole-cell isotopic compositions is robust. This separation reveals that isotopic fractionation of Cd only occurs once Cd is inside the cell, and is dominated by Cd translocation to the cell membranes (Fig. 3.9).

We also compared the Cd isotopic composition of subcellular isolates that were rinsed in HCl with those rinsed with 18.2 MΩ H_2O (Figs. 3.7). We found that the total amount of Cd recovered (for a comparable mass of cells) was $\approx$ 34$\times$ lower, despite all other experimental conditions remaining the same. The partitioning of Cd within the cell was also modified by HCl rinsing,

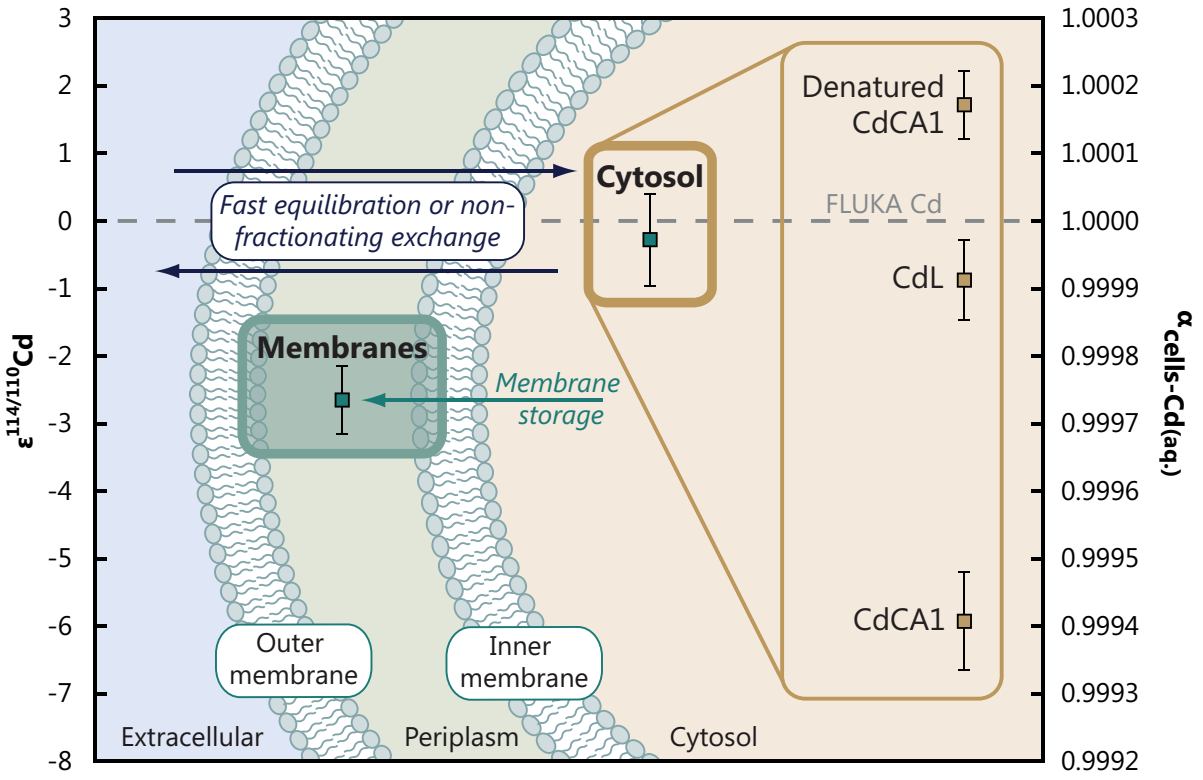

Figure 3.9: Proposed model for Cd isotopic fractionation in *E. coli*. Cd isotope compositions plotted on a schematic representation of the cell for each of the subcellular fractions, with interpretation. The measurements demonstrate that different components of E. coli cells exhibit multiple Cd isotope compositions. The bulk cytosolic measurement is isotopically indistinguishable from the growth solution, implying either rapid Cd isotopic equilibration across the membrane, or that the uptake of Cd into the cytosol does not fractionate Cd isotopes.

apparently causing a shift in the Cd load from cytosol to membranes (although the total amount of Cd present is lower). Further, the isotopic composition of the membranes was seen to shift to more negative Cd isotopic compositions; the cytosol remained unchanged. This likely explains why more intense washing techniques led to more fractionated isotopic compositions in whole cells (Figs. 3.2, 3.8). We were unable to isolate Cd from CdCA1 in HCl-rinsed cells, implying that the cleaning techniques were damaging the cells and causing Cd to leak from the cytosol and membranes.

3.4 Discussion

3.4.1 Intracellular mass balance for Cd

The macroscopic whole-cell experiments and subcellular mass balance both demonstrate that expression of the Cd enzyme, CdCA1, is not a significant contributor to the mass balance of Cd within the cell and hence whole-cell isotopic compositions (Fig. 3.6). Although Cd bound to CdCA1 has the most isotopically fractionated value observed, the small fraction of cellular Cd bound in this enzyme makes it insignificant to the overall cellular Cd isotope composition (in accord with observations from the macroscopic experiments; Fig. 3.2). Instead, the Cd sequestered into the cell membrane drives the whole-cell isotopic composition. Importantly, this observation also explains why cells not expressing CdCA1 exhibit identically light Cd isotope compositions as those cells expressing it (Fig. 3.2). The size and direction of the membrane-associated fractionation is in accord with Cd removal from seawater (Fig. 3.1).

3.4.2 Cellular Cd management

Transport of Cd^{2+} into the cytosol likely occurs because of close geochemical similarities to Zn^{2+} (and/or other divalent metals, e.g. Co^{2+}), which play an important role in many enzyme pathways (e.g. *Waldron and Robinson*, 2009; *Waldron et al.*, 2009). Zn limitation has been shown to increase Cd uptake in bacteria (*Laddaga and Silver*, 1985) and phytoplankton (*Cullen and Sherrell*, 2005), with Fe restriction also demonstrated to increase cellular Cd quotas in culture (*Lane et al.*, 2008). Previous research suggests that Cd is mistakenly imported by a wide range of microorganisms as they accumulate geochemically similar trace elements for physiological use (e.g. *Nies*, 1992), thereby removing Cd from seawater.

The toxicity of Cd requires that it be managed if it enters a cell. One role of the membranes in *E. coli*, and many other microorganisms, is to ensure that metal homeostasis is maintained by sensing, transporting, and storing metals for subsequent use (*Waldron and Robinson*, 2009).

E. coli cells have Cd management systems analogous to those of eukaryotic cells, including marine phytoplankton (*Prévéral et al.*, 2009). There is genetic evidence in both pro- and eukaryotes for gene products that manage or confer tolerance to heavy-metal stress, including to that from Cd (*Cobbett and Goldsbrough*, 2002; *Silver and Phung*, 2005). Once internalized, Cd can interfere with essential cellular machinery, particularly through displacement of metals from their correct binding site. The cellular concentrations of Cd, and other toxic metals, must therefore be tightly controlled to prevent damage to cells (*Waldron and Robinson*, 2009). The mechanism of Cd management – binding with cysteine-rich peptides such as phytochelatin or metallothionein (*Grill et al.*, 1987) – is a common, highly conserved feature of many organisms including bacteria, plants, fungi, and animals (*Prévéral et al.*, 2009). The fate of these Cd complexes depends on the organism in question, although they are commonly exported to a vacuole (*Mendoza-Cózatl et al.*, 2010; *Ortiz et al.*, 1995) or sometimes ejected from the cell (*Silver and Phung*, 2005; *Lee et al.*, 1996) where they cannot interfere with the critical cellular machinery in the cytosol. *E. coli*, which lack a vacuole, translocate Cd to their membranes (*Mitra et al.*, 1975) by binding Cd with glutathione, a precursor of (and functionally analogous to) phytochelatin (*Prévéral et al.*, 2009). Our isotope data suggest that this process of homeostasis can lead to the retention of isotopically light inert Cd complexes by organisms. This mechanism can account for the isotopic fractionation observed in experiments conducted both with and without expression of CdCA1 (Fig. 3.2).

3.4.3 Implications for the water column

The implication of these experiments is that biologically-mediated Cd isotope fractionation occurs from growth media as organisms inadvertently acquire Cd and sequester it into inert forms within the cell. Because all organisms share a common ability to manage Cd (*Prévéral et al.*, 2009, Sec. 3.4.2), but do not share CdCA1 (Table 3.1; *Park et al.*, 2007), we contend that metal homeostasis, rather than physiological function, drives the vertical isotopic (*Ripperger et al.*, 2007) and concentration gradients (*Boyle et al.*, 1976; *Bruland*, 1980) of Cd seen in the global

ocean. The fractionation observed with accidental uptake and homeostasis (i.e. membrane storage) in *E. coli* is consistent with the direction and magnitude of Cd isotopic fractionation for published seawater data (Fig. 3.1). It remains to be tested if there are different fractionation factors associated with various Cd-ligating peptides (e.g. phytochelatin vs. glutathione) and their ultimate fate within cells.

That homeostasis is the dominant mechanism in controlling Cd isotope partitioning in cells also reconciles the rare genetic occurrence for CdCA1 with existing Cd isotopic and concentration data for cultured phytoplankton (Table 3.1). Cultures of *Chlamydomonas reinhardtii* and *Chlorella* sp. have been shown to accumulate isotopically light Cd (*Lacan et al.*, 2006) even though analysis of their genomes reveals that no CdCA1-like sequences are present in either (Table 3.1). However, *C. reinhardtii* has been shown to possess a Cd-phytochelatin transporter that can internalize Cd in the cell vacuole (*Hanikenne et al.*, 2005). In addition, studies examining the trace-element content of phytoplankton in culture have shown that the Cd/P of *Emiliania huxleyi* is approximately five times higher than that of *T. weissflogii* when grown under identical conditions (*Ho et al.*, 2003), yet only the latter possesses a CdCA1 (*Park et al.*, 2007). Together, the limited culture and genetic data are consistent with the inadvertent uptake and homeostasis mechanism proposed here and offers an alternative explanation as to the cause of the Cd-P association seen in the global ocean (*Boyle et al.*, 1976; *Bruland*, 1980). In other words, all phytoplankton, regardless of their ability to utilize Cd, can contribute to the removal of Cd and fractionation of its isotopes in seawater (Fig. 3.1).

Inadvertent uptake and homeostasis may contribute to the distribution of other metals in the ocean. Even metals with well-understood enzymatic roles (e.g. Fe, Zn, Cu) may exhibit a homeostasis control in regions of higher concentration (e.g. upwelling zones of the ocean). Subcellular isotopic analysis, as performed for Cd in this study, may enable testing the relative importance of this mechanism for other metals.

3.5 Conclusions

- When performing cell culturing experiments, it is important to quantify any effects that cell harvesting or washing may have on the results. In the case of the experiments described here, more intense cell washing was shown to increase the apparent isotopic fractionation factor (i.e. more aggressively washed cells displayed isotopically lighter compositions).

- Using standard biochemical techniques, it is possible to pull cells apart and measure distinct intracellular isotopic compositions of different cellular components. In the case of Cd, this includes the catalytic metal atoms from the CdCA1 metalloenzyme that had been expressed, *in vivo*, in a heterologous system.

- The overexpression of CdCA1 metalloenzyme was not a significant contributor to the isotopic composition of whole bacterial cells, despite the enzyme being one of the dominant cellular functions (i.e. overexpression) and its extremely fractionated Cd isotope composition ($\epsilon^{114/110}\text{Cd}_{\text{CdCA1}} = -5.9 \pm 0.7$). The largest pool of internalized Cd in these cells was found to be non-specifically-bound Cd in the cytosol, with an 'unfractionated' Cd isotope composition similar to the growth medium ($\epsilon^{114/110}\text{Cd}_{\text{CdL}} = -0.9 \pm 0.6$).

- Cells both with and without overexpression of CdCA1 exhibited light Cd isotope compositions ($\alpha_{\text{cells}-\text{Cd}_{(\text{aq.})}} \approx 0.9996$). This fractionation was localized to the cell membranes, a process attributed to Cd homeostasis (i.e. avoiding toxicity) following the accidental import of Cd from the growth medium.

- This process of unavoidable uptake and subsequent homeostasis can explain the nutrient-like distribution of Cd in seawater, and may contribute to the elemental and isotopic distributions of other metals in seawater, even for those commonly considered as micronutrients.

Acknowledgements

We would like to thank Y. Xu for the CdCA1 construct for use in these experiments; P.F. Holdship for help with the ICPMS; and F.M.M. Morel for helpful discussions. T.J.H is supported by NERC (NE/G524060/1) and Nu Instruments. This work was funded by the Oxford-Princeton Research Partnership (R.E.M.R. and F.M.M. Morel), NERC, and the ERC (SP2-GA-2008-200915).

CHAPTER 4

Isotopic fractionation of cadmium into calcite

An reformatted version of this chapter was published as: *Horner, Rickaby, and Henderson* (2011) Isotopic fractionation of cadmium into calcite, *Earth Planet. Sci. Lett.*, *312*(1-2), 243–253, doi:10.1016/j.epsl.2011.10.004. It is reproduced here in thesis format.

"The Reason of making Experiments is, for the Discovery of the Method of Nature, in its Progress and Operations. Whosoever, therefore doth rightly make Experiments, doth design to enquire into some of these Operations."

–Robert Hooke

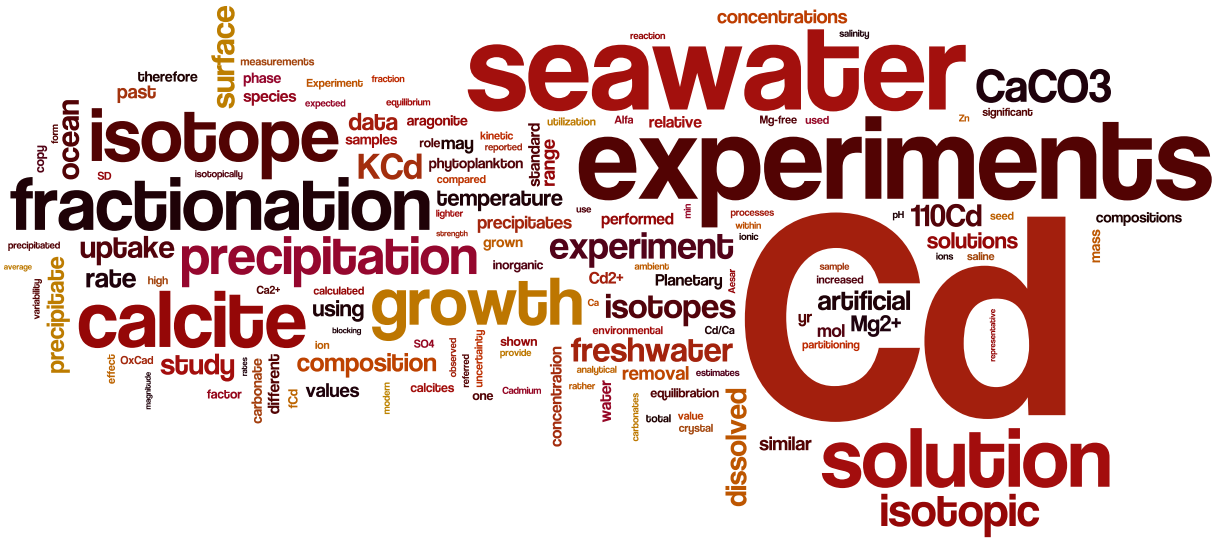

Abstract

Cadmium mimics the distribution of the macronutrient phosphate in the oceans, and has uses as a palaeoproxy of past ocean circulation and nutrient utilization. Isotopic analyses of dissolved Cd in modern seawater show potential as a new tool for disentangling phytoplankton utilization of Cd from abiotic processes, such as ocean mixing. Extending this information into the past requires the Cd isotope signal to be captured and faithfully preserved in a suitable sedimentary archive. However, the role that environmental factors, such as temperature, may play in controlling Cd isotope fractionation into such archives has not been assessed. To this end, we have performed controlled inorganic $CaCO_3$ precipitation experiments in artificial seawater solutions. We precipitated calcite under different precipitation rates, temperatures, salinities, and ambient [Mg^{2+}], before measuring Cd isotopic compositions by double spike MC-ICPMS. We find that the isotopic fractionation factor for Cd into calcite ($\alpha_{CaCO_3-Cd_{(aq)}}$) in seawater is always less than one (i.e. light isotopes of Cd are preferred in calcite). The fractionation factor has a value of 0.99955 ± 0.00012 and shows no response to temperature, [Mg^{2+}], or precipitation rate across the range studied. The constancy of this fractionation in seawater suggests that marine calcites may provide a record of the local seawater composition, without the need to correct for effects due to environmental variables. We also performed $CaCO_3$ growth in freshwater and, in contrast to calcite precipitated from artificial seawater solutions, no isotopic offset was recorded between the growth solution and calcite ($\alpha_{CaCO_3-Cd_{(aq)}} = 1.0000 \pm 0.0001$). Cadmium isotope fractionation during calcite growth can be explained by a kinetic isotope effect during the largely unidirectional incorporation of Cd at the mineral surface. The rate of Cd uptake

and isotopic fractionation are thus modulated by increased ion blocking of crystal surface sites at high salinity. The fractionation of Cd isotopes observed during precipitation of calcite has the same direction and similar magnitude to that implicated for Cd removal from the surface ocean by seawater measurements. However, flux calculations show that $CaCO_3$ precipitation is unlikely to play a significant role in setting the Cd isotope composition in seawater, compared to Cd utilization in phytoplankton soft tissue. Marine carbonates therefore record seawater Cd isotope chemistry – with potential as a palaeoceanographic proxy – rather than drive oceanic Cd isotope compositions.

4.1 Introduction

CADMIUM is an important micronutrient in the oceans and has been widely used as a proxy to reconstruct past ocean circulation and nutrient utilization. It exhibits a clear nutrient-like distribution in the modern ocean (*Boyle et al.*, 1976), which is generally ascribed to its role as an enzyme cofactor (although only one such cofactor role has so far been identified - carbonic anhydrase, e.g. *Price and Morel*, 1990; *Lane et al.*, 2005; *Xu et al.*, 2008). The nutrient-like behaviour of Cd, and particularly the close association with P (as PO_4^{3-}) in seawater, underpins its use as a palaeoproxy. Seawater phosphate concentrations are not generally recorded in sedimentary archives (*Henderson*, 2002), but Cd substitutes readily for Ca in $CaCO_3$ (*Lorens*, 1981; *Tesoriero and Pankow*, 1996) and is well-preserved in natural marine carbonates (*Boyle*, 1981). Cadmium has therefore seen widespread use to reconstruct the distribution of water masses in the past deep ocean (e.g. *Boyle and Keigwin*, 1987; *Boyle*, 1988) and to assess the extent of nutrient utilization in the surface ocean (e.g. *Rickaby and Elderfield*, 1999; *Elderfield and Rickaby*, 2000).

Recent isotopic analyses of dissolved Cd have shown that there are systematic variations, not only in the Cd concentration, but also in the Cd isotope composition of modern seawater (*Lacan et al.*, 2006; *Ripperger and Rehkämper*, 2007; *Ripperger et al.*, 2007; *Abouchami et al.*, 2011). These studies have demonstrated that Cd isotopes display behavior similar to those of Si (*de la Rocha et al.*, 1997; *Reynolds et al.*, 2006) or N (*Sigman et al.*, 1999) isotopes. As in these systems, Cd-depleted surface waters exhibit isotopically 'heavy' compositions, whereas deep waters have increasing Cd contents and isotopically 'lighter' signatures. This appears to reflect biological processes in the photic zone preferentially removing the lighter isotopes of Cd during metal uptake and regeneration of this signal at depth. This process has also been investigated for cultured phytoplankton, demonstrating that cultures were enriched in isotopically 'light' Cd due to biological uptake from the growth solution (*Lacan et al.*, 2006).

The isotopic data for seawater reveal additional information about processes controlling water-

column Cd distributions. Whilst some of the isotope data can be modelled by a closed-system Rayleigh fractionation of Cd isotopes during removal from surface seawater, some data fall away from this trend (*Ripperger et al.*, 2007; *Abouchami et al.*, 2011). These deviations from Rayleigh fractionation provide evidence of other processes, such as water-mass mixing, which cannot be resolved by measurement of [Cd] alone. Such data indicates that Cd isotopes have the potential to provide information that is complementary to [Cd] data, and may allow multiple oceanic processes to be deconvolved.

To extend the use of Cd isotopes into the past requires a suitable sedimentary archive with sufficiently high temporal and spatial resolution. It has been shown that the incorporation of Cd into foraminiferal tests occurs in proportion to the Cd concentration of the ambient seawater in which the test forms (*Boyle*, 1981; *Ripperger et al.*, 2008). Records of Cd/Ca are therefore assumed to reflect palaeo-Cd concentrations in seawater, once relevant corrections have been made for water-column depth (in benthic species, e.g. *Boyle*, 1988) or temperature (for planktonic species, e.g. *Rickaby and Elderfield*, 1999); temperature does not appear to significantly influence partitioning behaviour in bottom-dwellers (*Marchitto*, 2004). Foraminifera and other marine carbonates are also likely to be good substrates to record past Cd isotope compositions, but before they can be used as such, we must assess whether environmental variables, such as temperature, control the fractionation of Cd isotopes during uptake into calcite. The only study that reports Cd isotope compositions for calcium carbonate (*Wombacher et al.*, 2003) tentatively concludes that a synthetic aragonite exhibited isotopically light Cd relative to the growth solution, but there are no measurements of the fractionation into calcite, nor the variability of this fractionation. In this study, we have performed $CaCO_3$ precipitation experiments in artificial seawater solutions to understand the inorganic partitioning of Cd isotopes during growth of calcite. We investigated environmental controls which have been shown to exert specific controls on elemental and isotopic partitioning into calcite: precipitation rate, temperature, salinity, and ambient $[Mg^{2+}]$ to assess the variability in Cd isotopic partitioning.

4.2 Materials and Methods

4.2.1 Experimental design

The simplest way to determine Cd isotope fractionation would be to measure the difference in Cd isotope compositions between a precipitated calcite phase and a large dissolved Cd pool. In this case:

$$\alpha_{CaCO_3-Cd_{(aq)}} = \frac{R_{CaCO_3}}{R_{Cd_{(aq)}}} \tag{4.2.1}$$

where α_{CaCO_3-Cd} is the fractionation factor for Cd and R is the $^{114}Cd/^{110}Cd$ isotopic ratio of the relevant phase (denoted by subscript). This approach would be unlikely to yield a satisfactory value of $\alpha_{CaCO_3-Cd_{(aq)}}$ however, as the magnitude of the isotopic offset is only slightly larger than the analytical uncertainty. An alternative approach, given the high distribution coefficient for Cd into $CaCO_3$ (K_D^{Cd}), is to allow the dissolved Cd pool to decrease significantly during growth so that the partitioning of Cd isotopes into $CaCO_3$ follows a Rayleigh fractionation trend. Our experiments follow this approach because it leads to significantly larger final isotope deviations in the dissolved phase, thereby reducing uncertainty in estimates of $\alpha_{CaCO_3-Cd_{(aq)}}$.

4.2.2 Synthetic carbonate manufacture

Calcite was grown under carefully-controlled laboratory conditions in 12 separate experiments. Ten of these were conducted in solutions with similar ionic strength to seawater but with variable Mg^{2+} and SO_4^{2-}, at temperatures of 5, 20, & 30 °C; two of these experiments were carried out at $\sim 2\times$ and $4\times$ the rates of the other experiments. Two further experiments were carried out in de-ionized water (referred to as 'freshwater' experiments) at 20 °C.

Synthetic carbonates were precipitated in acid-cleaned borosilicate beakers which contained 500 mL of artificial seawater solution, kept at a constant temperature ($\pm$0.5 °C) in a 26 L

Table 4.1: Composition of artificial seawater solution used in this study (after *Kester et al.*, 1967).
[a] Mg^{2+} and SO_4^{2-} values shown are for the normal artificial seawater experiments, and are close to zero in the Mg-free experiments.
[b] HCO_3^- was not added because the artificial seawater solution was bubbled with air for approximately 18 hours prior to the start of any precipitation experiments, thus allowing the solution to reach chemical equilibrium.
[c] Cd^{2+} concentrations were set to $\approx 10^3\times$ Pacific Deep Water concentrations to ease analysis.

Ion	Artificial seawater content (g/kg)	Inventory form
Mg^{2+}	1.297 [a]	$MgCl_2 \cdot 6H_2O$
Ca^{2+}	0.413	$CaCl_2 \cdot 2H_2O$
Br^-	0.142	KBr
BO_3^{3-}	0.026	H_3BO_3
Sr^{2+}	0.008	$SrCl_2$
HCO_3^-	0 [b]	$NaHCO_3$
SO_4^{2-}	2.712 [a]	Na_2SO_4
F^-	0.001	NaF
K^+	0.387	KCl
Cl^-	19.353	NaCl
Na^+	11.634	NaCl
Li^+	1.75×10^{-4}	L-SVEC standard solution
U^{4+}	3.09×10^{-5}	Alfa Aesar standard solution
Ba^{2+}	1.35×10^{-4}	Alfa Aesar standard solution
Zn^{2+}	3.9×10^{-7}	Alfa Aesar standard solution
Cd^{2+}	1.35×10^{-4} [c]	Alfa Aesar standard solution - 'OxCad'

HAAKE DL30-V26/B open bath circulator. The seawater solutions (Table 4.1) were prepared using a similar method to *Kester et al.* (1967), with AnalaR salts for the major ions, and high-purity ICPMS (inductively coupled plasma mass spectrometry) standards for minor ions. (Standard solutions initially in NO_3^- form were converted to Cl^- form prior to use.)

Seawater solutions were bubbled with air at a flow rate of ~ 6.5 L min^{-1}, stirred with a borosilicate impeller (to prevent grinding of the calcite at the base of the beaker), and left to equilibrate with 0.10 g of seed calcite (Alfa Aesar Puratronic-grade, lot number B06R005) for at least 18 hours prior to starting $CaCO_3$ precipitation. During equilibration, the pH of the solution increased from $\sim$ 6 to between 7.5 and 8.0, reflecting slight dissolution of calcite as the system equilibrated. Calcium carbonate was precipitated using the dual syringe pump method (*Tesoriero and Pankow*, 1996), which has been used in previous studies (e.g. *Marriott et al.*, 2004a,b; *Bots et al.*, 2011) when studying elemental and isotopic partitioning of elements into calcite. Solutions of Na_2CO_3 and $CaCl_2$ were slowly pumped into a beaker containing the artificial seawater solution using a Linton Instruments KDS200 dual syringe pump, causing

$CaCO_3$ precipitation to proceed according to the reaction:

$$Na_2CO_3 + CaCl_2 \rightarrow CaCO_3 + 2NaCl \tag{4.2.2}$$

The concentrations of the Na_2CO_3 and $CaCl_2$ solutions were set so as to maintain a constant salinity of the growth solution. The rate of precipitation was controlled by pump speed which was assumed to control (linearly) surface-area-normalized crystal growth rate (given that the mass of seed calcite was identical in each experiment). Experiments were performed twice at each temperature; once in a solution nearly free of Mg^{2+} and SO_4^{2-}, and once with Mg^{2+} and SO_4^{2-} equal to modern seawater concentrations, with total ionic strengths of $\sim$ 0.6 M and $\sim$ 0.7 M, respectively (Table 4.1). Each water chemistry was expected to lead to a different $CaCO_3$ mineralogy (calcite or aragonite, respectively) but, as detailed below (Sec. 4.3.1), only calcite was precipitated in all cases.

In all experiments, the growth solution was rapidly depleted in Cd once $CaCO_3$ precipitation started, owing to the high equilibrium value of K_D^{Cd} (4170; *Prieto et al.*, 2003). Typically $50-90$ % of the Cd was utilized within $2.5-3$ hours, at which point experiments were stopped to measure the Cd isotope composition of the Cd remaining in solution. Sub-samples of the solution were also taken during the experiments. The pH of the growth solution during precipitation increased to $\sim$ 8.4 over the first 45 minutes of each experiment and then remained relatively constant, so that $\sim$ 70 % of the calcite in each experiment grew in stable conditions of pH $\sim$ 8.4 (Fig. 4.1a). A linear decrease in Cd/Ca with Cd concentration during the saline experiments (Fig. 4.1b) demonstrates that calcite growth was continuous and closely balanced by Ca^{2+} input.

Experiments were performed at 1.2 μmol Cd, which is approximately one thousand times the [Cd] of Pacific deep water (*Boyle et al.*, 1976). The dominant aqueous Cd species at this concentration and ionic strength is $CdCl_2$ in the saline experiments, and Cd^{2+} in the freshwater

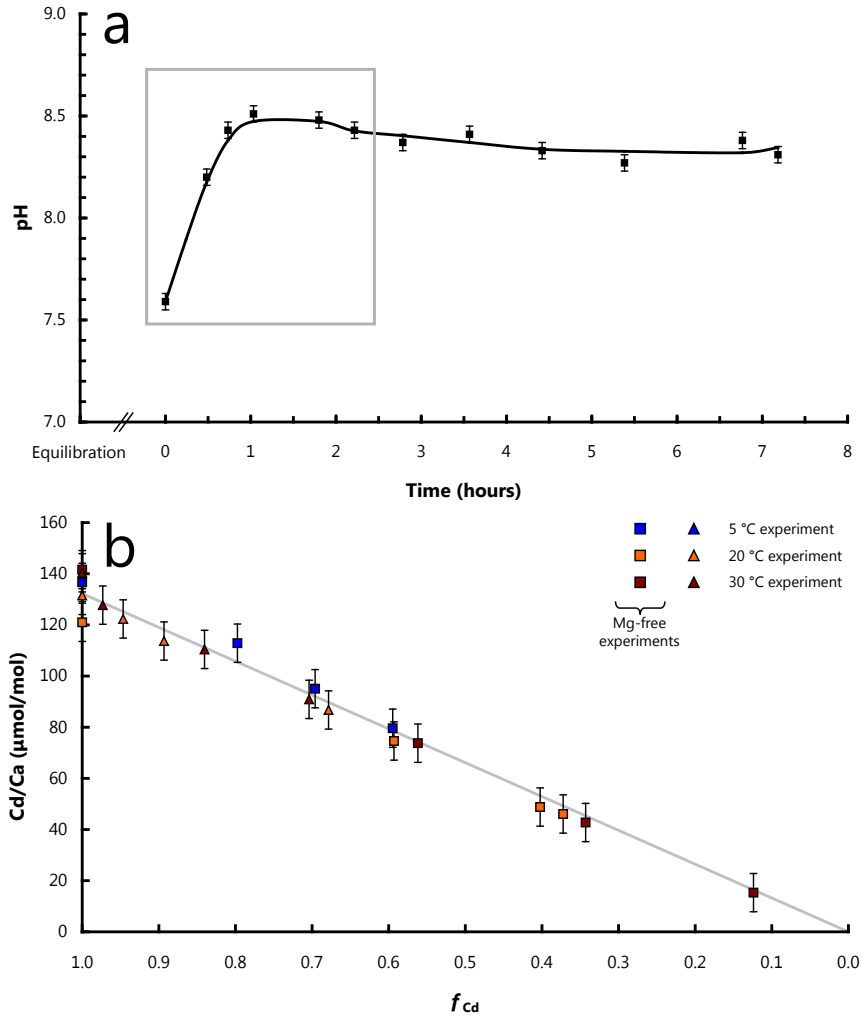

Figure 4.1: Growth-solution evolution during precipitation experiments in artificial seawater. (a) Evolution of the pH of the growth solution for an extended (eight hour) precipitation experiment. Time 0 represents activation of the dual syringe pump. The time before 0 hours ('equilibration') refers to the minimum of 18 hours in which the artificial seawater solution was equilibrated with the seed calcite. The majority of the experiments in this study were stopped after 2.5 hours (indicated by the grey box). **(b)** Plot of Cd/Ca vs. f_{Cd} (fraction of dissolved Cd remaining) for the growth solution over the course of representative experiments (#21, 22, 24, 25, & 26; $R^2 > 0.9$).

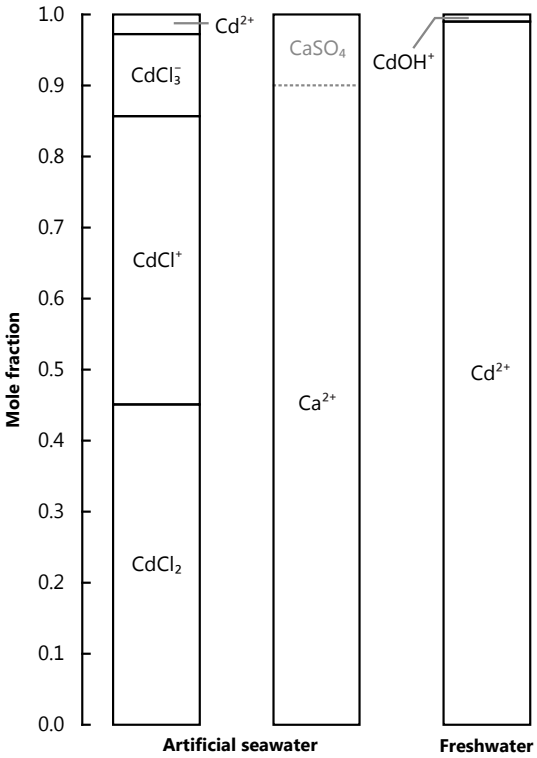

Figure 4.2: Relative abundances of inorganic aqueous Cd and Ca species in artificial seawater and freshwater experiments. Calculations performed using PHREEQC (*Parkhurst et al.*, 1999). Ca is present almost exclusively as dissolved Ca^{2+} in both freshwater and Mg-free seawater; however $\sim$ 10 % is expected to complex with SO_4^{2-} in the 'normal' seawater experiments (#18, 20, 22, 25). Species with abundances $<$ 1 % are omitted for clarity.

experiments (*Long and Angino*, 1977; *Sverjensky et al.*, 1997; *Byrne*, 2002; Fig. 4.2). All subsequent speciation and mineral saturation calculations were performed using the program PHREEQC (*Parkhurst et al.*, 1999).

The slight difference in ionic strength between the Mg-free and normal artificial seawater experiments is not expected to change overall Cd speciation by more than 1 %, although $\sim$ 10 % of the available Ca^{2+} is expected to complex with SO_4^{2-} in the normal [Mg] artificial seawater experiments (Fig. 4.2). The Cd content of the seawater solutions was kept low enough to avoid saturation with respect to pure $CdCO_3$ (otavite). The initial $\Omega_{otavite}$ (otavite saturation) was calculated as $<$ 0.1.

For the freshwater experiments, more of the dissolved Cd is speciated as Cd^{2+} ($\sim$ 99 % compared with $\sim$ 3 % in the seawater-type experiments; Fig. 4.2), equivalent to a 35-fold increase in 'available' Cd^{2+} concentrations. Consequently, $\Omega_{otavite}$ increased from 0 to $\leq$ 22.4 as the calcite

seed crystals dissolved to reach equilibrium with the growth solution, before decreasing again as Cd was removed from the growth solution. The rate of Cd uptake by the solid phase was at least 2× faster compared with the seawater experiments, presumably owing to the significantly higher $\Omega_{otavite}$. Therefore freshwater experiments were stopped after 1.2 hours of precipitation so as to measure the Cd isotope composition of the residual Cd in solution.

4.2.3 Sample processing and analysis

Preliminary Cd concentrations of solutions and carbonates were measured on a Thermo Scientific ELEMENT 2 ICPMS, to enable spiking with a suitable amount of $^{111}Cd-^{112}Cd$ double spike (mixed in Oxford with an Ag-normalized $^{111}Cd/^{112}Cd = 0.890654 \pm 0.000081$). These steps were carried out in laminar flow workstations at the University of Oxford; all acids used were purified by sub-boiling distillation in quartz glass stills and diluted (where necessary) with 18.2 MΩ H_2O. The artificial seawater solution was sampled at the start of every precipitation experiment to determine the Cd concentration of the solution, and to serve as a long term indicator of the reproducibility of our isotopic measurements. Solutions were filtered (using Whatman hardened ashless-grade cellulose filters in a Nalgene vacuum filtration system) and the precipitates rinsed with the growth solution and then Milli-Q H_2O thrice before drying at 75 °C for 15 minutes.

The spiked samples were passed through a two-stage separation chemistry to remove as much of the matrix as possible before mass spectrometry. The complete separation protocol is outlined in *Horner et al.* (2010), and represents a re-scaled version of those reported in previous studies (*Wombacher et al.*, 2003; *Ripperger and Rehkämper*, 2007). The final eluent from the second stage was dried down and converted to HNO_3^- form before being taken up in 2 % HNO_3 for mass spectrometry.

Mass spectrometric measurements were performed on a Nu Instruments multi-collector ICPMS at the University of Oxford. Samples were introduced into the mass spectrometer using an El-

emental Scientific PFA MicroFlow Nebulizer in conjunction with a Nu Instruments DSN-100 desolvation system at rates of $\sim$ 120 μL min^{-1}. The ion currents of ^{111}Cd, ^{112}Cd, ^{113}Cd, ^{114}Cd, ^{115}In, and ^{117}Sn were measured simultaneously in 40 $\times$ 10 s integrations, consuming $\sim$ 1 mL of solution per sample. Instrumental mass bias was assumed to follow the GPL (Generalized Power Law; *Maréchal et al.*, 1999) with the mass-dependence of the instrumental mass discrimination optimized at -0.15. Data reduction was performed using a MATLAB-based interpretation of the methods described by *Siebert et al.* (2001), with additional iterative loops for interference corrections (^{112}Sn on ^{112}Cd, ^{113}In on ^{113}Cd, and ^{114}Sn on ^{114}Cd). Isotopic data are reported as ϵ values (*Wombacher and Rehkämper*, 2004):

$$\epsilon^{114/110}\mathrm{Cd} = \left(\frac{^{114/110}\mathrm{Cd}_{\mathrm{sample}}}{^{114/110}\mathrm{Cd}_{\mathrm{standard}}} - 1 \right) \times 10,000 \tag{4.2.3}$$

relative to our in-house standard 'OxCad' (Alfa Aesar Specpure Cd concentration standard, lot number 81-081192A). The isotopic composition of OxCad, relative to BAM-I012 Cd (*Pritzkow et al.*, 2007) was determined to be $\epsilon^{114/110}\mathrm{Cd} = +4.9 \pm 0.9$ (2 SD, $n = 11$). For comparison with other laboratories, we also report (relative to BAM-I012 Cd) the isotopic composition of Alfa Cd Zürich (*Ripperger and Rehkämper*, 2007; *Ripperger et al.*, 2007) as $\epsilon^{114/110}\mathrm{Cd} = +13.0 \pm 1.1$ (2 SD, $n = 10$) and JMC Cd Mainz (*Schmitt et al.*, 2009a,b) as $\epsilon^{114/110}\mathrm{Cd} = +14.9 \pm 0.9$ (2 SD, $n = 16$). The long-term reproducibility for sample replicates taken through chemistry (excluding a single outlier) is ± 1.3 $\epsilon^{114/110}$Cd units (2 SD, $n = 28$), equivalent to ± 32 ppm AMU^{-1}. This level of uncertainty is approximately an order of magnitude smaller than the total variability surveyed in the samples analyzed in this study.

Uncertainties for the samples presented here are reported as either the long-term external reproducibility for sample replicates (± 1.3 $\epsilon^{114/110}$Cd) to two standard deviations, or as 2$\times$ standard error, whichever is the larger. The total analytical blank was 23 ± 14 pg Cd (1 SD, $n = 6$) which constitutes an insignificant (≤ 0.05 %) level of contamination relative to sample Cd; no blank correction was applied.

4.3 Results

4.3.1 Mineralogical data and elemental partitioning

Typical crystal morphologies from example experiments are shown in Fig. 4.3a-d. The mineralogy was analyzed by powder XRD (x-ray diffraction), confirming that all samples were calcite. The presence of Mg^{2+} in the normal seawater-type experiments is seen to change the growth morphology of the precipitates (Fig. 4.3d) but not the mineralogy (Fig. 4.3e; *Davis et al.*, 2000; *Han and Aizenberg*, 2003; *Wasylenki et al.*, 2005).

Distribution coefficients, K_D^{Cd}, are derived from:

$$K_D^{Cd} = \frac{x_{CdCO_3}}{x_{CaCO_3}} / \frac{(Cd^{2+})}{(Ca^{2+})} \tag{4.3.1}$$

where x_{CdCO_3} or x_{CaCO_3} refers to the mole fraction in the precipitate, and (Cd^{2+}) or (Ca^{2+}) to the activity of the free-aquo ion in the growth solution. Activities of the aqueous species were determined by measuring the total (analytical) concentrations of Cd and Ca by ICPMS, and calculating an activity using PHREEQC (*Parkhurst et al.*, 1999) based on the temperature (5, 20, or 30 °C), pH (fixed at 8.25), and ionic strength ($\sim$ 0, 0.6 or 0.7 M) of the growth solution. In this way, calculated values of K_D^{Cd} are directly comparable between different experiments as this formulation accounts for the different activities of the free-aquo ions when experiments are performed in different growth media.

Calculated values of K_D^{Cd} assume that all Cd removed from the growth solution was present in the calcite and that the elemental partition coefficient did not change with evolving Cd concentrations over the course of an experiment. The mass of precipitate recovered at the end of an experiment (corrected for mass of initial seed calcite, typically $\sim$ 50 % of the recovered material) was used to calculate x_{CdCO_3} and x_{CaCO_3}. The average [Cd]/[Ca] (analytical concentrations) in the growth solution were converted to activity ratios to yield an average K_D^{Cd} for

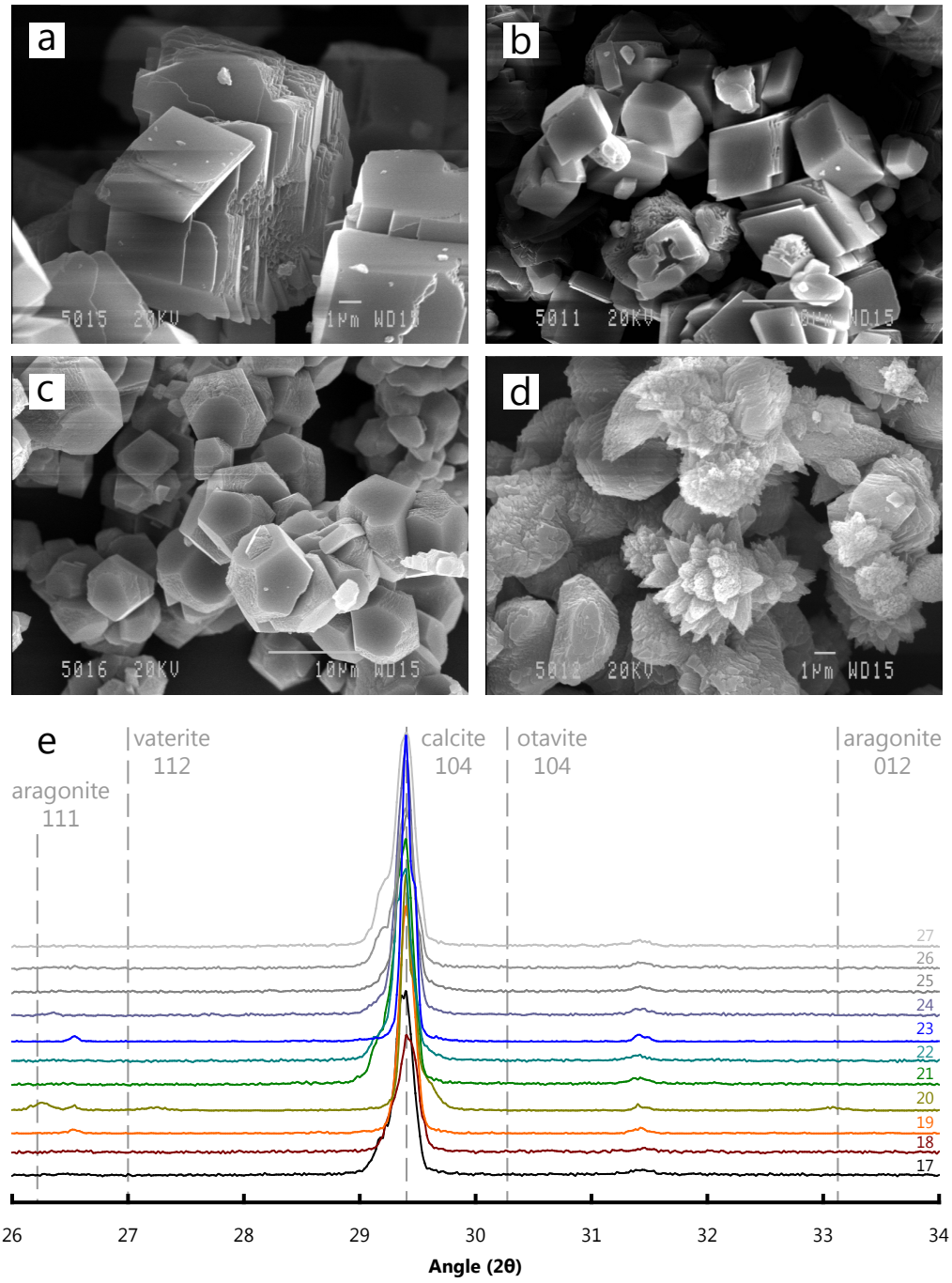

Figure 4.3: Secondary electron images of a selection of inorganic calcite precipitates from this study. These examples were grown at 50 nmol mg^{-1} min^{-1}; all experiment numbers correspond to Table 4.2. Scale bars are provided in the lower-right of each panel. **(a)** Crystals from Experiment #17 grown at 5 °C in the absence of Mg^{2+} showing well-defined rhombs and characteristic growth steps. **(b)** Crystals from Experiment #21 grown at 20 °C in the absence of Mg^{2+}. **(c)** Crystals from Experiment #19 grown at 30 °C in the absence of Mg^{2+}. **(d)** Crystals from Experiment #20 grown at 30 °C in the presence of Mg^{2+} showing crystal elongation ~ parallel to the *c*-axis relative to the *a*- and *b*-axes probably caused by Mg^{2+} acting as a growth inhibitor (*Han and Aizenberg*, 2003; *Davis et al.*, 2004). **(e)** XRD scans of the precipitates from this study showing intensity in the $26 - 34$ ° region (2θ). The *y*-axis has been re-scaled and plotted in relative units owing to the differences in absolute signal intensity between different analyses. These scans reveal the characteristic $\{10\bar{1}4\}$ diffraction peak of calcite at ≈ 29.4 °. The principal reflectors (I_1) for aragonite and vaterite are also shown (an additional aragonite (012) reflector, $I_2 = 0.6$, is also shown), demonstrating that other polymorphs of $CaCO_3$ were not present (with the possible exception of a minor aragonite reflection in Experiment #20).

each experiment. This approximation provided reasonable estimates that are within the range from previous studies (*Lorens*, 1981; *Tesoriero and Pankow*, 1996; Table 4.2). For the freshwater experiments, the mass of overgrowth could not be directly measured during equilibration, therefore the amount of $CaCO_3$ precipitation (and its Cd content) was taken to be equivalent to the concentration of Cd removed from solution (*Prieto et al.*, 2003). The large uncertainties for some of the K_D^{Cd} estimates are a consequence of allowing for possible incomplete recovery of $CaCO_3$ from the growth vessel prior to filtering.

Values of K_D^{Cd} in the 12 experiments of this study range from $4 - 2588$ and show systematic variation depending on experiment type. The freshwater experiments exhibit very low K_D^{Cd}, ranging from $4 - 19$. Values of K_D^{Cd} are much larger and variable in seawater experiments, ranging from $532 - 2588$, with the experiments containing Mg^{2+} and SO_4^{2-} being at the lower end of this range (average $K_D^{Cd} \approx 1100$ compared with ≈ 1900 for Mg-free experiments). Increasing precipitation rate decreases K_D^{Cd} from 2091 to 654 as growth rate quadruples (Fig. 4.4d).

4.3.2 Cadmium isotopic partioning data

Isotopic fractionation factors for Cd into $CaCO_3$, $\alpha_{CaCO_3-Cd_{(aq)}}$, are calculated, assuming Rayleigh fractionation (e.g. *de la Rocha et al.*, 1997), based on solution isotope values using:

$$\alpha_{CaCO_3-Cd_{(aq)}} = \frac{\ln\left(\frac{\epsilon^{114/110}Cd_{sol.}}{10{,}000} + 1\right)}{\ln\left(f_{Cd}\right)} + 1 \tag{4.3.2}$$

and from the precipitates with:

$$\alpha_{CaCO_3-Cd_{(aq)}} = \frac{\ln\left(\frac{\left(-\epsilon^{114/110}Cd_{carb.} - 10{,}000\right)(1-f_{Cd})}{10{,}000} + 1\right)}{\ln\left(f_{Cd}\right)} \tag{4.3.3}$$

where f_{Cd} is the fraction of dissolved Cd remaining. Isotopic compositions were always determined relative to the starting Cd in the growth solution, hence our choice of reference standard

Table 4.2: Summary of the results of this study.
[a] Precipitation rate, expressed in nmol per mg seed min^{-1}.
[b] Sample numbers refer to artificial seawater solutions unless otherwise stated.
[c] Number of independent isotopic measurements.
[d] See text for how K_D^{Cd} and associated uncertainty was calculated.
[e] No Na_2CO_3 or $CaCl_2$ were added in this experiment, so as to investigate Cd removal during equilibration only.
[†] This sample significantly deviates from the Rayleigh fractionation trend defined by the other samples in this study and is considered to be an outlier. It has been omitted from Fig. 4.4 and appears greyed-out in Fig. 4.5.
[§] It is not clear why the Cd concentration in this sample increased during $CaCO_3$ precipitation; the Cd isotope composition did not appear to be influenced by this, and it does not influence the results of this study.

Experiment #	Temp. (°C)	R [a]	Sample # [b]	$\epsilon^{114/110}$Cd	$\pm$ 2 SD	n [c]	f_{Cd}	$K_D^{Cd} \pm$ 2 SD [d]	$\alpha_{CaCO_3-Cd_{(aq)}} \pm$ 2 SD [e]
Mg-free artificial seawater experiments									
14	5	93	1	-	-	-	1.00	-	-
14	5	93	2	+6.6	1.3	1	0.12	-	0.99969 ± 0.00006
14	5	93	precipitate	−0.6	1.3	1	0.12	1554 ± 120	0.9998 ± 0.0004
17	5	50	1	−0.5	1.7	3	1.00	-	-
17	5	50	2	+6.2	1.6	1	0.14	-	0.99968 ± 0.000081
17	5	50	3	+9.3	1.3	1	0.06	-	0.99968 ± 0.00005
17	5	50	precipitate	−1.6	1.3	3	0.06	2091 ± 190	0.9990 ± 0.0008
19	30	50	1	+1.3	1.3	3	1.00	-	-
19	30	50	2	+6.3	1.3	1	0.24	-	0.99956 ± 0.00009
19	30	50	3	+10.9	1.4	2	0.10	-	0.99952 ± 0.00006
19	30	50	precipitate	−0.7	1.5	4	0.10	2129 ± 194	0.9997 ± 0.0006
21	20	50	1	+0.2	1.3	2	1.00	-	-
21	20	50	2	+4.2	2.8	4	0.59	-	0.99920 ± 0.00053
21	20	50	3	+6.3	1.3	5	0.40	-	0.99931 ± 0.00014
21	20	50	4	+8.6	1.6	8	0.37	-	0.99913 ± 0.00016
21	20	50	precipitate	−1.6	1.3	9	0.37	1050 ± 88	0.9997 ± 0.0002
24	30	50	1	−0.9	1.3	2	1.00	-	-
24	30	50	2	+11.2	1.3	2	0.12	-	0.99947 ± 0.00006
24	30	50	precipitate	−1.2	1.3	8	0.12	2239 ± 224	0.9996 ± 0.0004
26	5	199	1	−0.7	1.3	2	1.00	-	-
26	5	199	2	+3.9	1.5	5	0.59	-	0.99926 ± 0.00029
26	5	199	precipitate	−2.4	1.5	8	0.59	654 ± 65	0.9997 ± 0.0002

Experiment #	Temp. (°C)	R [a]	Sample # [b]	$\epsilon^{114/110}$Cd	± 2 SD	n [c]	f_{Cd}	$K_D^{Cd} \pm 2$ SD [d]	$\alpha_{CaCO_3-Cd_{(aq)}} \pm 2$ SD [e]
Normal artificial seawater experiments									
18	5	50	1	+0.8	1.3	3	1.00	-	-
18	5	50	2	+5.9	1.3	1	0.25	-	0.99957 ± 0.00009
18	5	50	3	+7.8	1.3	1	0.10	-	0.99966 ± 0.00006
18	5	50	precipitate	−2.9	2.3	3	0.10	2588 ± 370	0.9988 ± 0.0009
20	30	50	1	+0.3	1.3	3	1.00	-	-
20	30	50	2	+3.1	1.3	2	0.45	-	0.99961 ± 0.00016
20	30	50	3	+2.8	2.7	2	0.55	-	0.99953 ± 0.00045
20	30	50	precipitate	−1.1	2.3	4	0.55	772 ± 64	0.9999 ± 0.0002
22	20	50	1	+0.4	1.3	3	1.00	-	-
22	20	50	2	+2.0	1.3	4	0.89	-	0.99826 ± 0.00115
22	20	50	3	+2.4	1.3	4	0.68	-	0.99938 ± 0.00034
22	20	50	precipitate	−3.2	1.3	8	0.68	564 ± 71	0.9996 ± 0.0002
25	30	50	1	−0.4	1.3	3	1.00	-	-
25	30	50	2[†]	+3.4	1.3	5	0.97	-	-
25	30	50	3	+1.4	1.3	4	0.84	-	0.99918 ± 0.00075
25	30	50	4	+2.0	1.3	4	0.70	-	0.99942 ± 0.00037
25	30	50	precipitate	−2.4	1.3	8	0.70	532 ± 67	0.9997 ± 0.0002
Freshwater experiments									
23	20	- [e]	1	-	-	-	1.00	-	-
23	20	- [e]	2	+1.1	1.3	2	0.61	-	0.99979 ± 0.00026
23	20	- [e]	precipitate	-	-	-	0.61	12 ± 1	-
27	20	-	1	-	-	-	1.00	-	-
27	20	-	2	+0.8	1.3	3	0.29	-	0.99994 ± 0.00010
27	20	-	precipitate	-	-	-	0.29	19 ± 2	-
27	20	50	3	+0.7	1.3	2	0.33[§]	-	0.99994 ± 0.00012
27	20	50	4	+1.2	1.3	2	0.03	-	0.99997 ± 0.00004
27	20	50	precipitate	-	-	-	0.03	4 ± 1	-

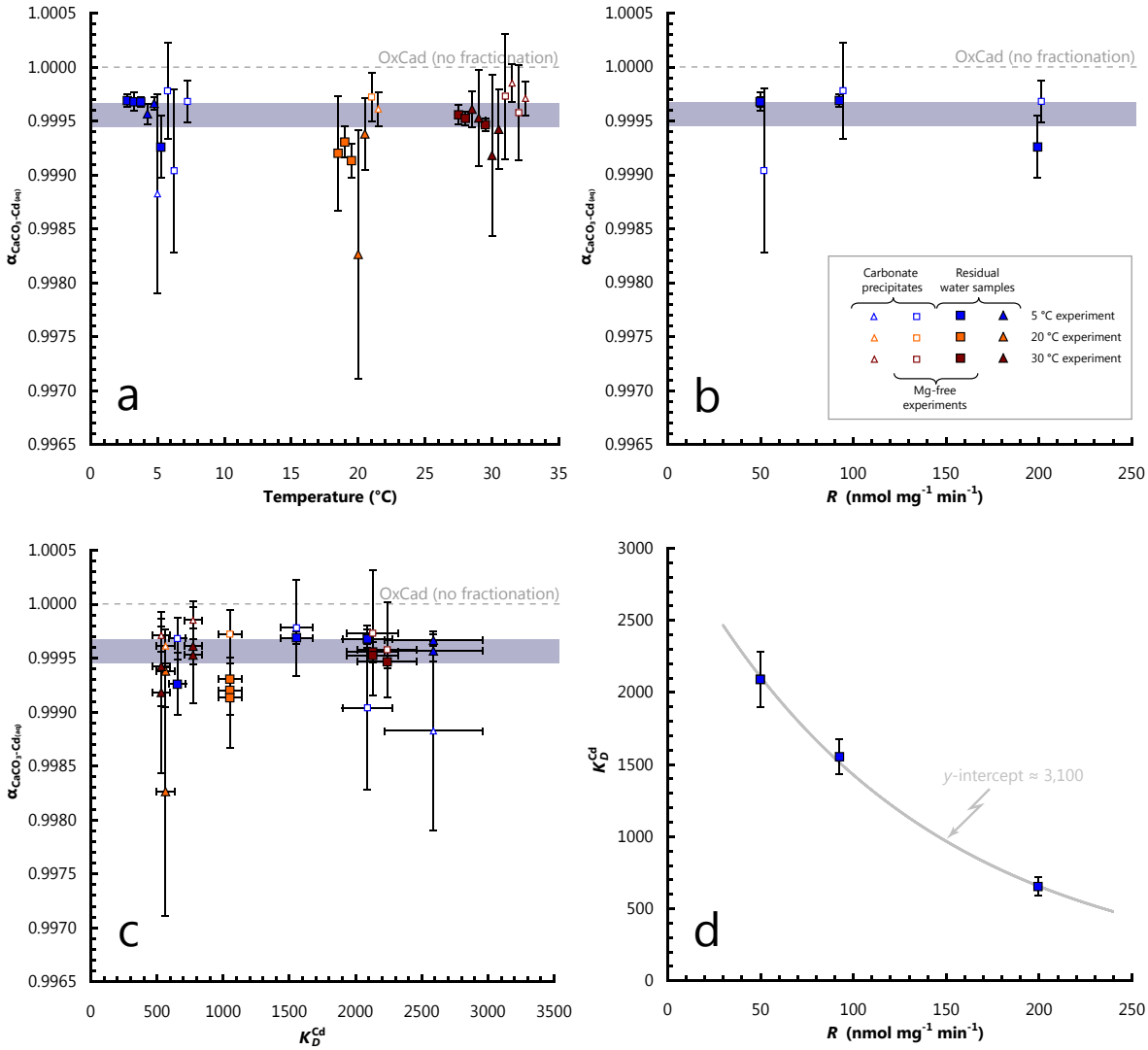

Figure 4.4: Summary of the seawater experiment data from this study. (a) $\alpha_{CaCO_3-Cd_{(aq)}}$ against temperature (data have been spaced for clarity of presentation; all experiments performed at 5, 20, & 30 °C). **(b)** $\alpha_{CaCO_3-Cd_{(aq)}}$ plotted against precipitation rate, R. **(c)** $\alpha_{CaCO_3-Cd_{(aq)}}$ against K_D^{Cd}. **(d)** K_D^{Cd} plotted against R. The exponential relationship seen suggests an equilibrium $K_D^{Cd} \approx 3100$, similar to theoretical value of 4170 (*Prieto et al.*, 2003). The mauve shaded area in panels **(a)–(c)** corresponds to $\alpha_{CaCO_3-Cd_{(aq)}} = 0.99955 \pm 0.00012$, the weighted average value of this study.

Table 4.3: Summary of previously reported isotopic offsets between various substrates and dissolved Cd. Offsets have been renormalized to $\epsilon^{114/110}$Cd notation, and are reported as $10,000\ \ln(\alpha_{\text{substrate}-\text{Cd}_{(aq)}}) \approx \epsilon^{114/110}\text{Cd}_{\text{substrate}} - \epsilon^{114/110}\text{Cd}_{\text{Cd}_{(aq)}}$.
[a]Includes water samples from $\geq$ 1000 m depth.
[b]Ranges reported for ACC (Antarctic Circumpolar Current) and Weddell Gyre.

Substrate	$10\ 000\ \ln(\alpha_{\text{substrate}-\text{Cd}_{(aq)}})$	Reference
Synthetic aragonite	-5.5 ± 4.5	*Wombacher et al.* (2003)
Cultured freshwater phytoplankton	-14 ± 6	*Lacan et al.* (2006)
North Pacific seawater[a]	-6 ± 6	*Lacan et al.* (2006)
Global seawater compilation[a]	-4.0 ± 2.0	*Ripperger et al.* (2007)
Southern Ocean seawater	-5.0 ± 1.0	*Rehkämper et al.* (2010)
Southern Ocean seawater[b]	-3.1 ± 1.1	*Abouchami et al.* (2011)
Inorganic seawater-derived calcites	-4.5 ± 1.2	This study

in this regard was not important. Significant error magnification occurred when calculating $\alpha_{\text{CaCO}_3-\text{Cd}_{(aq)}}$ from the $\epsilon^{114/110}$Cd values of the precipitates, because deviations of $\epsilon^{114/110}$Cd from the initial solution value were only $\sim 2\times$ the analytical uncertainty, and decreased with increasing Cd utilization. The isotopic composition of the precipitates was therefore used to corroborate, rather than determine, $\alpha_{\text{CaCO}_3-\text{Cd}_{(aq)}}$ for any given experiment.

Values of $\alpha_{\text{CaCO}_3-\text{Cd}_{(aq)}}$ can be compared with temperature (Fig. 4.4a), K_D^{Cd} (Fig. 4.4b), and precipitation rate (Fig. 4.4c), and are similar in all seawater experiments. Given the similarity in values of $\alpha_{\text{CaCO}_3-\text{Cd}_{(aq)}}$ between different seawater experiments, we have calculated $\alpha_{\text{CaCO}_3-\text{Cd}_{(aq)}}$ by combining the isotopic data from all ten experiments. A weighting is assigned to each point that is inversely proportional to both the fraction of dissolved Cd remaining in solution and the measurement uncertainty, $1/x$, so that samples with a low degree of Cd utilization or large uncertainties do not bias the calculation of $\alpha_{\text{CaCO}_3-\text{Cd}_{(aq)}}$. Taking this approach, our weighted sum (with weighted uncertainties) yields $\alpha_{\text{CaCO}_3-\text{Cd}_{(aq)}} = 0.99955 \pm 0.00012$ (2 SD, $n = 18$, Fig. 4.5). This is equivalent to the precipitates having a Cd isotope composition 4.5 ± 1.2 ϵ-units lighter than the seawater solution in which they formed. This is consistent with the Cd isotope composition ($\epsilon^{114/110}\text{Cd} = -5.5 \pm 4.5$) of the synthetic aragonite measured by *Wombacher et al.* (2003), within the larger uncertainties of that study (Table 4.3).

In contrast to the saline experiments, no Cd isotope fractionation was observed during uptake by calcite in freshwater (Table 4.2, Fig. 4.6). During these experiments, in addition to removal

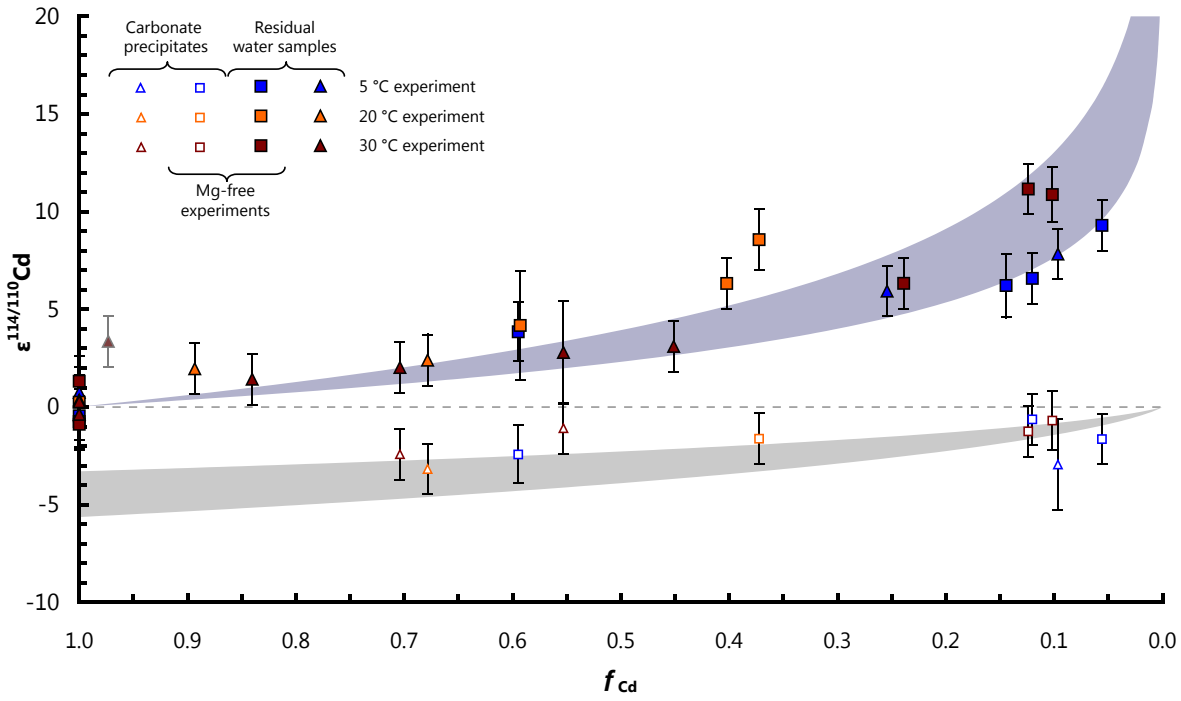

Figure 4.5: Cd isotope data for all measurements from the seawater experiments plotted against f_{Cd}. The best-fit isotopic evolution of the residual water and the precipitates are shown with the mauve and grey shaded curves, respectively for $\alpha_{CaCO_3-Cd_{(aq)}} = 0.99955 \pm 0.00012$.

of Cd by $CaCO_3$ precipitation, Cd was also removed from the growth solution during initial equilibration with the calcite seeds. This occurred because the growth solution (de-ionized water) was undersaturated with respect to calcite, causing Ca^{2+} and CO_3^{2-} to be released into solution as some of the seed calcite dissolved. The increase in $[Ca^{2+}]$ and $[CO_3^{2-}]$ increased $\Omega_{otavite}$, leading to precipitation of Cd-rich $CaCO_3$, removing $\sim$ 50 % of the initial Cd. This was similar to the beaker experiments described in *Prieto et al.* (2003), and as with their experiments, Cd removal from the growth solution slowed dramatically after several hours of equilibration. This Cd removal during equilibration did not result in any observable Cd isotopic fractionation in the solution (Table 4.2, Experiment #23). In a second freshwater experiment (Experiment #27), following the $\sim$ 18 hours of seed calcite equilibration, further Cd removal was induced by pumping in $CaCl_2$ and Na_2CO_3 (as with the saline experiments). The final $\alpha_{CaCO_3-Cd_{(aq)}}$ for the freshwater growth was 0.99997 ± 0.00004 (Table 4.2). Unlike the seawater experiments however, salinity could not be held constant and increased from zero to 0.08 by the end of calcite growth.

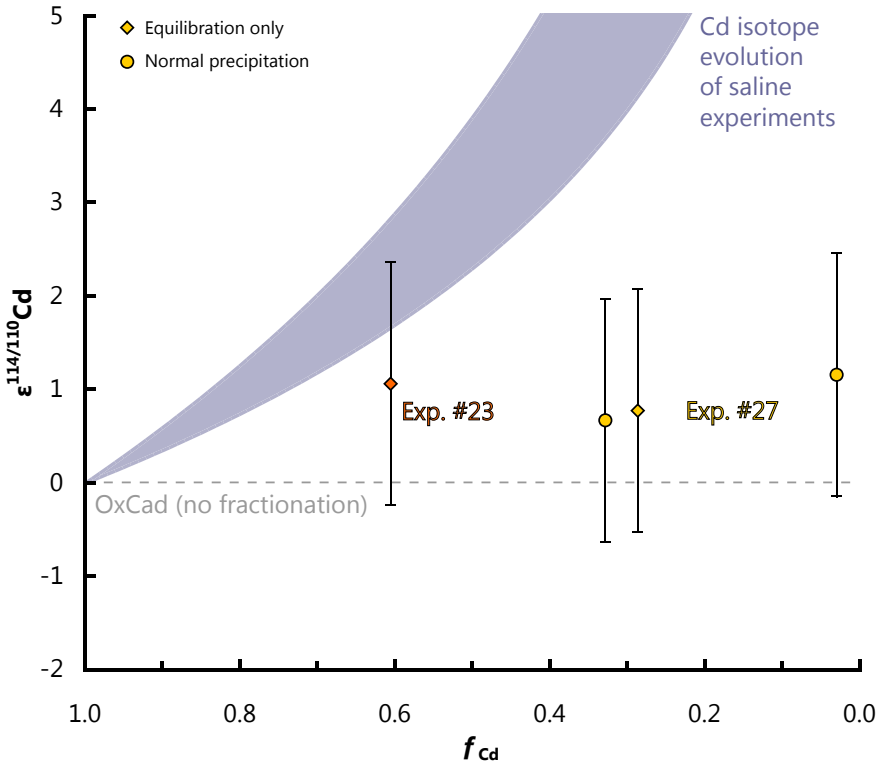

Figure 4.6: Cadmium isotope data for the two freshwater experiments plotted against f_{Cd}. These data illustrate the lack of any significant fractionation. The mauve shading illustrates the Cd isotope evolution of the seawater experiments for comparison.

4.4 Discussion

4.4.1 Invariance of the fractionation factor in seawater

The primary conclusion from the inorganic precipitation experiments in seawater solutions is that $\alpha_{CaCO_3-Cd_{(aq)}}$ is less than one (0.99955 ± 0.00012) and is remarkably insensitive to changes in temperature, ambient [Mg^{2+}], or precipitation rate (across the range studied). This invariance occurs despite a factor of five range in K_D^{Cd} for the seawater experiments (Fig. 4.4c). The lack of variation in $\alpha_{CaCO_3-Cd_{(aq)}}$ with environmental variables will simplify the use of Cd isotopes in palaeo-$\epsilon^{114/110}$Cd reconstructions because the range of variations studied here is comparable to those expected in the surface ocean. Consequently, values of $\epsilon^{114/110}$Cd recovered from natural biogenic calcites, if they behave in a similar manner to laboratory-synthesized calcites, may be representative of past seawater $\epsilon^{114/110}$Cd (with a uniform offset), rather than reflecting changes in temperature- or Mg^{2+}-dependent variability in $\alpha_{CaCO_3-Cd_{(aq)}}$. However, studies of Cd isotopes derived from $CaCO_3$ in lacustrine or riverine environments may be subject to different controls on $\alpha_{CaCO_3-Cd_{(aq)}}$ than in seawater, as this study demonstrates the importance of ionic strength in modulating Cd isotope fractionation. The ability to reconstruct past ocean Cd isotopes will provide information about past micronutrient cycles to complement that from Cd/Ca and other palaeonutrient proxies.

4.4.2 The effect of salinity and the mechanism of Cd isotope fractionation

Calcite growth in freshwater yields an $\alpha_{CaCO_3-Cd_{(aq)}}$ within error of one, in contrast to the fractionated calcites in the seawater experiments. We suggest that the mechanism of Cd isotope fractionation during calcite growth is related to kinetic isotope effects at the mineral surface, modified by competition with other ions (e.g. Na^+).

In some isotope systems (e.g. boron), the presence of more than one dissolved species with isotopic offsets between the species is an important control on the isotopic composition of

minerals derived from solutions (i.e. if one dissolved phase is incorporated in preference to another). Such an effect is also seen for Zn isotopes, with Zn^{2+} having different isotope compositions than chlorinated forms of Zn (*Fujii et al.*, 2010; *Black et al.*, 2011). Like Zn, Cd is also complexed by chloro-ligands (although much more so than Zn) in seawater (*Byrne*, 2002), with only ~ 3 % present as Cd^{2+} (Fig. 4.2). This might suggest a similar isotope effect for Cd, assuming analagous behaviour for Zn and Cd. For Zn, the heavier isotopes are favoured in the Zn^{2+} species. If this is also true for Cd, given that only Cd in the Cd^{2+} form is likely to be incorporated into calcium carbonate (*Davis et al.*, 1987; *Reeder*, 1996), carbonates would be isotopically heavier than the bulk solution composition; the opposite of the effect that is observed. This logic argues against a dominant role for fractionation between chemical species in the solution in generating isotopically light calcite growth.

The observation that the solid phase is enriched in the lighter isotopes of Cd compared to the growth solution (in the seawater experiments), despite the strong bonding of Cd in calcite, argues against equilibrium isotope fractionation during mineral growth (e.g. *Johnson et al.*, 2004; *DePaolo*, 2011). Kinetic isotope fractionation at the calcite surface, with the lighter isotopes of Cd preferentially incorporated into the solid phase, is a more likely explanation for the observations.

The incorporation of Cd into calcite can be thought of as a largely unidirectional process. For the calcite to grow, the forward reaction must dominate over the back reaction and, because of the high equilibrium K_D for Cd, return of Cd to the solution phase is likely to be minor. In such a situation, where the reaction can be considered unidirectional, the kinetics of isotope fractionation become important, with the faster reaction of the lighter isotopes leading to a light Cd isotope signature in the calcite.

The different response of the freshwater and saline experiments also provides information about the processes inducing fractionation. Although K_D^{Cd} is calculated from the activity of Cd^{2+}, exchange of Cd^{2+} in solution with Cd bound in chloro-complexes ($CdCl_x^{2-x}$) is fast (e.g.

Margerum et al., 1978). If considering the kinetics, it is more relevant to compare the rate of Cd uptake into the solid relative to the bulk solution chemistry. On that logic, uptake of Cd into the solid was observed to be $> 2\times$ faster in the freshwater experiments than the seawater experiments during precipitation. Thus, it appears that this kinetic fractionation can be modulated by ion blocking at the crystal surface in the seawater media. Major ions (particularly Na^+ and K^+) retard crystal growth by overwhelming surface sites, and decrease Cd uptake during calcite growth. The magnitude of this ion blocking effect depends on the concentration of major ions in the growth solution. In the seawater experiments, the precipitates exhibit particularly high distribution coefficients, suggesting slower Cd uptake and isotopic selection ($K_D^{Cd} \sim 500 - 2500$, $\alpha_{CaCO_3-Cd_{(aq)}} = 0.99955 \pm 0.00012$). In the freshwater experiments where almost all Cd is speciated as Cd^{2+} and $\Omega_{otavite}$ is > 1, Cd uptake occurs much more rapidly from the immediate growth environment and is effectively quantitative, so that no fractionation is observed. This is evidenced by the much lower K_D^{Cd} values of $\sim 5 - 20$ (e.g. *Putnis*, 2010), and unfractionated Cd isotope compositions ($\alpha_{CaCO_3-Cd_{(aq)}} = 1$). Only when Cd uptake is inhibited by ion blocking does the kinetic effect become apparent, despite variation in other environmental variables such as temperature or ambient $[Mg^{2+}]$.

If kinetic fractionation is the dominant control then there are some instances where the constancy in $\alpha_{CaCO_3-Cd_{(aq)}}$ for calcite grown in seawater may break down. At very slow precipitation rates, the back reaction (calcite dissolution) might become important, resulting in a decreased isotopic fractionation factor (e.g. *Fantle and DePaolo*, 2007; *DePaolo*, 2011). The same may also apply at very fast precipitation rates and/or supersaturation where quantitative removal of Cd occurs, such that no fractionation is observed. The freshwater examples presented here broadly confirm this, as these experiments had larger $\Omega_{otavite}$ and therefore exhibited $> 2\times$ faster Cd uptake rates, and reduced K_D^{Cd} (*Putnis*, 2010). Additionally, the range of temperatures investigated, whilst representative of the range relevant to the surface ocean, is relatively narrow in an absolute sense; decreased fractionation may be expected at very high temperatures (e.g. *DePaolo*, 2011; *Wombacher et al.*, 2011).

4.4.3 The role of $CaCO_3$ precipitation in setting surface ocean Cd isotope compositions

The value of $\alpha_{CaCO_3-Cd_{(aq)}}$ in seawater experiments in this study is similar in both direction and magnitude to previous estimates of $\alpha_{x-Cd_{(aq)}}$, based on Cd isotope and concentration data in surface seawater (where x is a removal phase, often assumed to be phytoplankton; *Ripperger et al.*, 2007; *Abouchami et al.*, 2011; Table 4.3). It is therefore possible that $CaCO_3$ precipitation in the ocean could account for the observed variability in oceanic $\epsilon^{114/110}$Cd values, rather than or as well as biological activity. This would imply that records of past seawater $\epsilon^{114/110}$Cd, and even potentially Cd/Ca, are not representative of nutrient availability and uptake by phytoplankton soft tissue, as is currently accepted in the literature, but by the calcium carbonate portion of productivity.

The removal of dissolved Cd from surface seawater is affected by two types of particulate material: calcium carbonate (referred to here as PIC, particulate inorganic carbon) and organic soft tissue (referred to here as POC, particulate organic carbon). PIC removes Cd via substitution of Cd for Ca in the $CaCO_3$ lattice, whereas POC removes Cd that is organically-bound in phytoplankton. The size of the PIC flux can be estimated using the Cd/Ca of planktonic foraminiferal tests (*Rickaby et al.*, 2000) and assuming a similar ratio for other calcifying organisms for which scant data is available (e.g. coccoliths, pteropods, etc.). Planktonic forams constitute $\sim$ 50 % of the total $CaCO_3$ production in surface waters (*Schiebel*, 2002), therefore this estimate may provide reasonable values of PIC-bound Cd requirements. The annual Cd uptake of pelagic calcifiers is estimated as $2 - 10 \times 10^6$ mol Cd yr^{-1} (using the estimate of $CaCO_3$ productivity of 58×10^{12} mol C yr^{-1} from *Milliman et al.*, 1999). To estimate POC-bound Cd, we use the elemental stoichiometry of common phytoplankton from *Ho et al.* (2003); *Cullen and Sherrell* (2005), which extend the Redfield formula to include transition elements. An average Cd/C ratio of biomass in the ocean of $1.6 - 1.7 \times 10^{-6}$ (*Ho et al.*, 2003; *Cullen and Sherrell*, 2005) equates to a global Cd requirement for phytoplankton of between $9,500 - 14,000 \times 10^6$ mol Cd yr^{-1} using a

range of global net primary production of $5.9 - 8.0 \times 10^{15}$ mol C yr^{-1} (*Jin et al.*, 2006). These calculations indicate that POC-bound Cd requirements are three-four orders of magnitude greater than those of PIC. Despite the similarity in estimates of $\alpha_{x-Cd_{(aq)}}$ from our experiments and that indicated by seawater measurements, we can largely discount the role of $CaCO_3$ production in determining the Cd isotope composition of surface seawater.

Our assessment of the fractionation of Cd isotopes into calcium carbonate provides an additional constraint on the global Cd isotope budget. The main input and removal fluxes of Cd to/from the ocean are summarized in Fig. 4.7, based largely on *Rosenthal et al.* (1995). This budget is balanced within the significant uncertainties that exist on all fluxes. Hydrothermal vents are unlikely to add significant Cd because, although the vents release $2 - 26 \times 10^6$ mol Cd yr^{-1} to the deep ocean (*Von Damm et al.*, 1985; *van Geen et al.*, 1995), this is removed by rapid scavenging into sulphide phases (*German et al.*, 1991). The two remaining significant inputs of Cd into the ocean are rivers and dust. Estimates of the relative magnitudes of these fluxes range from $4 - 15 \times 10^6$ mol Cd yr^{-1} and $2 - 11 \times 10^6$ mol Cd yr^{-1} for rivers and dust, respectively (*Martin and Thomas*, 1994; *Rosenthal et al.*, 1995; *van Geen et al.*, 1995). Suboxic and fully anoxic sediment sinks are assumed to be the largest removal flux of $6 - 24 \times 10^6$ mol Cd yr^{-1} (*Rosenthal et al.*, 1995). A PIC-bound Cd sink may constitute between $0.4 - 1.8 \times 10^6$ mol Cd yr^{-1} accumulation on the sea-floor in $CaCO_3$ (using estimates of $CaCO_3$ from *Milliman et al.*, 1999; Fig. 4.7). When considered in the context of the PIC and POC Cd requirements, our results suggest that the Cd content and isotopic composition of calcium carbonate precipitated in the ocean record – rather than drive – the observed variability in seawater $\epsilon^{114/110}$Cd.

4.5 Conclusions

- The isotopic fractionation factor for Cd during inorganic calcite growth in a seawater matrix is $\alpha_{CaCO_3-Cd_{(aq)}} = 0.99955 \pm 0.00012$ and is insensitive to temperature, ambient $[Mg^{2+}]$, or precipitation rate (across the range studied). This result suggests, assum-

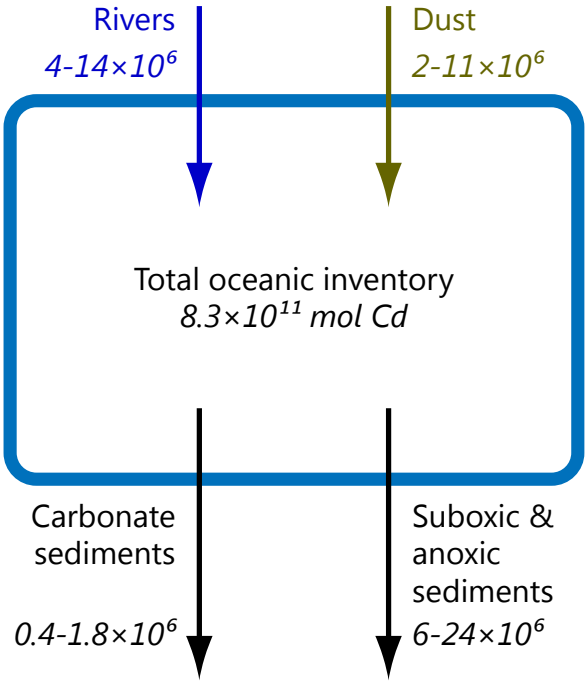

Figure 4.7: Schematic marine Cd cycling model. Estimated flux ranges are given in mol Cd yr^{-1} (after *Rosenthal et al.*, 1995).

ing that biogenic calcites fractionate Cd in a similar manner to inorganic calcites, that records of calcium carbonate $\epsilon^{114/110}$Cd may be representative of variations in seawater $\epsilon^{114/110}$Cd in the past, rather than changes in $\alpha_{CaCO_3-Cd_{(aq)}}$ with time (caused by varying environmental parameters).

- In contrast to calcite grown in seawater, $\alpha_{CaCO_3-Cd_{(aq)}}$ for calcites grown in freshwater is within uncertainty of one (i.e. no isotopic fractionation).

- We hypothesize that the mechanism of Cd isotope fractionation is related to kinetic isotope effects during the largely unidirectional incorporation of Cd at the mineral surface. This process becomes more pronounced at high salinity, probably due to ion blocking of surface sites, which decreases the rate of Cd uptake.

- Calcium carbonate production in the modern ocean does not play a significant role in determining the Cd isotope composition of surface seawater, with organically-bound Cd the dominant uptake mechanism in surface waters. Calcium carbonate sediments are only a minor sink for Cd in the modern ocean, but are a potentially valuable record of

past seawater $\epsilon^{114/110}$Cd.

Acknowledgements

We would like to thank the following people for their input throughout this study: A.J. Mason & N.S. Belshaw for keeping the mass spectrometers running; C.C. Day, S.G. Nielsen, A.L. Thomas, C.L. Blättler, & M. Rehkämper for helpful discussions; S. Wyatt for keeping the reagents flowing; W. Abouchami, S.J.G. Galer, & F. Wombacher for supplying reference standards; A.J. White for help with electron microscopy; R.B. Pearce and F. Minoletti for performing x-ray analyses; an anonymous referee, and M. Prieto for a particularly helpful and constructive review. T.J.H. is supported by Natural Environment Research Council (NERC) grant NE/G524060/1 with additional funding from Nu Instruments.

CHAPTER 5

Cadmium isotope evidence of Rayleigh fractionation during deep-sea coral biomineralization

A modified version of this chapter is in preparation for publication as: Horner, Henderson, Rickaby, and Adkins (in prep.) Cadmium isotope evidence of Rayleigh fractionation during deep-sea coral biomineralization.

"There has never been any doubt that corals write valuable information into their skeletons; it is their language that has remained blurry and ambiguous."

–*Barnes and Lough* (1996)

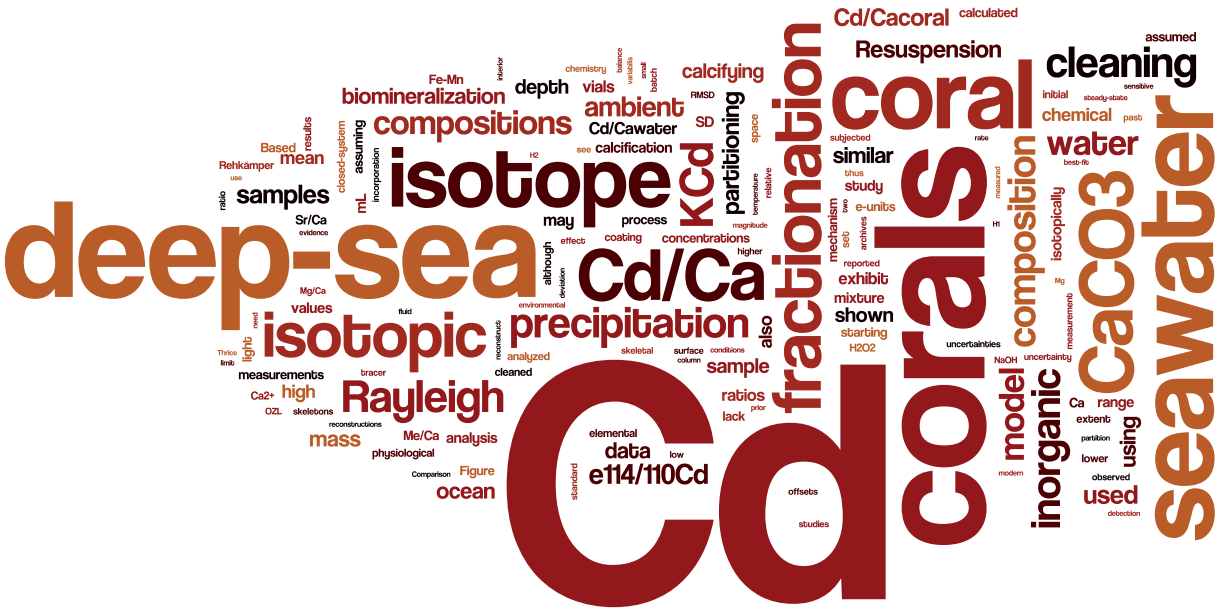

Abstract

The $CaCO_3$ skeletons of corals and other marine carbonates are valuable archives of past environmental conditions, and can be used to reconstruct past changes in seawater chemistry. The application of Cd isotopes, or any other tracer to palaeoceanography first requires that a suitable archive be identified. A complication arises as the majority of these archives are biominerals and contain a physiological overprint which must be deconvolved from the environmental signal for it to be meaningful in a palaeoceanographic sense. Unlike surface-dwelling corals, deep-sea corals grow in near-constant environments and lack photosymbionts, thereby allowing for the independent study of biomineralization. The similar ionic radii of Cd^{2+} and Ca^{2+} and the high equilibrium partition coefficient of Cd relative to Ca into $CaCO_3$, render Cd a sensitive tracer of coral biomineralization. Here we analyze a suite of modern deep-sea coral specimens for Cd/Ca and Cd isotope compositions. We find that the corals can be split into two populations: those which closely mimic assumed ambient seawater Cd/Ca and those which display high Cd/Ca that also shows some systematic variation along the length of the coral septa. This grouping does not correlate with water column depth, $Cd/Ca_{water\ est.}$, or coral species. Whilst the corals which mimic seawater Cd/Ca have Cd isotopic compositions similar to seawater ($\alpha_{coral-Cd_{SW}} \approx 1$), the high Cd/Ca corals exhibit light Cd isotope compositions similar to those observed during inorganic $CaCO_3$ precipitation ($\alpha_{coral-Cd_{SW}} = 0.99938 \pm 0.00019$). Together, the Cd/Ca and Cd isotope compositions of corraline $CaCO_3$ follow the predicted trend for closed-system Rayleigh fractionation in the calcifying space. These data demonstrate that Cd is highly sensitive to the balance between seawater exchange and $CaCO_3$ precipitation

and supports the commonly used Rayleigh fractionation model for deep-sea coral biomineralization. The lack of isotopic offsets between some corals and seawater will facilitate the application of Cd isotopes in deep-sea corals to palaeoceanography. Deep-sea corals may be used to reconstruct deep-ocean Cd isotope chemistry without the need for any environmental corrections (e.g. coral species, water depth, etc.), so long as corals are screened for high Cd/Ca prior to isotopic analysis.

5.1 Introduction

CADMIUM exhibits a nutrient-like profile in the modern ocean similar to that of P (as PO_4^{3-}; *Boyle et al.*, 1976). By measuring the Cd content of calcareous fossils, the Cd-P association has been extensively used to reconstruct past water mass distributions (e.g. *Boyle*, 1988) and the extent of nutrient utilization in the surface ocean (e.g. *Elderfield and Rickaby*, 2000). Recent developments in Cd isotope mass spectrometry have demonstrated that removal of Cd from seawater by phytoplankton leads to isotopic fractionation in culture (*Lacan et al.*, 2006) and the open ocean (*Ripperger and Rehkämper*, 2007; *Ripperger et al.*, 2007; *Abouchami et al.*, 2011; *Xue et al.*, 2011). Combined measurement of Cd isotopes and concentrations in seawater therefore allows multiple oceanic processes to be assessed (e.g. water-mass mixing and nutrient utilization).

Extending the utility of Cd isotope measurements to assess past ocean conditions requires sedimentary archives with sufficient temporal and spatial resolution, and with a high fidelity for the ambient seawater signal. Since many sedimentary archives are biominerals, they frequently exhibit a physiological component or 'vital effect', which complicates interpretation of the seawater signal (e.g. *Erez*, 1978; *McConnaughey*, 1989; *Adkins et al.*, 2003). By studying modern samples from controlled or near-constant environments, it is possible to understand the nature of the 'vital effect' and use this to interpret environmental signals obtained from fossil samples. Here we have chosen to assess the suitability of deep-sea corals to record ambient seawater Cd isotope compositions.

Unlike the surface ocean, the ocean interior (below $\sim$ 1,000 m) is largely homogeneous for Cd isotope compositions (*Ripperger et al.*, 2007; *Xue et al.*, 2011). This is thought to be a consequence of near-quantitative Cd removal from surface waters by marine phytoplankton and subsequent remineralization of this organic matter into the abyssal ocean (*Ripperger et al.*, 2007). Decay of phytoplankton organic matter increases [Cd] and effectively 'resets' deep ocean Cd isotope compositions. (This general water column structure is in accord with that observed for

the N isotope composition of dissolved nitrate; e.g. *Sigman et al.*, 1999, 2009.) Only two high-precision Cd isotopic water column profiles are currently published (*Ripperger et al.*, 2007; *Xue et al.*, 2011). Based on the current literature, we make the operational assumption that the deep ocean is entirely homogeneous for Cd isotopes, although future studies may reveal water column structure that is not currently evident. Because the samples we selected are from within the ocean interior, any observed skeletal compositional variability is entirely attributable to the process(es) of biomineralization, rather than water mass compositional variability or seasonality.

Deep-sea corals are ubiquitous in the water column and are typically found on seamounts between $500 - 2,500$ m (*Robinson et al.*, 2007). Deep-sea corals have linear growth rates on the order of mm yr^{-1} (*Adkins et al.*, 2004), allowing high-resolution water column reconstructions (e.g. *Smith et al.*, 1997; *Adkins et al.*, 1998). Previous studies have shown that deep-sea corals record the Nd isotopic composition of seawater (*van de Flierdt et al.*, 2010), ^{14}C concentrations (*Adkins et al.*, 1998; *Mangini et al.*, 1998; *Goldstein et al.*, 2001; *Adkins et al.*, 2002), and have been used to reconstruct seawater Cd/Ca (*Adkins et al.*, 1998).

To summarize some of the important aspects of deep-sea coral biomineralization, seawater is transported to the site of calcification (*Gagnon et al.*, 2012) through small paracellular pores ($\sim 10^1$ Å; *Tambutté et al.*, 2012). The pH of the calcifying fluid (seawater) is subsequently increased by a membrane-hosted Ca-type ATPase (or 'alkalinity pump') which removes H^+ and imports Ca^{2+} (*Al-Horani et al.*, 2003a,b; *Zoccola et al.*, 2004). Precipitation of $CaCO_3$ then occurs on an organic matrix (*Tambutté et al.*, 2007a) containing carbonic anhydrase (*Tambutté et al.*, 2007b), which serves to lower the activation energy of calcification. An important distinction between surface and deep-sea corals is the lack of photosymbionts. Because deep-sea corals cannot photosynthesize, they must consume POM (particulate organic matter) present in deep-ocean currents or sinking through the water column. Despite this, radiocarbon analysis of skeletal $CaCO_3$ has demonstrated that deep-sea corals precipitate their aragonitic skeletons from seawater DIC (dissolved inorganic carbon), and not POM (*Adkins et al.*, 2003).

Using these physiological constraints as a starting point, the trace element and isotopic composition of deep-sea coral $CaCO_3$ will reflect a combination of the environmental conditions both in the calcification environment (i.e. modified seawater) and the biologically-mediated partitioning of elements into a mineral phase. This partitioning should follow either a batch or steady-state model. In a batch process, the partitioning will follow a Rayleigh fractionation evolution (*Rayleigh*, 1896), whereby a 'parcel' of seawater is transported to the calcification site and precipitation occurs in a closed system until the seawater is eventually refreshed (*Elderfield et al.*, 1996; *Gagnon et al.*, 2007; *Gaetani et al.*, 2011; *Gagnon et al.*, 2012). In a steady-state model, seawater transport and calcification occur simultaneously and continuously (*Sinclair and Risk*, 2006; *Gagnon et al.*, 2012). High-precision co-located trace element profiles have so far been unable to distinguish between these models (e.g. *Gagnon et al.*, 2012). In reality, both models are essentially end-members of the same process, whereby the residence time of the seawater reservoir and the $CaCO_3$ precipitation rate determines the extent of Rayleigh vs. steady-state precipitation. In either scenario, the net result is that there should be systematic variation in geochemical tracers (e.g. Cd/Ca and Cd isotopes) that can be related to the coral physiology.

Here we apply a new isotopic tracer to deep-sea corals to test the nature of elemental and isotopic partitioning during skeletal biomineralization. Previous studies have shown that Cd has a high equilibrium partition coefficient into $CaCO_3$ (*Lorens*, 1981; *Tesoriero and Pankow*, 1996; *Prieto et al.*, 2003) and an isotopic fractionation factor (into inorganic calcite) that is insensitive to changes in temperature, ambient $[Mg^{2+}]$, or precipitation rate (Chapter 4). There is currently no calibration study that tests Cd isotope partitioning into inorganic aragonite. The results from a single synthetic aragonite are in agreement with the magnitude and direction of Cd isotopic fractionation observed during inorganic calcite precipitation (*Wombacher et al.*, 2003; Chapter 5). Assuming similar behaviour to inorganic calcite partitioning, the Cd/Ca and Cd isotope composition of deep-sea corals growing in a water mass of given Cd isotopic composition, should depend entirely on the balance between the rate of seawater turnover and $CaCO_3$ precipitation from the calcifying fluid. By examining a suite of modern samples, our investigation also per-

mits the investigation of the suitability of deep-sea corals as potential archives of past seawater Cd isotope compositions.

5.2 Methods

5.2.1 Samples

A suite of 11 modern deep-sea scleractinian corals were selected for analysis (Fig. 5.1). Samples were originally collected by means of benthic trawling, were recovered from drilling, or in some cases, collected by the manned submersible ALVIN directly from the seabed. The corals are kept in an extensive collection at Caltech, except for OZL 548 and OZL 549, which were recovered from Integrated Ocean Drilling Program Expedition 325 (e.g. *Beaman et al.*, in prep.). The sample set comprises nine specimens of *Demophyllum dianthus*, one *Madrepora oculata*, and one *Enallopsammia rostrata*. Six of the specimens were subsampled to examine spatial patterns of Cd/Ca and Cd isotopes within-coral. The specimens sample all major ocean basins, with a mean depth in the water column of $\approx 1,200$ (total range $750 - 2150$; Table 5.1). To examine the effect of chemical cleaning on Cd/Ca and Cd isotopes, a single specimen of *Solenosmilia variabilis* (unknown age) with a well-developed Fe-Mn coating was also selected for analysis (Fig. 5.2).

5.2.2 Deep-sea coral cleaning methods

The purpose of chemical cleaning is to remove non lattice-bound (i.e. contaminating) phases from the coral skeleton. Chemical cleaning methods followed established protocols, based largely on *Cheng et al.* (2000). A detailed step-by-step procedure is provided in Table 5.2. Briefly, corals were subjected to a series of chemical treatments whilst submersed in a sonicating vessel at 35 kHz. The exterior walls of the corals were pre-cleaned using H_2O and oxidizing solutions in 8 mL vials before crushing and transferring to 1.5 mL centrifuge vials. Corals were further

Table 5.1: Water column properties for the deep-sea coral samples analyzed in this study.

Sample name	Subsample	Latitude (+N,-S)	Longitude (+E,-W)	Depth (m)	$[PO_4^{3-}]^{\dagger}$ (μmol kg^{-1})	$[Cd]_{water\ est.}$* (nmol kg^{-1})	$(Cd/Ca)_{water\ est.}$* μmol mol^{-1}	$Cd/Ca^{\ddagger}_{coral}$ μmol mol^{-1}	K_D^{Cd}*	±2 SD*
JFA36.3	(1)	60.0417	-29.6667	1125	1.06	0.26	0.026	0.362	14.2	2.3
	(3)	60.0417	-29.6667	1125	1.06	0.26	0.026	0.192	7.5	1.2
	(2A)	60.0417	-29.6667	1125	1.06	0.26	0.026	0.204	8.0	1.3
JFA42.10	(1)	38.6900	-27.5533	1388	1.38	0.36	0.035	0.297	8.6	1.1
	(2)	38.6900	-27.5533	1388	1.38	0.36	0.035	0.302	8.7	1.1
	(3)	38.6900	-27.5533	1388	1.38	0.36	0.035	0.334	9.6	1.2
JFA68.1	-	-22.3150	43.0183	753	1.84	0.50	0.049	0.096	2.0	0.2
JFA84.1	-	-24.9067	-44.4333	1000	2.15	0.61	0.059	0.138	2.3	0.2
JFA41.26	(1)	38.2050	-26.4350	1113	1.08	0.27	0.026	0.457	17.5	2.8
	(2)	38.2050	-26.4350	1113	1.08	0.27	0.026	0.409	15.7	2.5
	(3)	38.2050	-26.4350	1113	1.08	0.27	0.026	0.033	1.3	0.2
84820-1	(1)	0.2333	-91.6000	806	2.98	0.92	0.090	1.002	11.2	0.6
	(2)	0.2333	-91.6000	806	2.98	0.92	0.090	0.876	9.8	0.5
	(3)	0.2333	-91.6000	806	2.98	0.92	0.090	0.617	6.9	0.4
78459	-	38.7500	-72.6500	2145	1.19	0.30	0.029	0.038	1.3	0.2
CEO804 H1	-	58.0000	-21.0000	1720	1.16	0.29	0.028	0.036	1.3	0.2
NBP0805 H2	-	-54.4000	-62.1000	816	2.16	0.61	0.060	0.104	1.7	0.1
OZL 548	(C)	-17.2901	146.9413	1100	2.32	0.67	0.065	0.077	1.2	0.1
	(D)	-17.2901	146.9413	1100	2.32	0.67	0.065	0.077	1.2	0.1
OZL 549	(A)	-17.2901	146.9413	1100	2.32	0.67	0.065	0.089	1.4	0.1
	(B)	-17.2901	146.9413	1100	2.32	0.67	0.065	0.092	1.4	0.1
B10 (cleaning exp.)	Cleaned	38.2030	-60.5350	1713	-	-	-	0.181	-	-
	Not cleaned	38.2030	-60.5350	1713	-	-	-	0.213	-	-

* See text for how this was calculated (and associated uncertainties).
† PO_4^{3-} data from the World Ocean Atlas (*Garcia et al.*, 2010)
‡ Uncertainty on Cd/Ca is less than 0.1 % relative standard deviation.

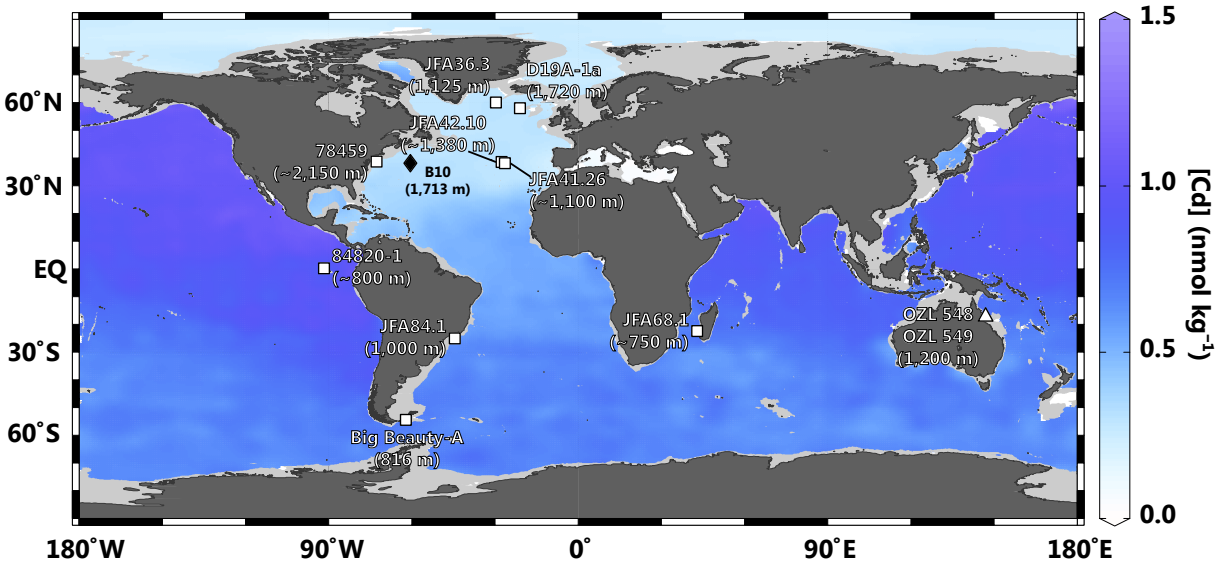

Figure 5.1: Map of the deep-sea coral sample locations used in this study. The colour shading represents estimated Cd concentrations at 1,200 m depth (corresponding to the mean depth of the sample set; see Sec. 5.4.1 for how [Cd] was estimated). *D. dianthus* are plotted as squares; *M. oculata* and *E. rostrata* are from the same location and plotted as a triangle; coral B10 (cleaning experiment; *S. variabilis*) is plotted as the filled diamond. Map drafted in Ocean Data View (*Schlitzer*, 2011).

pre-cleaned before transferring to acid-cleaned 1.5 mL centrifige vials and step-cleaned using alternating combinations of oxidizing and reducing agents, before leaching in dilute HNO_3 and EDTA (ethylenediaminetetraacetic acid). A final leach in dilute HNO_3 was performed in 7 mL polytetrafluoroethylene vials before digestion in 1 M HCl; 25 ± 9 % (1 SD) of the corraline aragonite was lost during chemical cleaning. All cleaning agents used were ultra-high purity (i.e. trace-metal clean), except in the case of N_2H_4, which was reagent grade. Coral cleaning was undertaken in Class 10 laminar flow workstations at The Oxford Isotope Laboratory for Earth Tracers (Class 1,000 clean facility).

5.2.3 Purification and analysis of Cd

Following dissolution, an aliquot containing ~ 20 μg of Ca was taken from each coral for multi-element analysis. Measurements were performed on a Thermo Scientific ELEMENT 2 HR-ICPMS (high-resolution inductively-coupled plasma mass spectrometer). The concentrations of Cd, Ba, U, Mg, Al, Mn, Fe, Zn, and Sr were quantified using a multi-point external standard calibration (typically two or three points, plus origin); Ca was used as the internal standard.

Table 5.2: Deep-sea coral cleaning procedure used in this study. The protocol is largely adapted from *Cheng et al.* (2000).

Reagent	Sonication	Repeat
8 mL polypropylene bottles		
18.2 MΩ H_2O	20 min.	Until supernatant remains clear
30 % H_2O_2 − 1 M NaOH mixture*	20 min.	-
18.2 MΩ H_2O	Resuspension only	Thrice
18.2 MΩ H_2O	1 min.	Twice
30 % H_2O_2 − 1 % $HClO_4$ mixture*	1 min.	-
18.2 MΩ H_2O	Resuspension only	Thrice
18.2 MΩ H_2O	1 min.	Twice
Crush samples and transfer to new vials		
1.5 mL polypropylene centrifuge vials		
18.2 MΩ H_2O	20 min.	Until supernatant remains clear
30 % H_2O_2 − 1 M NaOH mixture	20 min.	-
18.2 MΩ H_2O	Resuspension only	Thrice
18.2 MΩ H_2O	1 min.	Twice
Conc. CH_3OH	20 min.	-
18.2 MΩ H_2O	Resuspension only	Twice
18.2 MΩ H_2O	1 min.	Twice
30 % H_2O_2 − 1 % $HClO_4$ mixture	1 min.	-
18.2 MΩ H_2O	Resuspension only	Thrice
18.2 MΩ H_2O	1 min.	Twice
Use only acid-cleaned vials from this point		
1.5 mL polypropylene centrifuge vials		
Conc. CH_3OH	20 min.	-
18.2 MΩ H_2O	Resuspension only	Twice
18.2 MΩ H_2O	1 min.	Twice
0.2 % ΔHNO_3 †	1 min.	-
18.2 MΩ H_2O	Resuspension only	Twice
18.2 MΩ H_2O	1 min.	Twice
30 % H_2O_2 − 1 M NaOH mixture	20 min.	Shake for 2 min. post sonication
18.2 MΩ H_2O	Resuspension only	Twice
18.2 MΩ H_2O	1 min.	Twice
$C_6H_8O_7$−N_2H_4−NH_3 mixture‡	20 min.	-
18.2 MΩ H_2O	Resuspension only	Twice
18.2 MΩ H_2O	1 min.	Twice
30 % H_2O_2 − 1 M NaOH mixture	20 min.	Shake for 2 min. post sonication
18.2 MΩ H_2O	Resuspension only	Twice
18.2 MΩ H_2O	1 min.	Twice
0.2 % ΔHNO_3	1 min.	-
18.2 MΩ H_2O	Resuspension only	Twice
18.2 MΩ H_2O	1 min.	Twice
EDTA−1 M NaOH mixture	20 min.	-
18.2 MΩ H_2O	Resuspension only	Twice
18.2 MΩ H_2O	1 min.	Twice
Small (3 − 7 mL) polytetrafluoroethylene vials		
0.2 % ΔHNO_3	1 min.	-
18.2 MΩ H_2O	Resuspension only	Twice
Dry samples and re-weigh; ready for dissolution		

* Reagents mixed in a 1 : 1 ratio
† Δ denotes quartz-distilled
‡ Reagents mixed in a ratio of 1.6 : 1 : 13.3; N_2H_4 is deadly toxic, prepare in fume hood

Based on the measured Cd concentrations, a suitable amount of Cd double spike (^{111}Cd-^{113}Cd; see Chapter 2) was added to each sample prior to extraction chromatography.

Purification of Cd from the coral matrix followed existing chromatographic protocols described in detail elsewhere (e.g. *Wombacher et al.*, 2003; *Ripperger and Rehkämper*, 2007; Chapter 2). Following separation, samples were analyzed on a Nu Instruments multiple-collector ICPMS in 40×10 s integrations. Data reduction was performed offline using a MATLAB-based script to deconvolve sample isotopic compositions from spike-sample mixtures and isobaric Sn and In interferences. Cd isotope ratios are reported relative to NIST SRM 3108 Cd (*Abouchami et al.*, 2012), using the ϵ-notation (*Wombacher and Rehkämper*, 2004):

$$\epsilon^{114/110}\mathrm{Cd} = \left(\frac{^{114/110}\mathrm{Cd}_{\mathrm{sample}}}{^{114/110}\mathrm{Cd}_{\mathrm{NIST\ SRM\ 3108}}} - 1 \right) \times 10,000 \tag{5.2.1}$$

Uncertainties are calculated in three ways: $2\times$ SD of sample replicates (when $n \geq 5$), $2\times$ SD of the standard replicates from the same analysis session with similar [Cd] and spike:sample ratios as the samples themselves (this has previously been shown to be a good approximation of sample uncertainty; *Ripperger and Rehkämper*, 2007), or $2\times$ SE of the 40 integrations during the sample measurement; the reported uncertainty is always the largest of the three. The mean measurement uncertainty (≈ 0.8 ϵ-units) is significantly improved compared to previous work (± 1.3 ϵ-units; *Horner et al.*, 2011; Chapter 4) by means of a new double spike for instrumental mass bias correction (Chapter 2).

5.3 Results

5.3.1 Stepped cleaning results

The results for the cleaning experiment on coral B10 (*S. variabilis*) are shown in Fig. 5.2a. Nearly all elements show a decrease in their Me/Ca ratio post-chemical cleaning (except for Sr/Ca,

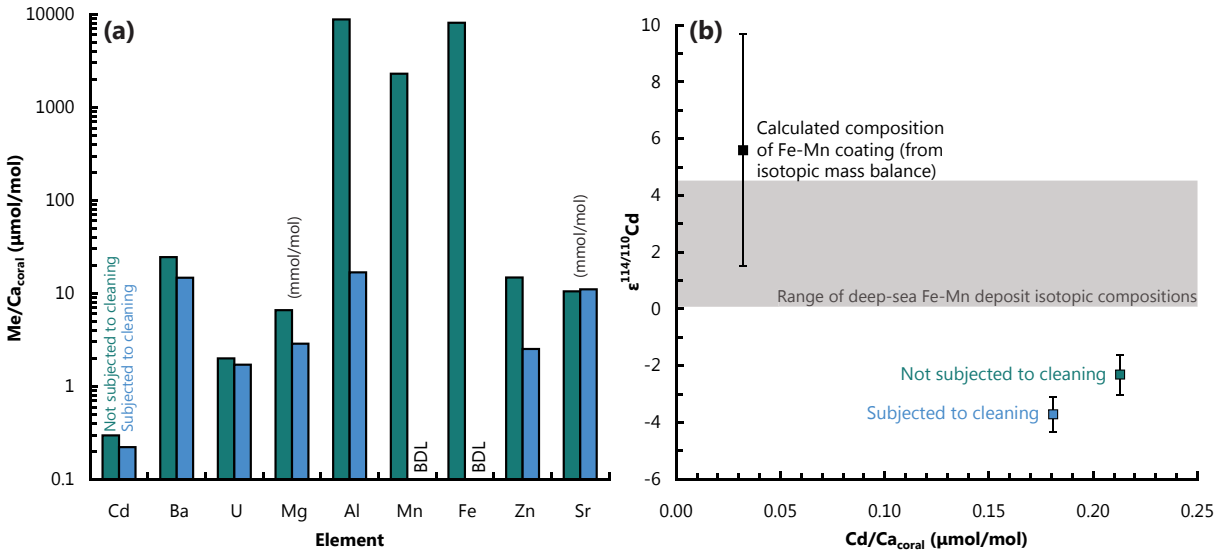

Figure 5.2: Deep-sea coral cleaning results. (a) Comparison of Me/Ca ratios for coral B10 (*S. variabilis*) before and after chemical cleaning. Mg/Ca and Sr/Ca are reported in mmol/mol. (BDL, below detection limit.) (b) Effect of chemical cleaning on the Cd isotope and Cd/Ca for coral B10.

which is within measurement uncertainty). Once the Fe-Mn coating had been chemically removed, both Fe/Ca and Mn/Ca were lower than the limit of detection. The small decrease in Cd/Ca between the uncleaned and cleaned coral suggests that the Fe-Mn coating contained very little of the extant Cd. This result is unsurprising given the high equilibrium partition coefficient for Cd into $CaCO_3$.

In addition to Me/Ca analysis, the Cd isotopic composition of coral B10 was also measured (Fig. 5.2b). The uncleaned specimen exhibited a Cd isotope composition of $\epsilon^{114/110}\text{Cd} = -2.3 \pm 0.7$ whereas the cleaned specimen was isotopically lighter with $\epsilon^{114/110}\text{Cd} = -3.7 \pm 0.6$. Based on an isotopic mass balance, the Cd isotope composition of the Fe-Mn coating was $\epsilon^{114/110}\text{Cd} = +5.6 \pm 4.1$, with a Cd content of $\sim 30\ \mu\text{g g}^{-1}$ (assuming that the coating was entirely composed of Fe and Mn with trace Cd). Both the Cd isotope composition and Cd content are similar to the ranges reported for deep-sea Fe-Mn deposits (*Schmitt et al.*, 2009b; *Horner et al.*, 2010).

5.3.2 Cd/Ca and Cd isotopic results

The corals exhibit a wide range in both Cd/Ca and Cd isotopic compositions (Fig. 5.3). Cd/Ca varies from 0.03 to 1.0 μmol mol^{-1} and Cd isotope compositions from -3.8 to $+4.5$ ϵ-units.

Table 5.3: Cd isotope and multi-element geochemical data for the deep-sea corals analyzed in this study.

Sample name	Subsample	$\epsilon^{114/110}$Cd	±2 SD	n†	$\alpha_{\text{coral}-\text{Cd}_{(\text{aq.})}}$*	±2 SD*	Multi-element data‡						
							Sr/Ca	Ba/Ca	U/Ca	Mg/Ca	Al/Ca	Mn/Ca	Fe/Ca
JFA36.3	(1)	-1.4	0.6	2	0.99949	0.00006	11.5	10.9	2.5	2.4	30.9	0.8	BDL
	(3)	0.3	0.8	1	0.99966	0.00008	11.5	10.5	1.8	2.9	26.4	0.8	BDL
	(2A)	-1.4	1.0	2	0.99949	0.00010	10.9	9.2	1.9	2.5	22.0	0.2	BDL
JFA42.10	(1)	1.0	0.8	5	0.99973	0.00008	10.7	8.8	2.3	2.3	23.3	1.5	BDL
	(2)	-	-	-	-	-	11.0	9.4	2.5	2.4	18.2	1.4	BDL
	(3)	0.2	0.7	1	0.99964	0.00007	11.1	9.4	2.3	2.5	17.7	3.9	BDL
JFA68.1	-	3.3	0.7	1	0.99996	0.00007	11.1	11.7	2.5	2.3	35.1	BDL	BDL
JFA84.1	-	2.6	0.6	1	0.99989	0.00006	11.4	13.6	1.9	2.7	30.4	2.7	BDL
JFA41.26	(1)	-0.1	0.5	7	0.99962	0.00005	11.0	9.0	2.8	2.0	13.4	BDL	BDL
	(2)	-0.6	0.6	4	0.99957	0.00006	11.1	9.2	2.0	2.8	45.8	0.5	3.6
	(3)	4.5	0.8	1	1.00008	0.00008	11.2	8.9	2.0	2.9	10.2	BDL	BDL
84820-1	(1)	-3.8	0.6	3	0.99925	0.00006	11.2	16.1	2.9	1.8	17.3	BDL	BDL
	(2)	-3.8	0.6	3	0.99925	0.00006	11.1	15.7	2.4	2.1	22.9	BDL	BDL
	(3)	-1.4	0.8	1	0.99949	0.00008	11.3	16.6	2.8	2.0	26.3	BDL	2.7
78459	-	3.6	0.6	1	0.99999	0.00006	10.7	9.0	1.9	2.4	18.6	BDL	BDL
CEO804 H1	-	2.4	1.1	1	0.99987	0.00011	10.7	8.4	1.2	2.5	-	0.3	4.6
NBP0805 H2	-	2.7	1.0	1	0.99990	0.00010	10.7	13.0	1.6	2.0	-	0.2	3.1
OZL 548	(C)	4.0	0.9	1	1.00003	0.00009	11.3	18.6	2.5	1.7	-	0.7	3.8
	(D)	4.2	0.9	1	1.00005	0.00009	11.2	19.0	2.5	1.7	-	0.8	5.2
OZL 549	(A)	4.1	1.2	1	1.00004	0.00012	11.3	19.3	2.6	1.8	-	1.7	9.1
	(B)	3.2	1.1	1	0.99995	0.00011	11.4	19.9	2.6	1.7	-	1.6	7.0
B10	Cleaned	-3.7	0.6	4	-	-	11.1	14.7	1.7	2.9	16.8	BDL	BDL
	Not cleaned	-2.3	0.7	2	-	-	10.5	24.5	2.0	6.6	8821	2301	8127

* See text for calculation and discussion of associated uncertainties

† Number of independent isotopic measurements

‡ Reported in μmol mol^{-1} except for Sr/Ca and Mg/Ca (mmol mol^{-1}); BDL, below detection limit.

Measurement uncertainties on Me/Ca ratios are typically $5-10$ % relative standard deviation.

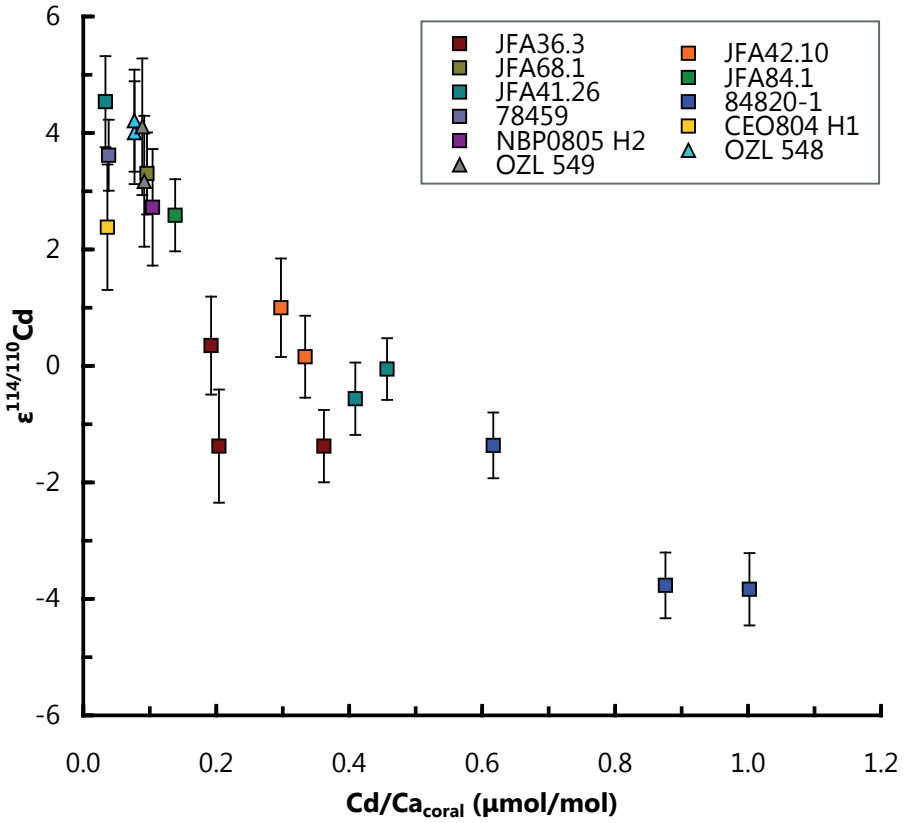

Figure 5.3: Deep-sea coral Cd isotope and Cd/Ca results. *D. dianthus* are shown as squares; OZL corals (*M. oculata* and *E. rostrata*) are shown as triangles. Cd isotope compositions against Cd/Ca_{coral} for all deep-sea corals analyzed.

Generally, the corals with lowest Cd/Ca have the isotopically heaviest compositions, whereas the higher Cd/Ca samples exhibit increasingly light Cd isotope values. The variability in Cd/Ca and $\epsilon^{114/110}$Cd does not correlate with other commonly measured Me/Ca proxies (e.g. Sr/Ca, Ba/Ca, U/Ca, etc.; maximum $R^2 \leq 0.3$; Table 5.3), nor with coral species, and cannot be attributed to insufficient chemical cleaning, as all corals displayed Fe/Ca and Mn/Ca ratios that were below, or close to, the limit of detection (~ 1 μmol mol^{-1}). There is no clear relationship between $\epsilon^{114/110}$Cd or Cd/Ca_{coral} with other water mass properties (e.g. depth, latitude, longitude, etc.; maximum $R^2 \leq 0.4$; Table 5.1).

5.4 Discussion

5.4.1 Elemental and isotopic partitioning of Cd

In the following discussion, we assume that the bulk – if not all – of the Cd precipitated in deep-sea coral skeletons is sourced from Cd dissolved in seawater, and not POM. The physiological constraints on skeletogenesis outlined in Sec. 5.1 suggest that seawater is the predominant source of dissolved ions (with the exception of Ca^{2+}). Additionally, radiocarbon measurements have demonstrated that 8 % of deep-sea coral skeletal C is sourced from POM (as an upper limit, but generally much less; *Adkins et al.*, 2003). We can estimate the proportion of skeletal Cd from POM by making several assumptions: Cd/C_{POM} is similar to average phytoplankton ($\approx 1.6 \times 10^{-6}$ mol mol^{-1}; *Ho et al.*, 2003); an average seawater Cd/DIC at 1,200 m depth of $\approx 2.7 \times 10^{-7}$ mol mol^{-1}; and that corals incorporate Cd into their skeleton in proportion to Cd/C_{POM} and Cd/DIC. Based on the upper limit of 8 % skeletal C sourced from POM (*Adkins et al.*, 2003), $\sim$ 70 % of skeletal Cd is sourced from dissolved Cd in seawater.

Elemental partitioning of Cd

The Cd concentration of the ocean interior is variable, and increases systematically between the Atlantic, Southern, Indian, and Pacific Oceans because of ocean circulation and the remineralization of Cd-bearing organic matter at depth (*Boyle*, 1988; Fig. 5.1). As such, Cd/Ca_{coral} reflects both the Cd/Ca of the ambient seawater and any physiological modulation during Cd incorporation into skeletal $CaCO_3$. Given that $[Cd]_{water}$ is not available for the coral collection sites, and the general sparsity of $[Cd]_{water}$ measurements, Cd/Ca_{water} must be estimated.

The global correlation of Cd and P permits estimation of $[Cd]_{water}$ from PO_4^{3-} measurements. The current database of co-located Cd and PO_4^{3-} measurements contains $\approx$ 1,200 data points (collated in *Rehkämper et al.*, 2011). Using this database, a polynomial relationship between $[PO_4^{3-}]$ (μmol kg^{-1}) and [Cd] (nmol kg^{-1}) was calculated. The model:

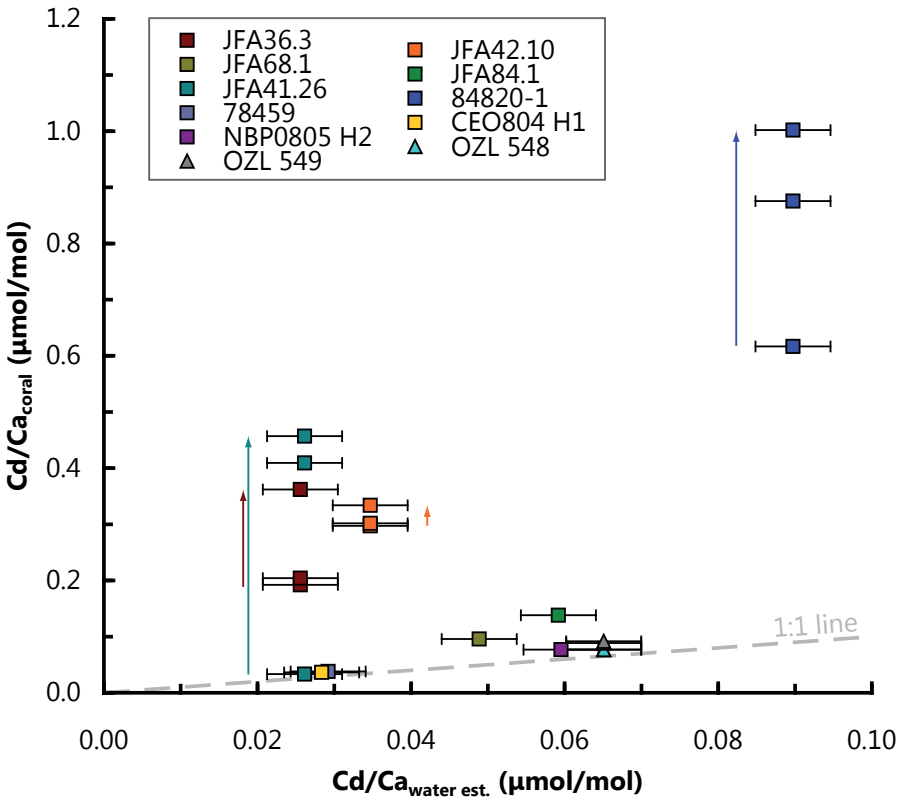

Figure 5.4: Deep-sea coral Cd elemental partitioning. Cd/Ca_{coral} against $Cd/Ca_{water\ est.}$ (see Sec. 5.4.1 for description of how $Cd/Ca_{water\ est.}$ was calculated). The $1:1$ line (i.e. $Cd/Ca_{coral} = Cd/Ca_{water\ est.}$; $K_D^{Cd} = 1$) is shown as the dashed grey line. Of the 11 corals analyzed, four significantly deviate from the $1:1$ line and show increasing Cd/Ca along the length of the coral (subsamples of the same coral and direction of coral growth are indicated by the respective arrows).

$$[\mathrm{Cd}] = 0.2146(\pm 0.0075) \times [\mathrm{PO_4^{3-}}] + 0.0321(\pm 0.0032) \times [\mathrm{PO_4^{3-}}]^2 \quad (5.4.1)$$

fits the data with an RMSD (root-mean-square deviation) = 0.1 nmol kg^{-1}; the uncertainties on the polynomial coefficients are ±1 SD). Spatially-averaged [Cd] values were obtained from mean annual [PO_4^{3-}] estimates (World Ocean Atlas; *Garcia et al.*, 2010). A depth slice of $[Cd]_{\text{water est.}}$ at 1,200 m (corresponding to the mean deep-sea coral recovery depth for this study) is shown in Fig. 5.1. Assuming a constant [Ca] of 10.3 mmol kg^{-1}, $Cd/Ca_{\text{water est.}}$ was calculated for each site (Table 5.3), and by comparison with Cd/Ca_{coral}, converted to an empirical partition coefficient, K_D^{Cd}, using:

$$K_D^{Cd} = \left(\frac{Cd}{Ca}\right)_{\text{coral}} / \left(\frac{Cd}{Ca}\right)_{\text{water est.}} \quad (5.4.2)$$

In this notation, $Cd/Ca_{\text{water est.}}$ refers to the total (analytical) concentrations, and does not make assumptions regarding aqueous speciation (i.e. $K_D^{Cd} = 1$ means that both the coral and water mass have identical Cd/Ca). Comparison of Cd/Ca_{coral} and $Cd/Ca_{\text{water est.}}$ reveals that four corals are significantly enriched in Cd compared to the ambient water mass (Fig. 5.4). Cd/Ca_{coral} also appears to increase along the length of the coral (higher Cd/Ca_{coral} towards the most recent growth). The remaining seven corals exhibit Cd/Ca ratios similar to the ambient water mass (i.e. $K_D^{Cd} \approx 1$; Fig. 5.4).

Isotopic partitioning of Cd

Unlike the Cd concentration, the Cd isotope composition of the ocean interior is thought to be largely homogeneous ($\epsilon^{114/110}Cd \approx +3$; *Ripperger et al.*, 2007; *Xue et al.*, 2011). The lack of variation has been attributed to the near-quantitative uptake of Cd from surface seawater (by phytoplankton) and subsequent remineralization at depth (*Ripperger et al.*, 2007; *Rehkämper et al.*, 2011). Based on this observation, deep-sea coral Cd isotope compositions can be expressed as

fractionation factors, α (i.e. the deviation between the assumed ambient seawater composition and the coral):

$$\alpha_{\text{coral}-\text{Cd}_{(\text{aq.})}} = \frac{R_{\text{coral}}}{R_{\text{Cd}_{(\text{aq.})}}} \tag{5.4.3}$$

where R_{coral} and $R_{\text{Cd}_{(\text{aq.})}}$ refer to the $^{114/110}$Cd ratio of the coral and the ambient seawater, respectively. Fractionation factors were calculated for each coral assuming an initial seawater composition of $\epsilon^{114/110}\text{Cd} = +3.7$ (see Sec. 5.4.3; Table 5.3). Normalization demonstrates that corals are either isotopically similar to assumed ambient seawater ($\alpha_{\text{coral}-\text{Cd}_{(\text{aq.})}} \approx 1$) or enriched in the light isotopes of Cd ($\alpha_{\text{coral}-\text{Cd}_{(\text{aq.})}} < 1$).

There is tentative evidence to suggest that the abyssal Atlantic may be isotopically heavier than the Pacific by about $1-2$ ϵ-units (cf. *Ripperger et al.*, 2007; *Xue et al.*, 2011). This may account for some of the scatter between the deep-sea coral Cd isotope compositions. The sparse coverage of seawater Cd isotope measurements does not permit the normalization of corals to different seawater starting $\epsilon^{114/110}$Cd values, although as more seawater profiles are measured (as part of the GEOTRACES program; *GEOTRACES Planning Group*, 2006), better normalizations may be possible.

5.4.2 Comparison with inorganic $CaCO_3$ precipitation

Calculated K_D^{Cd} and $\alpha_{\text{coral}-\text{Cd}_{(\text{aq.})}}$ values for the deep-sea corals can be directly compared with inorganic precipitation experiments (Fig. 5.5). Variations in extrinsic water mass properties, such as temperature, precipitation rate, or Mg concentration, affect K_D^{Cd}, both for inorganic precipitates (e.g. *Lorens*, 1981; *Tesoriero and Pankow*, 1996; *Prieto et al.*, 2003; Fig. 5.5) and biogenic $CaCO_3$ (e.g. *Rickaby and Elderfield*, 1999). Cd isotopic fractionation into inorganic calcite is not affected by these variables (*Horner et al.*, 2011; Chapter 4), with a mean $\alpha_{\text{inorg. CaCO}_3-\text{Cd}_{(\text{aq.})}} = 0.99955 \pm 0.00012$ across a wide range of K_D^{Cd} values (i.e. carbonates are 4.5 ± 1.2 ϵ-units lighter

than the ambient seawater; Fig. 5.5). The proposed mechanism for Cd isotopic fractionation during incorporation into inorganic $CaCO_3$ is thought to relate to a kinetic isotope effect at the mineral surface, modulated by ion blocking of crystal surface sites (*Horner et al.*, 2011). Although this inorganic data is for calcite rather than the aragonite of deep-sea corals, it represents the only present assessment of Cd isotope fractionation into $CaCO_3$.

Using inorganic $CaCO_3$ values as a starting point, the deep-sea corals can be split into two populations. The first population has low Cd/Ca (< 0.2 μmol mol^{-1}; $K_D^{Cd} < 4$) and unfractionated Cd isotope compositions ($\alpha_{coral-Cd_{(aq.)}} \approx 1$) whereas the second possesses higher Cd/Ca (> 0.2 μmol mol^{-1}; $K_D^{Cd} > 4$) and light Cd isotope compositions (mean $\alpha_{coral-Cd_{(aq.)}} = 0.99952$). This second group of corals exhibit a similar magnitude of Cd isotopic fractionation to that during inorganic calcite growth ($\alpha_{inorg.\ CaCO_3-Cd_{(aq.)}} = 0.99955$; *Horner et al.*, 2011). Based on the inorganic experiments, the Cd isotopic composition of deep-sea coral $CaCO_3$ should be insensitive to conditions in the calcification environment. Observed Cd isotope variation of deep-sea coral $CaCO_3$ should instead reflect the biologically-mediated partitioning of Cd into $CaCO_3$. The similarity of isotopic fractionation patterns between inorganic and deep-sea coral $CaCO_3$ implies that a similar mechanism may be controlling Cd (and Cd isotope) partitioning. This is not entirely surprising given the low degree of physiological mediation of calcification in deep-sea corals (e.g. *Barnes*, 1970). The organic matrix – the calcification template – may not play a significant role in modulating Cd isotope partitioning into deep-sea corals, but instead acts as a passive catalyst for precipitation (e.g. *Rickaby and Schrag*, 2005).

5.4.3 Evidence of Rayleigh fractionation

The direction and maximum magnitude and direction of Cd isotope fractionation observed in deep-sea coral $CaCO_3$ is in agreement with inorganically-precipitated $CaCO_3$, although this does not explain the low-K_D^{Cd} corals with$\alpha_{coral-Cd_{(aq.)}} \approx 1$. The observation that these 'unfractionated' corals also exhibit low K_D^{Cd} values (Fig. 5.5) implies that a common process controls

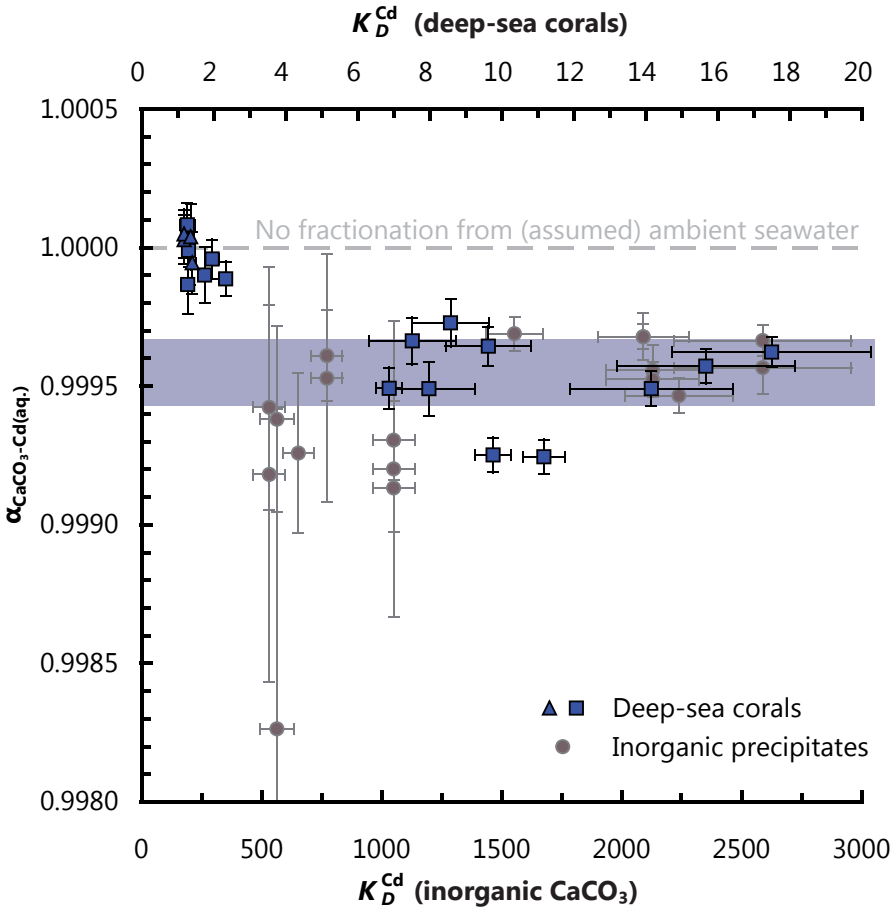

Figure 5.5: Comparison of deep-sea corals with inorganic $CaCO_3$ precipitates. The expected Cd isotopic fractionation for inorganic $CaCO_3$ is shown as the purple shaded bar ($\alpha_{\text{inorg.}CaCO_3-Cd_{(aq.)}} = 0.99955 \pm 0.00012$; *Horner et al.*, 2011), and is near-constant across a wide-range of K_D^{Cd} values. The much larger K_D^{Cd} values of inorganically-precipitated $CaCO_3$ reflects a slight difference in the calculation method as follows: in the inorganic K_D^{Cd} formulation, the activity of the free aquo-ion (e.g. Cd^{2+} or Ca^{2+}) is used instead of the total concentration. Since the activity ratio of Cd/Ca in the calcifying space is not known for deep-sea corals, the empirical formulation of K_D^{Cd} is used (i.e. total analytical concentrations).

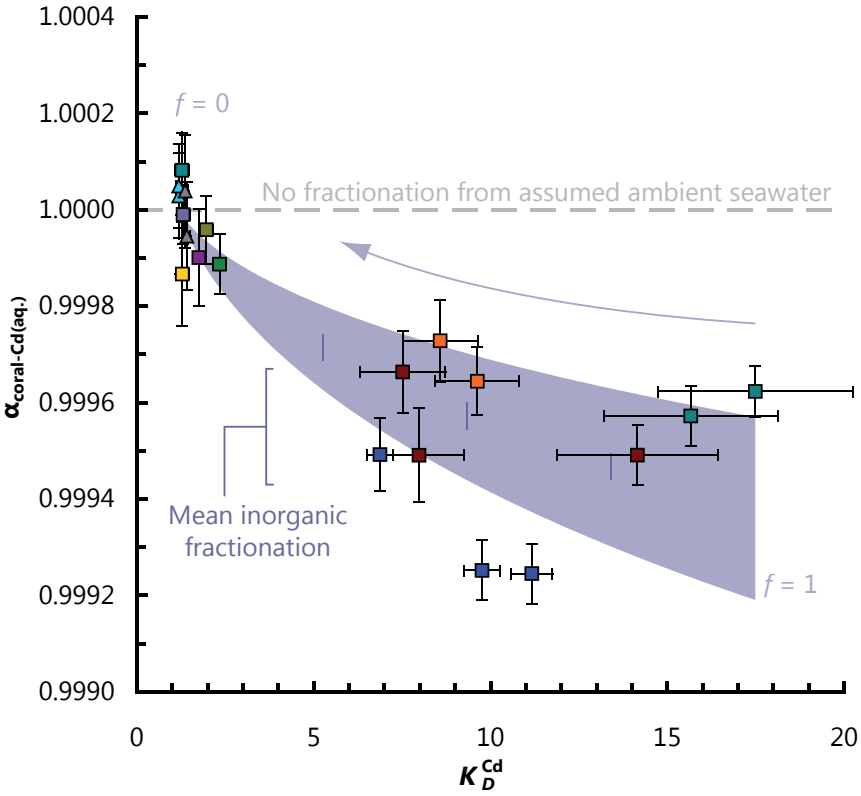

Figure 5.6: Closed-system Rayleigh fractionation during deep-sea coral biomineralization. Coral symbols as in Figs. 5.3, 5.4. The best-fit closed system Rayleigh model for the accumulated product is shown as the purple shaded region, assuming an initial seawater composition of $\epsilon^{114/110}\text{Cd} = +3.7$. Rayleigh fractionation proceeds from $f = 1$ to $f = 0$ (i.e. the fraction of dissolved Cd remaining in the calcifying space; Eq. 5.4.4), as denoted by the arrow. (Additional 'notches' are shown at $f = 0.75$, 0.50, and 0.25.) The range of fractionation factors used is $\alpha_{\text{coral}-\text{Cd}_{(\text{aq.})}} = 0.99919 - 0.99957$, as this range corresponds to the RMSD minimum in Fig 5.7d.

both K_D^{Cd} and $\alpha_{\text{coral}-\text{Cd}_{(\text{aq.})}}$.

A Rayleigh-type process has previously been invoked to explain elemental partitioning into biogenic $CaCO_3$ in calcareous foraminifera and corals (e.g. *Elderfield et al.*, 1996; *Gagnon et al.*, 2007). By using the same elemental and isotopic tracer, we can test the applicability of the Rayleigh fractionation model without the need to compare multiple Me/Ca ratios (e.g. Mg/Ca, Sr/Ca, Ba/Ca). We start by assuming that the corals will follow the closed-system trend for the accumulated product, $R_{\text{acc.}}$, a reasonable assumption given the physiological constrains on skeletogenesis (e.g. *Adkins et al.*, 2003; *Tambutté et al.*, 2012):

$$R_{\text{acc.}} = \frac{1 - f^{\alpha_{\text{coral}-\text{Cd}_{(\text{aq.})}}}}{1 - f} \tag{5.4.4}$$

where f is the proportion of Cd remaining in the calcifying space after a given amount of $CaCO_3$ precipitation. If $f = 1$ and $f = 0$ are set by the corals with the highest and lowest K_D^{Cd}, respectively, the Cd isotopic composition of deep-sea coral $CaCO_3$ should depend solely on the extent of $CaCO_3$ precipitation. (The sensitivity of the model to the assumption that $f = 1$ corresponds to $K_D^{Cd} = 17.5$ is shown in Fig. 5.7.) Once precipitation from the initial 'parcel' of seawater begins, the first skeletal $CaCO_3$ will have an elevated Cd/Ca (relative to the starting seawater because of the high equilibrium K_D^{Cd} for Cd into $CaCO_3$) and a light Cd isotope composition (the magnitude of isotopic fractionation is set by $\alpha_{coral-Cd_{(aq.)}}$). As precipitation continues, the cumulative Cd/Ca and $\epsilon^{114/110}$Cd of the skeleton will tend towards the starting seawater composition (i.e. $\alpha_{coral-Cd_{(aq.)}} \approx 1$; $K_D^{Cd} \approx 1$; Fig. 5.6).

The Rayleigh model is shown for a range of $\alpha_{coral-Cd_{(aq.)}}$ between $0.99919 - 0.99957$ in Fig. 5.6, corresponding to an RMSD misfit of < 1.5 ϵ-units. The sensitivity of the parameters in the Rayleigh model was investigated over a range of $\alpha_{coral-Cd_{(aq.)}}$, starting seawater compositions, as well as the range of f values (Fig. 5.7). The misfit is expressed as the RMSD between the corals and the model. The best-fit parameters were identified (using the interior-point method, e.g. *Wright*, 2004) as $\alpha_{coral-Cd_{(aq.)}} = 0.99938$ and a starting seawater composition of $\epsilon^{114/110}Cd = +3.7$ (best-fit model RMSD $= 1.3$ ϵ-units). That the best-fit convergence occurs at values of $\epsilon^{114/110}$Cd and $\alpha_{coral-Cd_{(aq.)}}$ that are representative of the interior ocean $\epsilon^{114/110}$Cd (*Ripperger et al.*, 2007; *Xue et al.*, 2011) and experimentally-determined $\alpha_{calcite-Cd_{(aq.)}}$ (*Horner et al.*, 2011), gives us confidence in the model.

Because Cd has a large inorganic partition coefficient into $CaCO_3$ and [Cd] << [Ca] (in seawater), Cd is a particularly sensitive tracer of Rayleigh fractionation during skeletal biomineralization. This is because the initial pool of Cd will be rapidly depleted by $CaCO_3$ precipitation if the original seawater 'parcel' is not periodically refreshed. The ability of the Rayleigh model to capture the main features of the dataset, including the corals which do not exhibit any Cd isotope fractionation, suggests that this relatively simple biomineralization model is applicable for Cd and Cd isotope incorporation into deep-sea coral $CaCO_3$ during skeletogenesis.

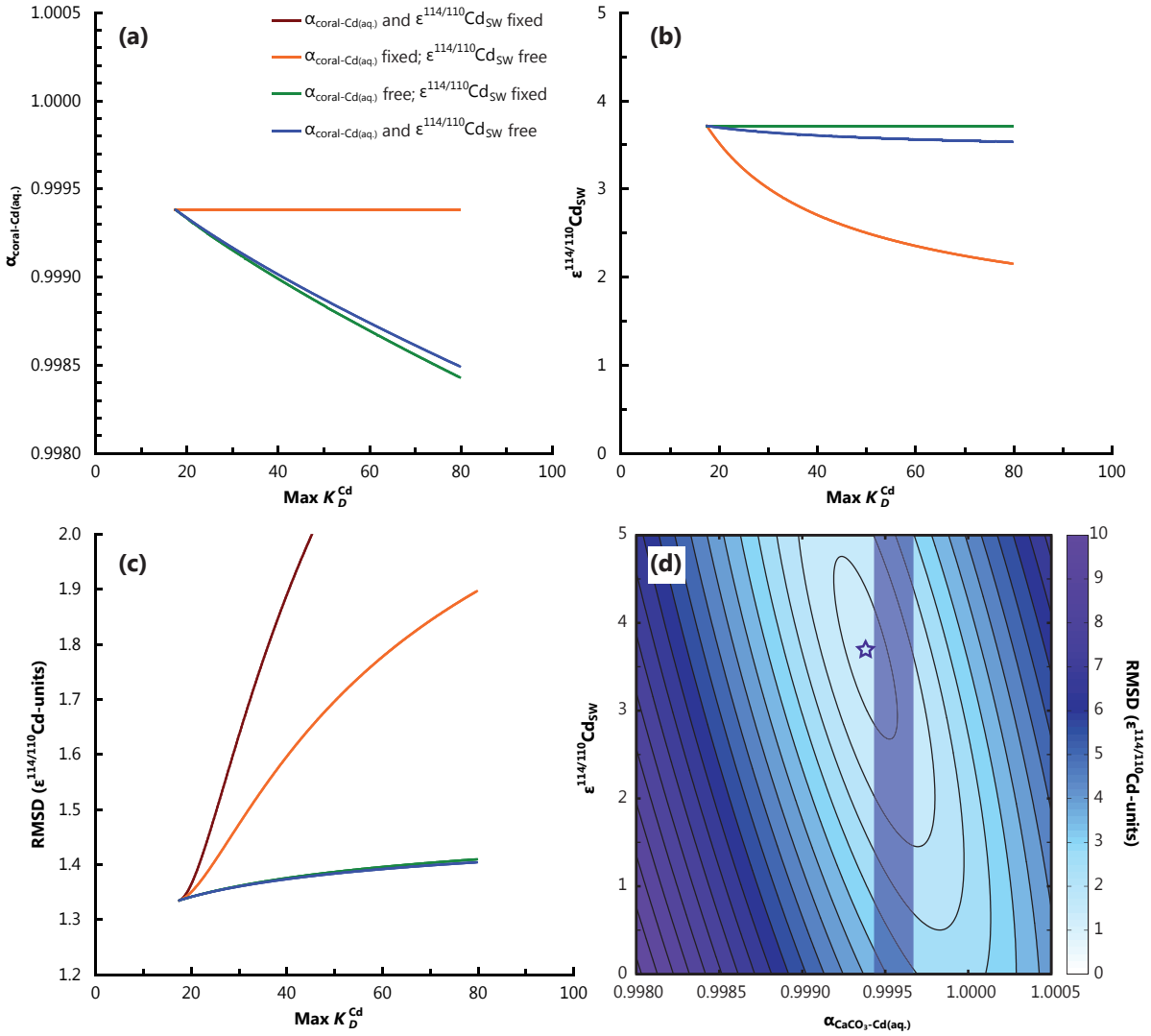

Figure 5.7: Sensitivity of the Rayleigh model to initial parameters. In the Rayleigh model (shown in Fig. 5.6), $f = 1$ is set by the coral with the highest value of K_D^{Cd}. In panels (a)–(c) the effect of changing the maximum value of K_D^{Cd} (i.e. we assume that there other deep-sea corals with higher K_D^{Cd} values that we have yet to find and analyze) is investigated across four scenarios: $\epsilon^{114/110}Cd_{SW}$ initial and $\alpha_{coral-Cd_{(aq.)}}$ are fixed across the range of K_D^{Cd} (at +3.7 and 0.99938, respectively); $\alpha_{coral-Cd_{(aq.)}} = 0.99938$ but $\epsilon^{114/110}Cd_{SW}$ is free; $\alpha_{coral-Cd_{(aq.)}}$ is free but $\epsilon^{114/110}Cd_{SW} = +3.7$; both $\alpha_{coral-Cd_{(aq.)}}$ and $\epsilon^{114/110}Cd_{SW}$ are free. Best-fit (lowest RMSD) 'free' parameters were optimized for each value of K_D^{Cd} using the interior-point method. (a) Best-fit $\alpha_{coral-Cd_{(aq.)}}$ and (b) initial $\epsilon^{114/110}Cd_{SW}$ across a range of maximum K_D^{Cd}. (c) RMSD-misfit for the scenarios shown in (a) and (b), demonstrating that the best-fit between the model and data occurs when the maximum $K_D^{Cd} = 17.5$ (i.e. set by the highest observed value). (d) RMSD misfit of the Rayleigh model across a range of initial $\epsilon^{114/110}Cd_{SW}$ and $\alpha_{coral-Cd_{(aq.)}}$ for a maximum $K_D^{Cd} = 17.5$. The global minimum – the star – corresponds to parameters used in Fig. 5.6. The vertical shaded bar represents the Cd isotope fractionation expected for inorganic $CaCO_3$ precipitation (*Horner et al.*, 2011).

5.4.4 A possible mechanism and implications for palaeoceanography

Although the model may account for the spread in the data, it does not address the reason for varying degrees of closed-system Rayleigh fractionation observed in deep-sea corals. The model implies that the high-K_D^{Cd} and isotopically fractionated corals are refreshing their Cd – and therefore seawater – supply faster than $CaCO_3$ precipitation. With each batch of seawater transport, only a small proportion of the initially-present Cd is removed (i.e. $f > 0.5$; Fig. 5.6) before the system is refreshed and the next batch of precipitation begins. The low-K_D^{Cd} and isotopically 'normal' corals appear to precipitate almost all of the Cd present in the calcifying fluid before the seawater is refreshed.

Since the extent of Cd enrichment and Cd isotopic fractionation is related to the rate of seawater turnover, the driving mechanism is likely to be physiological. Whilst DIC can 'leak' into the calcifying space (*Adkins et al.*, 2003), charged metal ions cannot, thus the starting Cd/Ca and Cd isotope composition of the calcifying fluid are fixed at the time of seawater vacuolization (although Cd/Ca can be lowered by alkalinity pumping, i.e. Ca^{2+} import coupled with H^+ antiport). The extent of Rayleigh fractionation (f) observed for Cd/Ca and Cd isotopes is then set by the balance between closed-system $CaCO_3$ precipitation relative to the rate of seawater resupply. This pattern can then be modulated by the amount of alkalinity pumping in the coral (i.e. $Ca^{2+} - 2H^+$ exchange) prior to $CaCO_3$ precipitation (*Adkins et al.*, 2003; *Al-Horani et al.*, 2003a; *Zoccola et al.*, 2004; *Gagnon et al.*, 2012). If alkalinity pumping continues, the Cd/Ca of the calcifying space will continue to decrease, and a higher proportion of the vacuolized Cd will be precipitated into the corraline $CaCO_3$ ($f \rightarrow 0$). The reason(s) for the varying rates of seawater turnover relative to $CaCO_3$ precipitation (and potentially alkalinity pumping) remain to be identified, although we can rule out depth, $[Cd]_{water\ est.}$, or ocean basin as the primary driving mechanism. In the absence of more detailed physiological information, this tentative mechanism should only be considered as a working hypothesis.

The data presented here can also be considered as a 'core-top' study with which to interpret

palaeoceanographic records of Cd isotopes from deep-sea corals. The lack of Cd isotope offsets between the low-K_D^{Cd} corals enables the direct reconstruction of deep-ocean seawater Cd isotope chemistry, if the corals are accurately dated. Importantly, the Rayleigh model presented here demonstrates that these reconstructions need not account for differences in coral species, temperature, or depth, as the dominant control on fractionation is set by the extent of Rayleigh fractionation. Future studies examining Cd isotopes from deep-sea corals should screen samples for high Cd/Ca prior to Cd isotopic analysis (this could be done before chemical cleaning as the majority of the Cd in deep-sea corals is lattice-bound; Fig. 5.2). Based on the data in Fig. 5.3, a cutoff of $Cd/Ca_{coral} \sim 0.2$ μmol mol^{-1} should be used, although samples recovered from lower Cd/Ca_{water} basins (e.g. the Atlantic) should use a lower cutoff (perhaps as low as $Cd/Ca_{coral} \sim 0.1$ μmol mol^{-1}). If the proximate cause of the high K_D^{Cd} corals can be successfully identified, these corals may also prove useful in reconstructing local seawater conditions (rather than seawater Cd isotope chemistry). The Rayleigh mechanism for Cd isotopes posited here for deep-sea corals may also be applicable to other calcifying organisms that vacuolize seawater prior to $CaCO_3$ precipitation (e.g. calcareous foraminifera; *Bentov et al.*, 2009, or other species of coral), negating the need for species-specific calibrations. Further core-top studies are required to investigate this model of Cd isotopic incorporation into $CaCO_3$ before Cd isotopes can be routinely applied to palaeoceanography.

5.5 Conclusions

- Deep-sea corals fall into two groups for Cd/Ca and Cd isotopes: a group with low K_D^{Cd} and 'unfractionated' Cd isotope compositions (i.e. $\alpha_{coral-Cd_{(aq.)}} \approx 1$); and a group with variable and high K_D^{Cd} and isotopically light Cd isotope compositions (i.e. $\alpha_{coral-Cd_{(aq.)}} < 1$). The grouping is not related to ocean basin, depth, or $[Cd]_{seawater}$.

- The isotopically light corals exhibit the same magnitude of Cd isotopic fractionation as seen during inorganic $CaCO_3$ precipitation, suggesting a similar mechanism of Cd

isotope fractionation ($\alpha_{\text{coral}-\text{Cd}_{(\text{aq.})}} = 0.99938 \pm 0.00019$; $\alpha_{\text{inorg. CaCO}_3-\text{Cd}_{(\text{aq.})}} = 0.99955 \pm 0.00012$).

- The Cd/Ca and Cd isotope composition of deep-sea coral skeletons follows the predicted trend for closed-system Rayleigh fractionation from a semi-enclosed calcifying space during skeletogenesis.

- The lack of species-specific or other offsets in Cd isotope compositions between some corals and ambient seawater will enable deep-sea corals to be used in temporal reconstructions of seawater Cd isotope chemistry, although reconnaissance screening for high Cd/Ca should take place before samples are processed for isotopic analysis.

Acknowledgements

We would like to thank P.F. Holdship for performing multi-element ICPMS analyses; N. Thiagarajan for help with coral sampling; M.E. Auro for advice on chemical cleaning techniques; Z. Xue for sharing the seawater Cd-PO_4^{3-} database; A.C Gagnon and J.A. Murtaugh for discussions; A.L. Thomas and L.F. Robinson for sharing samples. T.J.H is supported by NERC (NE/G524060/1) and Nu Instruments.

Chapter 6

Conclusions, outlook, and closing remarks

"Although nature commences with reason and ends in experience it is necessary for us to do the opposite, that is to commence with experience and from this to proceed to investigate the reason."

–attributed to Leonardo da Vinci

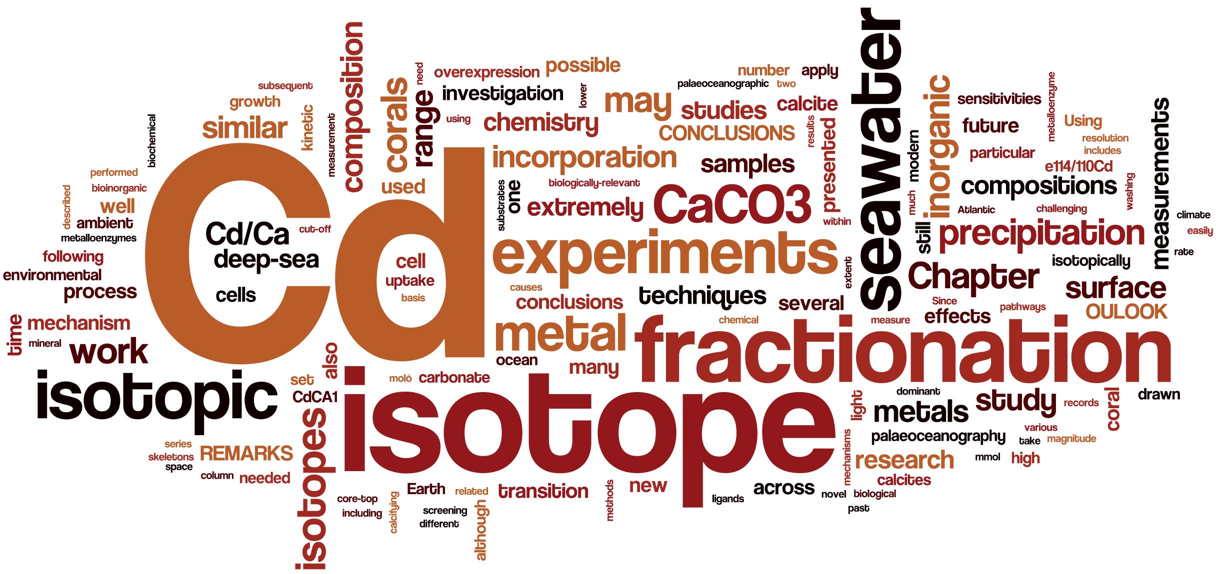

6.1 Conclusions

THE work presented in this thesis addresses the two major questions outlined in the Introduction. *Why* does Cd behave like an algal nutrient, and *how* can measurements of [Cd] and Cd isotopes be applied to palaeoceanography? The preceding chapters presented a number of novel studies into the causes of Cd isotope fractionation in the marine realm and offer several new conclusions.

In Chapter 2, the methods required to measure Cd isotopes in geological materials both precisely and accurately are discussed. This step-by-step guide describes the analytical considerations that are the common basis to the measurement of many isotope systems. This includes a detailed description of instrumental mass bias calculations and subsequent corrections (i.e. the double spike), as well as the chemical separation procedures. From this it is possible to apply Cd isotope measurements to actual samples.

In Chapter 3, Cd isotopes are applied to address the *why?* Using a systematic experimental approach, the following conclusions can be drawn from the work:

- When performing cell culturing experiments, it is important to quantify any effects that cell harvesting or washing may have on the results. In the case of the experiments described here, more intense cell washing was shown to increase the apparent isotopic fractionation factor (i.e. more aggressively washed cells displayed isotopically lighter compositions).

- Using standard biochemical techniques, it is possible to pull cells apart and measure distinct intracellular isotopic compositions of different cellular components. In the case of Cd, this includes the catalytic metal atoms from the CdCA1 metalloenzyme that had been expressed, *in vivo*, in a heterologous system.

- The overexpression of CdCA1 metalloenzyme was not a significant contributor to the isotopic composition of whole bacterial cells, despite the enzyme being one of the dominant

cellular functions (i.e. overexpression) and its extremely fractionated Cd isotope composition ($\epsilon^{114/110}Cd_{CdCA1} = -5.9 \pm 0.7$). The largest pool of internalized Cd in these cells was found to be non-specifically-bound Cd in the cytosol, with an 'unfractionated' Cd isotope composition similar to the growth medium ($\epsilon^{114/110}Cd_{CdL} = -0.9 \pm 0.6$).

- Cells both with and without overexpression of CdCA1 exhibited light Cd isotope compositions ($\alpha_{cells-Cd_{(aq.)}} \approx 0.9996$). This fractionation was localized to the cell membranes, a process attributed to Cd homeostasis (i.e. avoiding toxicity) following the accidental import of Cd from the growth medium.

- This process of unavoidable uptake and subsequent homeostasis can explain the nutrient-like distribution of Cd in seawater, and may contribute to the elemental and isotopic distributions of other metals in seawater, even for those commonly considered as micronutrients.

The *how* is addressed across two Chapters (i.e. *how* can measurements of [Cd] and Cd isotopes be applied to palaeoceanography?). In Chapter 4, a series of inorganic precipitation experiments are used to calculate fractionation factors for Cd during incorporation into calcite across a range of environmental conditions. From these experiments, the following conclusions may be drawn:

- The isotopic fractionation factor for Cd during inorganic calcite growth in a seawater matrix is $\alpha_{CaCO_3-Cd_{(aq)}} = 0.99955 \pm 0.00012$ and is insensitive to temperature, ambient [Mg^{2+}], or precipitation rate (across the range studied). This result suggests, assuming that biogenic calcites fractionate Cd in a similar manner to inorganic calcites, that records of calcium carbonate $\epsilon^{114/110}$Cd may be representative of variations in seawater $\epsilon^{114/110}$Cd in the past, rather than changes in $\alpha_{CaCO_3-Cd_{(aq)}}$ with time (caused by varying environmental parameters).

- In contrast to calcite grown in seawater, $\alpha_{CaCO_3-Cd_{(aq)}}$ for calcites grown in freshwater is within uncertainty of one (i.e. no isotopic fractionation).

- The contrasting isotopic behaviour of Cd during incorporation into calcite during saline vs. freshwater experiments points towards a salinity control on Cd isotope fractionation. The mechanism of Cd isotope fractionation may be related to kinetic isotope effects during the largely unidirectional incorporation of Cd at the mineral surface. This process becomes more pronounced at high salinity, probably due to ion blocking of surface sites, which decreases the rate of Cd uptake.

- Calcium carbonate production in the modern ocean does not play a significant role in determining the Cd isotope composition of surface seawater. Organically-bound Cd provides the dominant uptake mechanism in surface waters. Calcium carbonate sediments are only a minor sink for Cd in the modern ocean, but are a potentially valuable record of past seawater $\epsilon^{114/110}$Cd.

Using the inorganic experiments as a reference point, the *how* is realized by applying Cd isotopes to natural $CaCO_3$ samples (Chapter 5). By using modern samples, this study acts as both an investigation studying Cd incorporation into natural $CaCO_3$ skeletons during biomineralization processes, as well as a 'core-top' study, which must precede any eventual palaeoceanographic application. A number of conclusions can be drawn from the results:

- Deep-sea corals appear to fall into two groups for Cd/Ca and Cd isotopes: one with low K_D^{Cd} and $\alpha_{coral-Cd_{(aq.)}} \approx 1$, the other with variable and high K_D^{Cd} and Cd isotope compositions that are lighter than seawater. The grouping is not related to ocean basin, depth, or $[Cd]_{seawater}$.

- The isotopically light corals exhibit the same magnitude of Cd isotopic fractionation as seen during inorganic $CaCO_3$ precipitation ($\alpha_{coral-Cd_{(aq.)}} = 0.99938 \pm 0.00019$; $\alpha_{inorg.\ CaCO_3} = 0.99955 \pm 0.00012$). The similar magnitude between corals and inorganic precipitation

suggests a similar mechanism of Cd isotope fractionation, i.e. a kinetic isotope effect at the mineral surface during Cd incorporation.

- The Cd/Ca and Cd isotope composition of deep-sea coral skeletons follows the predicted trend for closed-system Rayleigh fractionation from a semi-enclosed calcifying space during skeletogenesis. The Cd/Ca and Cd isotope composition of deep-sea coral $CaCO_3$ appears to depend only (within measurement uncertainty) on the balance between $CaCO_3$ precipitation and seawater turnover.

- The extent of alkalinity pumping into the calcifying space ($Ca^{2+} \rightleftharpoons 2H^+$ exchange), a physiological effect, may be controlling the extent of Rayleigh fractionation (i.e. the extent of Cd removal from the calcification space, f). More alkalinity pumping further lowers Cd/Ca (by increasing $[Ca^{2+}]$, leading to a higher proportion of the vacuolized Cd being precipitated into skeletal $CaCO_3$ ($f \rightarrow 0$). The driving process behind this is presently unknown.

- The lack of species-specific or other offsets in Cd isotope compositions between some corals and ambient seawater will enable deep-sea corals to be used in temporal reconstructions of seawater Cd isotope chemistry, although reconnaissance screening for high Cd/Ca should take place before samples are processed for isotopic analysis. A Cd/Ca cut-off of ~ 0.2 μmol mol^{-1} should be used during screening, although samples recovered from the Atlantic, where $Cd/Ca_{seawater}$ is much lower, should use a lower cut-off of as low as ~ 0.1 μmol mol^{-1}.

The work presented in this thesis, through careful experimental and proxy approaches, tries to *why* Cd behaves the way it does in the modern ocean. The recent interest in Cd isotopes reflects the powerful nature of this tool in chemical oceanography. The experiments described in Chapter 3 show that Cd isotopic compositions should reflect marine productivity in general, which if captured by an appropriate archive, could be invaluable for past productivity reconstructions over a range of timescales. To help understand Cd isotope signals from such

archives, a reference framework must be established (i.e. *how* can Cd isotopes be applied to palaeoceanography?). The experiments described in Chapter 4 represent the first step towards establishing a mechanistic understanding of how Cd isotope compositions are recorded and transcribed into geological archives. Based on these experiments, the 'core-top' study of Chapter 5 explores how we might best interpret palaeoceanographic records using examples from the modern oceans.

6.2 Outlook

My hope is that this work will form the basis of future studies – not just for Cd – but more generally for other transition metals. In particular, the method that was developed in Chapter 3 is widely applicable to other metal isotope systems and opens numerous possibilities for further study. Several other themes for future investigation also emerge from the work presented here, which are outlined below.

Expanding the database of seawater metal isotope measurements. Improving the spatial resolution of the metal isotope dataset in seawater is of great importance so that palaeoceanographic records can be placed in the correct context. These additional measurements are needed – not just for Cd – but for all of the bioactive transition metals. In particular, the global marine distributions of these elements (and the processes that control them; e.g. biological, physical, or chemical) are poorly understood and require detailed analysis. Hopefully, much of this will be realized through the international GEOTRACES program (*GEOTRACES Planning Group*, 2006), and our understanding of the water column structure for many transition metals (and their isotopes) will be greatly improved. At present, the resolution is still extremely sparse – a consequence of the challenging nature of the measurements – although several groups are working to address this, using a range of novel pre-concentration techniques.

New combinations of biochemistry and isotope geochemistry. The fusion of biological and isotopic methods in Chapter 3 offers several new possible directions. Since Cd only has one

known biochemical function, this work has effectively exhausted the set of known enzymes in which Cd operates. There are still many other possible targets with which to apply this technique to other metal isotope systems (e.g. of the 1,371 sequenced enzymes, $\sim$ 50 % are metalloenzymes; *Waldron et al.*, 2009). These will allow the ivestigation of metal isotope fractionation along specific physiological pathways. These pathways can range from the expression/inhibition of individual metalloenzymes to the effect of various metal ion transporters in regulating cellular metal isotope fractionation, and may be useful in the hunt for isotopic 'biosignatures' (e.g. *Bullen*, 2011).

Much also remains to be done in the investigation of the bioinorganic cycling of Cd. In particular, the isotopic effects associated with various Cd-ligating peptides (i.e. $\alpha_{\text{peptide}-\text{Cd}_{(\text{aq.})}}$), examined as a set of *in vitro* experiments would set the reference framework in which to interpret future *in vivo* studies. These studies need only take the form of simple beaker experiments, and could be readily modified to investigate a number of easily-obtained or manufactured ligands (e.g. histidine, cysteine, metallothionein, glutathione, phytochelatin, etc.) as well as several biologically-relevant inorganic ligands (e.g. EDTA, hydrogen sulphide, citrate, hydroxyl, etc.). These Cd chelating experiments could also be extended to study similar effects in other biologically-relevant transition metals.

Investigating the causes and sensitivities of metal isotope fractionation during $CaCO_3$ precipitation. Much like the laboratory analogue experiments described for investigating the bioinorganic chemistry of Cd, similar work is needed in the area of $CaCO_3$ precipitation. The exact mechanism of Cd (and many other metals, e.g. Ca) isotope fractionation during incorporation into the $CaCO_3$ lattice is still elusive, and experiments could be performed to test certain hypothetical mechanisms (and their sensitivities). The *surface kinetic model* presented by *DePaolo* (2011) posits that metal isotope fractionation occurs during the de/rehydration step; experiments performed in different media that modify the cation-H_2O-hydration complex (e.g. ethanol, methanol, etc.) could alter or entirely circumvent this reaction step and elucidate fractionation mechanisms.

Applying Cd isotopes to palaeoceanography. The 'core-top' study presented in Chapter 5 represents the first of its kind for Cd isotopes. As such, there is still a long way to go before Cd isotopes are routinely applied in palaeoceanographic studies. More deep-sea coral analyses are in progress, including the first high-resolution time series from the north Atlantic seamounts across the most recent deglaciation. This time interval is also under investigation by another research group, who are examining a suite of Southern Ocean deep-sea corals. Other suitable substrates for Cd isotope measurements in palaeoceanography are needed. These could include other types of coral, including surface-dwelling zooxanthellate corals (work also ongoing) as well as calcareous microfossils (e.g. forams). The responses and environmental sensitivities of these substrates will also need to be investigated.

6.3 Closing remarks

My goals for future research are to use and develop non-traditional isotopic techniques to study topical problems in chemical oceanography, biogeochemistry, and climate. In particular, I am interested in applying metal stable isotope 'toolboxes' to probe the links between the nutrient chemistry of the oceans, the efficiency of the biological pump, phytoplankton physiology, and (palaeo)climate. Since my undergraduate research project I have been fascinated by the range of approaches that can be used to tackle problems in Earth Sciences.

The work we do as Earth scientists allows us to apply a range of often developmental and sometimes challenging techniques for the purpose of problem solving on a scale as large as the Earth itself. It is the continual learning of new techniques and skills, meeting new people with interesting ideas and different approaches – and most importantly – good research, that I have enjoyed the most during my time at Oxford, and hope to enjoy for many years to come.

References

Abouchami, W., S. J. G. Galer, H. J. W. de Baar, A. C. Alderkamp, R. Middag, P. Laan, H. Feldmann, and M. O. Andreae (2011), Modulation of the Southern Ocean cadmium isotope signature by ocean circulation and primary productivity, *Earth Planet. Sci. Lett.*, *305*(1-2), 83–91, doi:10.1016/j.epsl.2011.02.044.

Abouchami, W., S. J. G. Galer, T. J. Horner, M. Rehkämper, F. Wombacher, Z. Xue, M. Lambelet, M. Gault-Ringold, C. Stirling, M. Schönbächler, A. E. Shiel, D. Weis, and P. F. Holdship (2012), A Common Reference Material for Cadmium Isotope Studies – NIST SRM 3108 Cd, *Geostand. Geoanal. Res.*, *x*(y), z, doi:10.1111/j.1751-908X.2012.00175.x.

Adkins, J. F., H. Cheng, E. A. Boyle, E. R. M. Druffel, and R. L. Edwards (1998), Deep-Sea Coral Evidence for Rapid Change in Ventilation of the Deep North Atlantic 15,400 Years Ago, *Science*, *280*(5364), 725–728, doi:10.1126/science.280.5364.725.

Adkins, J. F., S. Griffin, M. Kashgarian, H. Cheng, E. M. Druffel, E. A. Boyle, R. L. Edwards, and C. Shen (2002), Radiocarbon dating of deep-sea corals, *Radiocarbon*, *44*(2), 567–580, doi: journals.uair.arizona.edu/index.php/radiocarbon/article/view/4127.

Adkins, J. F., E. A. Boyle, W. B. Curry, and A. Lutringer (2003), Stable isotopes in deep-seacorals and a new mechanism for "vital effects", *Geochim. Cosmochim. Acta*, *67*(6), 1129–1143, doi: 10.1016/S0016-7037(02)01203-6.

Adkins, J. F., G. M. Henderson, S. L. Wang, S. O'Shea, and F. Mokadem (2004), Growth rates of the deep-sea scleractinia *Desmophyllum cristagalli* and *Enallopsammia rostrata*, *Earth Planet. Sci. Lett.*, *227*(3), 481–490, doi:10.1016/j.epsl.2004.08.022.

Al-Horani, F. A., S. M. Al-Moghrabi, and D. De Beer (2003a), The mechanism of calcification and its relation to photosynthesis and respiration in the scleractinian coral *Galaxea fascicularis*, *Mar. Biol.*, *142*(3), 419–426, doi:10.1007/s00227-002-0981-8.

Al-Horani, F. A., S. M. Al-Moghrabi, and D. de Beer (2003b), Microsensor study of photosynthesis and calcification in the scleractinian coral, *Galaxea fascicularis*: active internal carbon cycle, *J. Exp. Mar. Biol. Ecol.*, *288*(1), 1–15, doi:10.1016/S0022-0981(02)00578-6.

Archer, C., and D. Vance (2004), Mass discrimination correction in multiple-collector plasma source mass spectrometry: an example using Cu and Zn isotopes, *J. Anal. At. Spectrom.*, *19*(5), 656–665, doi:10.1039/B315853E.

Aston, F. W. (1925), CXIX. The mass-spectra of chemical elements.–Part VI. Accelerated anode rays continued, *Philos. Mag.*, *49*(294), 1191–1201, doi:10.1080/14786442508634698.

Baker, R. G. A., M. Schönbächler, M. Rehkämper, H. M. Williams, and A. N. Halliday (2010), The thallium isotope composition of carbonaceous chondrites–New evidence for live ^{205}Pb in the early solar system, *Earth Planet. Sci. Lett.*, *291*(1-4), 39–47, doi:10.1016/j.epsl.2009.12.044.

Balistrieri, L. S., D. M. Borrok, R. B. Wanty, and W. I. Ridley (2008), Fractionation of Cu and Zn isotopes during adsorption onto amorphous Fe (III) oxyhydroxide: experimental mixing of acid rock drainage and ambient river water, *Geochim. Cosmochim. Acta*, *72*(2), 311–328, doi:10.1016/j.gca.2007.11.013.

Barling, J., G. L. Arnold, and A. D. Anbar (2001), Natural mass-dependent variations in the isotopic composition of molybdenum, *Earth Planet. Sci. Lett.*, *193*(3), 447–457, doi:10.1016/S0012-821X(01)00514-3.

Barnes, D. J. (1970), Coral skeletons: an explanation of their growth and structure, *Science*, *170*(3964), 1305–1308, doi:10.1126/science.170.3964.1305.

Barnes, D. J., and J. M. Lough (1996), Coral skeletons: storage and recovery of environmental information, *Global Change Biol.*, *2*(6), 569–582, doi:10.1111/j.1365-2486.1996.tb00068.x.

Beaman, R. J., J. M. Webster, A. Puga-Bernabéa, A. L. Thomas, and G. Jacobsen (in prep.), Discovery of a cold-water coral bank on a landslide block from the Great Barrier Reef margin, north-eastern Australia, *Deep Sea Res. Part I*.

Beard, B. L., C. M. Johnson, L. Cox, H. Sun, K. H. Nealson, and C. Aguilar (1999), Iron isotope biosignatures, *Science*, *285*(5435), 1889–1892, doi:10.1126/science.285.5435.1889.

Belshaw, N. S., P. A. Freedman, R. K. O'Nions, M. Frank, and Y. Guo (1998), A new variable dispersion double-focusing plasma mass spectrometer with performance illustrated for pb isotopes, *Int. J. Mass spectrom.*, *181*(1-3), 51–58, doi:10.1016/S1387-3806(98)14150-7.

Bentov, S., C. Brownlee, and J. Erez (2009), The role of seawater endocytosis in the biomineralization process in calcareous foraminifera, *Proc. Natl. Acad. Sci.*, *106*(51), 21,500–21,504, doi:10.1073/pnas.0906636106.

Bermin, J., D. Vance, C. Archer, and P. J. Statham (2006), The determination of the isotopic composition of Cu and Zn in seawater, *Chem. Geol.*, *226*(3-4), 280–297, doi:10.1016/j.chemgeo.2005.09.025.

Black, J. R., A. Kavner, and E. A. Schauble (2011), Calculation of equilibrium stable isotope partition function ratios for aqueous zinc complexes and metallic zinc, *Geochim. Cosmochim. Acta*, *75*(3), 769–783, doi:10.1016/j.gca.2010.11.019.

Bots, P., L. G. Benning, R. E. M. Rickaby, and S. Shaw (2011), The role of SO_4 in the switch from calcite to aragonite seas, *Geology*, *39*(4), 331–334, doi:10.1130/G31619.1.

Boyle, E. A. (1981), Cadmium, zinc, copper, and barium in foraminifera tests, *Earth Planet. Sci. Lett.*, *53*(1), 11–35, doi:10.1016/0012-821X(81)90022-4.

Boyle, E. A. (1988), Cadmium: Chemical tracer of deepwater paleoceanography, *Paleoceanography*, *3*(4), 471–489, doi:10.1029/PA003i004p00471.

Boyle, E. A. (1992), Cadmium and δ^{13}C Paleochemical Ocean Distributions During the Stage 2 Glacial Maximum, *Annu. Rev. Earth Planet. Sci.*, *20*(1), 245–287, doi:10.1146/annurev.ea.20.050192.001333.

Boyle, E. A., and L. Keigwin (1987), North Atlantic thermohaline circulation during the past 20,000 years linked to high-latitude surface temperature, *Nature*, *330*, 35–40, doi:10.1038/330035a0.

Boyle, E. A., and L. D. Keigwin (1982), Deep Circulation of the North Atlantic over the Last 200,000 Years: Geochemical Evidence, *Science*, *218*(4574), 784–787, doi:10.1126/science.218.4574.784.

Boyle, E. A., F. Sclater, and J. M. Edmond (1976), On the marine geochemistry of cadmium, *Nature*, *263*(5572), 42–44, doi:10.1038/263042a0.

Bradford, M. M. (1976), A rapid and sensitive method for the quantitation of microgram quantities of protein utilizing the principle of protein-dye binding, *Anal. Biochem.*, *72*(1-2), 248–254, doi:10.1016/0003-2697(76)90527-3.

Brand, L. E., W. G. Sunda, and R. R. L. G&lard (1983), Limitation of marine phytoplankton reproductive rates by zinc, manganese, and iron1, *Limnol. Oceanogr*, *28*(6), 1182–1198, doi:www.jstor.org/stable/2836278.

Bruland, K. W. (1980), Oceanographic distributions of cadmium, zinc, nickel, and copper in the North Pacific, *Earth Planet. Sci. Lett.*, *47*(2), 176–198, doi:10.1016/0012-821X(80)90035-7.

Bullen, T. D. (2011), Stable isotopes of transition and post-transition metals as tracers in environmental studies, in *Handbook of Environmental Isotope Geochemistry*, *Adv. Isot. Geochem.*, vol. 2, edited by M. M. Baskaran, 1st ed., pp. 177–203, Springer Berlin Heidelberg, Heidelberg, doi:10.1007/978-3-642-10637-8_10.

Byrne, R. H. (2002), Inorganic speciation of dissolved elements in seawater: the influence of pH on concentration ratios, *Geochem. Trans.*, *3*(1), 11, doi:10.1186/1467-4866-3-11.

Cameron, V., D. Vance, C. Archer, and C. H. House (2009), A biomarker based on the stable isotopes of nickel, *Proc. Natl. Acad. Sci.*, *106*(27), 10,944–10,948, doi:10.1073/pnas.0900726106.

Cardinal, D., L. Y. Alleman, J. de Jong, K. Ziegler, and L. André (2003), Isotopic composition of silicon measured by multicollector plasma source mass spectrometry in dry plasma mode, *J. Anal. At. Spectrom.*, *18*(3), 213–218, doi:10.1039/B210109B.

Cheng, H., J. F. Adkins, R. L. Edwards, and E. A. Boyle (2000), U-Th dating of deep-sea corals, *Geochim. Cosmochim. Acta*, *64*(14), 2401–2416, doi:10.1016/S0016-7037(99)00422-6.

Cobbett, C., and P. Goldsbrough (2002), Phytochelatins and metallothioneins: roles in heavy metal detoxification and homeostasis, *Annu. Rev. Plant Biol.*, *53*(1), 159–182, doi:10.1146/annurev.arplant.53.100301.135154.

Collier, R., and J. Edmond (1984), The trace element geochemistry of marine biogenic particulate matter, *Prog. Oceanogr.*, *13*(2), 113–199, doi:10.1016/0079-6611(84)90008-9.

Cullen, J. (2006), On the nonlinear relationship between dissolved cadmium and phosphate in the modern global ocean: Could chronic iron limitation of phytoplankton growth cause the kink?, *Limnol. Oceanogr.*, *51*(3), 1369–1380, doi:www.jstor.org/stable/3841183.

Cullen, J. T., and R. M. Sherrell (2005), Effects of dissolved carbon dioxide, zinc, and manganese on the cadmium to phosphorus ratio in natural phytoplankton assemblages, *Limnol. Oceanogr.*, *50*(4), 1193–1204, doi:www.jstor.org/stable/3597398.

Cullen, J. T., T. W. Lane, F. M. M. Morel, and R. M. Sherrell (1999), Modulation of cadmium uptake in phytoplankton by seawater CO_2 concentration, *Nature*, *402*(6758), 165–167, doi:10.1038/46007.

Davis, J. A., C. C. Fuller, and A. D. Cook (1987), A model for trace metal sorption processes at the calcite surface: Adsorption of Cd^{2+} and subsequent solid solution formation, *Geochim. Cosmochim. Acta*, *51*(6), 1477–1490, doi:10.1016/0016-7037(87)90330-9.

Davis, K. J., P. M. Dove, and J. J. De Yoreo (2000), The role of Mg^{2+} as an impurity in calcite growth, *Science*, *290*(5494), 1134, doi:10.1126/science.290.5494.1134.

Davis, K. J., P. M. Dove, L. E. Wasylenki, and J. J. De Yoreo (2004), Morphological consequences of differential Mg^{2+} incorporation at structurally distinct steps on calcite, *Am. Mineral.*, *89*(5-6), 714.

de Baar, H. J. W., P. M. Saager, R. F. Nolting, and J. van der Meer (1994), Cadmium versus phosphate in the world ocean, *Mar. Chem.*, *46*(3), 261–281, doi:10.1016/0304-4203(94)90082-5.

De La Rocha, C. L. (2006), Opal-based isotopic proxies of paleoenvironmental conditions, *Global Biogeochem. Cycles*, *20*(4), GB4S09, doi:10.1029/2005GB002664.

de la Rocha, C. L., M. A. Brzezinski, and M. J. DeNiro (1997), Fractionation of silicon isotopes by marine diatoms during biogenic silica formation, *Geochim. Cosmochim. Acta*, *61*(23), 5051–5056, doi:10.1016/S0016-7037(97)00300-1.

De Laeter, J. R., J. K. Böhlke, P. De Bièvre, H. Hidaka, H. S. Peiser, K. J. R. Rosman, and P. D. P. Taylor (2003), Atomic weights of the elements: review 2000, *Pure Appl. Chem.*, *75*(6), 683–800, doi:10.1351/pac200375060683.

DePaolo, D. J. (2011), Surface kinetic model for isotopic and trace element fractionation during precipitation of calcite from aqueous solutions, *Geochim. Cosmochim. Acta*, *75*(4), 1039–1056, doi:10.1016/j.gca.2010.11.020.

Dodson, M. H. (1963), A theoretical study of the use of internal standards for precise isotopic analysis by the surface ionization technique: Part I - General first-order algebraic solutions, *J. Sci. Instrum.*, *40*, 289, doi:10.1088/0950-7671/40/6/307.

Eilam, Y., H. Lavi, and N. Grossowicz (1985), Cytoplasmic Ca^{2+} homeostasis maintained by a vacuolar Ca^{2+} transport system in the yeast *Saccharomyces cerevisiae*, *J. Gen. Microbiol.*, *131*(3), 623–629, doi:10.1099/00221287-131-3-623.

Elderfield, H., and R. E. M. Rickaby (2000), Oceanic Cd/P ratio and nutrient utilization in the glacial Southern Ocean, *Nature*, *405*(6784), 305–310, doi:10.1038/35012507.

Elderfield, H., C. J. Bertram, and J. Erez (1996), A biomineralization model for the incorporation of trace elements into foraminiferal calcium carbonate, *Earth Planet. Sci. Lett.*, *142*(3), 409–423, doi:10.1016/0012-821X(96)00105-7.

Erez, J. (1978), Vital effect on stable-isotope composition seen in foraminifera and coral skeletons, *Nature*, *273*(5659), 199–202, doi:10.1038/273199a0.

Fantle, M. S., and D. J. DePaolo (2007), Ca isotopes in carbonate sediment and pore fluid from ODP Site 807A: The Ca^{2+}(aq)-calcite equilibrium fractionation factor and calcite recrystallization rates in Pleistocene sediments, *Geochim. Cosmochim. Acta*, *71*(10), 2524–2546, doi:10.1016/j.gca.2007.03.006.

Field, C. B., M. J. Behrenfeld, J. T. Randerson, and P. Falkowski (1998), Primary Production of the Biosphere: Integrating Terrestrial and Oceanic Components, *Science*, *281*(5374), 237–240, doi:10.1126/science.281.5374.237.

Frank, M. (2002), Radiogenic isotopes: tracers of past ocean circulation and erosional input, *Rev. Geophys.*, *40*(1), 1001, doi:10.1029/2000RG000094.

Frew, R. D., and K. A. Hunter (1992), Influence of Southern Ocean waters on the cadmium–phosphate properties of the global ocean, *Nature*, *360*(6400), 144–146, doi:10.1038/360144a0.

Friedlingstein, P., R. A. Houghton, G. Marland, J. Hackler, T. A. Boden, T. J. Conway, J. G. Canadell, M. R. Raupach, P. Ciais, and C. Le Quéré (2010), Update on CO_2 emissions, *Nat. Geosci.*, *3*(12), 811–812, doi:10.1038/ngeo1022.

Fujii, T., F. Moynier, P. Telouk, and M. Abe (2010), Experimental and Theoretical Investigation of Isotope Fractionation of Zinc between Aqua, Chloro, and Macrocyclic Complexes, *J. Phys. Chem. A*, *114*(7), 2543–2552, doi:10.1021/jp908642f.

Gaetani, G. A., A. L. Cohen, Z. Wang, and J. Crusius (2011), Rayleigh-based, multi-element coral thermometry: A biomineralization approach to developing climate proxies, *Geochim. Cosmochim. Acta*, *75*(7), 1920–1932, doi:10.1016/j.gca.2011.01.010.

Gagnon, A. C., J. F. Adkins, D. P. Fernandez, and L. F. Robinson (2007), Sr/Ca and Mg/Ca vital effects correlated with skeletal architecture in a scleractinian deep-sea coral and the role of Rayleigh fractionation, *Earth Planet. Sci. Lett.*, *261*(1-2), 280–295, doi:10.1016/j.epsl.2007.07.013.

Gagnon, A. C., J. F. Adkins, and J. Erez (2012), Seawater transport during coral biomineralization, *Earth and Planetary Science Letters*, *329*, 150–161, doi:10.1016/j.epsl.2012.03.005.

Galer, S. (1999), Optimal double and triple spiking for high precision lead isotopic measurement, *Chem. Geol.*, *157*(3-4), 255–274, doi:10.1016/S0009-2541(98)00203-4.

Garcia, H. E., R. A. Locarnini, T. P. Boyer, J. I. Antonov, M. M. Zweng, O. K. Baranova, and D. R. Johnson (2010), World Ocean Atlas 2009, Volume 4: Nutrients (phosphate, nitrate, silicate), in *World Ocean Atlas 2009*, *NOAA Atlas NESDIS*, vol. 71, edited by S. Levitus, 5th ed., p. 398, U.S. Government Printing Office, Washington, D.C., doi:www.nodc.noaa.gov/OC5/WOA09/pubwoa09.html.

Gault-Ringold, M., and C. H. Stirling (2012), Anomalous isotopic shifts associated with organic resin residues during cadmium isotopic analysis by double spike MC-ICPMS, *J. Anal. At. Spectrom.*, *37*, 449–459, doi:10.1039/C2JA10360E.

Gault-Ringold, M., T. Adu, C. H. Stirling, R. D. Frew, and K. A. Hunter (2012), Anomalous biogeochemical behavior of cadmium in subantarctic surface waters: Mechanistic constraints from cadmium isotopes, *Earth Planet. Sci. Lett.*, *341*, 94–103, doi:10.1016/j.epsl.2012.06.005.

GEOTRACES Planning Group (2006), *GEOTRACES Science Plan*, 79 pp., Scientific Committee on Oceanic Research, Baltimore, MD.

German, C. R., A. C. Campbell, and J. M. Edmond (1991), Hydrothermal scavenging at the Mid-Atlantic Ridge: Modification of trace element dissolved fluxes, *Earth Planet. Sci. Lett.*, *107*(1), 101–114, doi:10.1016/0012-821X(91)90047-L.

Goldstein, S. J., D. W. Lea, S. Chakraborty, M. Kashgarian, and M. T. Murrell (2001), Uranium-series and radiocarbon geochronology of deep-sea corals: implications for Southern Ocean ventilation rates and the oceanic carbon cycle, *Earth Planet. Sci. Lett.*, *193*(1), 167–182, doi:10.1016/S0012-821X(01)00494-0.

Grill, E., E. L. Winnacker, and M. H. Zenk (1987), Phytochelatins, a class of heavy-metal-binding peptides from plants, are functionally analogous to metallothioneins, *Proc. Natl. Acad. Sci.*, *84*(2), 439–443, doi:www.pnas.org/content/84/2/439.

Halliday, A. N., D.-C. Lee, J. N. Christensen, A. J. Walder, P. A. Freedman, C. E. Jones, C. M. Hall, W. Yi, and D. Teagle (1995), Recent developments in inductively coupled plasma magnetic sector multiple collector mass spectrometry, *Int. J. Mass Spectrom. Ion Processes*, *146*, 21–33, doi:10.1016/0168-1176(95)04200-5.

Han, Y. J., and J. Aizenberg (2003), Effect of magnesium ions on oriented growth of calcite on carboxylic acid functionalized self-assembled monolayer, *J. Am. Chem. Soc.*, *125*(14), 4032–4033, doi:10.1021/ja034094z.

Hanikenne, M., P. Motte, M. C. S. Wu, T. Wang, R. Loppes, and R. F. Matagne (2005), A mitochondrial half-size ABC transporter is involved in cadmium tolerance in *Chlamydomonas reinhardtii*, *Plant Cell Environ.*, *28*(7), 863–873, doi:10.1111/j.1365-3040.2005.01335.x.

Hedges, J. I., and R. G. Keil (1995), Sedimentary organic matter preservation: an assessment and speculative synthesis, *Mar. Chem.*, *49*(2-3), 81–115, doi:10.1016/0304-4203(95)00008-F.

Henderson, G. M. (2002), New oceanic proxies for paleoclimate, *Earth Planet. Sci. Lett.*, *203*(1), 1–13, doi:10.1016/S0012-821X(02)00809-9.

Ho, T. Y., A. Quigg, Z. V. Finkel, A. J. Milligan, K. Wyman, P. G. Falkowski, and F. M. M. Morel (2003), The elemental composition of some marine phytoplankton, *J. Phycol.*, *39*(6), 1145–1159, doi:10.1111/j.0022-3646.2003.03-090.x.

Horner, T. J., M. Schönbächler, M. Rehkämper, S. G. Nielsen, H. Williams, A. N. Halliday, Z. Xue, and J. R. Hein (2010), Ferromanganese crusts as archives of deep water Cd isotope compositions, *Geochem. Geophys. Geosyst.*, *11*, Q04001, doi:10.1029/2009GC002987.

Horner, T. J., R. E. M. Rickaby, and G. M. Henderson (2011), Isotopic fractionation of cadmium into calcite, *Earth Planet. Sci. Lett.*, *312*(1-2), 243–253, doi:10.1016/j.epsl.2011.10.004.

Jin, X., N. Gruber, J. P. Dunne, J. L. Sarmiento, and R. A. Armstrong (2006), Diagnosing the contribution of phytoplankton functional groups to the production and export of particulate organic carbon, $CaCO_3$, and opal from global nutrient and alkalinity distributions , *Global Biogeochem. Cycles*, *20*(2), GB2015, doi:10.1029/2005GB002532.

John, S. G., R. W. Geis, M. A. Saito, and E. A. Boyle (2007), Zinc isotope fractionation during high-affinity and low-affinity zinc transport by the marine diatom *Thalassiosira oceanica*, *Limnol. Oceanog.*, *52*(6), 2710–2714, doi:www.jstor.org/stable/4502415.

Johnson, C. M., B. L. Beard, and F. Albarede (2004), Overview and General Concepts, in *Geochemistry of non-traditional stable isotopes*, *Rev. Mineral. Geochem.*, vol. 55, edited by C. M. Johnson, B. L. Beard, and F. Albarede, pp. 1–24, Mineralogical Society of America, doi:10.2138/gsrmg.55.1.1.

Juillot, F., C. Maréchal, M. Ponthieu, S. Cacaly, G. Morin, M. Benedetti, J. L. Hazemann, O. Proux, and F. Guyot (2008), Zn isotopic fractionation caused by sorption on goethite and 2-lines ferrihydrite, *Geochim. Cosmochim. Acta*, *72*(19), 4886–4900, doi:10.1016/j.gca.2008.07.007.

Karl, D. M. (2000), Aquatic ecology: Phosphorus, the staff of life, *Nature*, *406*(6791), 31–33, doi:10.1038/35017683.

Kenney, J. P. L., and J. B. Fein (2011), Importance of extracellular polysaccharides on proton and Cd binding to bacterial biomass: A comparative study, *Chem. Geol.*, *286*(3-4), 109–117, doi:10.1016/j.chemgeo.2011.04.011.

Kester, D. R., I. W. Duedall, D. N. Connors, and R. Pytkowicz (1967), Preparation of artificial seawater, *Limnol. Oceanogr.*, *12*(1), 176–179, doi:www.jstor.org/stable/2833179.

Knox, F., and M. B. McElroy (1984), Changes in Atmospheric CO_2: Influence of the Marine Biota at High Latitude, *J. Geophys. Res.*, *89*(D3), 4629–4637, doi:10.1029/JD089iD03p04629.

Lacan, F., R. Francois, Y. Ji, and R. M. Sherrell (2006), Cadmium isotopic composition in the ocean, *Geochim. Cosmochim. Acta*, *70*(20), 5104–5118, doi:10.1016/j.gca.2006.07.036.

Laddaga, R. A., and S. Silver (1985), Cadmium uptake in *Escherichia coli* K-12, *J. Bacteriol.*, *162*(3), 1100, doi:jb.asm.org/cgi/content/abstract/162/3/1100.

Laemmli, U. K. (1970), Cleavage of structural proteins during the assembly of the head of bacteriophage T4, *Nature*, *227*(5259), 680–685, doi:10.1038/227680a0.

Lane, E. S., K. Jang, J. T. Cullen, and M. T. Maldonado (2008), The interaction between inorganic iron and cadmium uptake in the marine diatom *Thalassiosira oceanica*, *Limnol. Oceanog.*, *53*(5), 1784–1789, doi:www.jstor.org/stable/40058297.

Lane, E. S., D. M. Semeniuk, R. F. Strzepek, J. T. Cullen, and M. T. Maldonado (2009), Effects of iron limitation on intracellular cadmium of cultured phytoplankton: Implications for surface dissolved cadmium to phosphate ratios, *Mar. Chem.*, *115*(3-4), 155–162, doi:10.1016/j.marchem.2009.07.008.

Lane, T. W., M. A. Saito, G. N. George, I. J. Pickering, R. C. Prince, and F. M. M. Morel (2005), A cadmium enzyme from a marine diatom, *Nature*, *435*(7038), 42, doi:10.1038/435042a.

Larner, F., M. Rehkämper, B. J. Coles, K. Kreissig, D. J. Weiss, B. Sampson, C. Unsworth, and S. Strekopytov (2011), A new separation procedure for Cu prior to stable isotope analysis by MC-ICP-MS, *J. Anal. At. Spectrom.*, *26*(8), 1627–1632, doi:10.1039/C1JA10067J.

Lea, D. W. (2006), Elemental and Isotopic Proxies of Past Ocean Temperatures, in *The Oceans and Marine Geochemistry*, *Treatise Geochem.*, vol. 6, edited by H. Elderfield, 1st ed., pp. 365–390, Elsevier, Amsterdam, doi:10.1016/B0-08-043751-6/06114-4.

Lee, J. G., S. B. Roberts, and F. M. M. Morel (1995), Cadmium: a nutrient for the marine diatom *Thalassiosira weissflogii*, *Limnol. Oceanogr.*, *40*(6), 1056–1063, doi:www.jstor.org/stable/2838702.

Lee, J. G., B. A. Ahner, and F. M. M. Morel (1996), Export of cadmium and phytochelatin by the marine diatom *Thalassiosira weissflogii*, *Environ. Sci. Technol.*, *30*(6), 1814–1821, doi:10.1021/es950331p.

Levasseur, S., M. Frank, J. R. Hein, and A. N. Halliday (2004), The global variation in the iron isotope composition of marine hydrogenetic ferromanganese deposits: implications for seawater chemistry?, *Earth Planet. Sci. Lett.*, *224*(1-2), 91–105, doi:10.1016/j.epsl.2004.05.010.

Lockemann, G., and R. E. Oesper (1953), Friedrich stromeyer and the history of chemical laboratory instruction, *J. Chem. Educ.*, *30*(4), 202, doi:10.1021/ed030p202.

Long, D. T., and E. E. Angino (1977), Chemical speciation of Cd, Cu, Pb, and Zn in mixed freshwater, seawater, and brine solutions, *Geochim. Cosmochim. Acta*, *41*(9), 1183–1191, doi:10.1016/0016-7037(77)90064-3.

Lorens, R. B. (1981), Sr, Cd, Mn and Co distribution coefficients in calcite as a function of calcite precipitation rate, *Geochim. Cosmochim. Acta*, *45*(4), 553–561, doi:10.1016/0016-7037(81)90188-5.

Lynch-Stieglitz, J. (2006), Tracers of past ocean circulation, in *The Oceans and Marine Geochemistry*, *Treatise Geochem.*, vol. 6, edited by H. Elderfield, 1st ed., pp. 433–452, Elsevier, Amsterdam, doi:10.1016/B0-08-043751-6/06117-X.

Mangini, A., M. Lomitschka, R. Eichstädter, N. Frank, S. Vogler, G. Bonani, I. Hajdas, and J. Patzold (1998), Coral provides way to age deep water, *Nature*, *392*(6674), 347–348, doi:10.1038/32804.

Marchitto, T. M. (2004), Lack of a significant temperature influence on the incorporation of cd into benthic foraminiferal tests, *Geochem. Geophys. Geosyst.*, *5*, Q10D11, doi:10.1029/2004GC000753.

Maréchal, C. N., P. Télouk, and F. Albarède (1999), Precise analysis of copper and zinc isotopic compositions by plasma-source mass spectrometry, *Chem. Geol.*, *156*(1-4), 251–273, doi:10.1016/S0009-2541(98)00191-0.

Maréchal, C. N., E. Nicolas, C. Douchet, and F. Albarède (2000), Abundance of zinc isotopes as a marine biogeochemical tracer, *Geochem. Geophys. Geosys.*, *1*(5), 1015, doi:10.1029/1999GC000029.

Margerum, D. W., G. R. Cayley, D. C. Weatherburn, and G. K. Pagenkopf (1978), Kinetics and mechanisms of complex formation and ligand exchange, in *Coordination Chemistry*, vol. 2, edited by A. E. Martell, pp. 1–220, American Chemical Society Monograph Series, Washington, DC.

Marriott, C. S., G. M. Henderson, N. S. Belshaw, and A. W. Tudhope (2004a), Temperature dependence of δ^7Li, δ^{44}Ca and Li/Ca during growth of calcium carbonate, *Earth Planet. Sci. Lett.*, *222*(2), 615–624, doi:10.1016/j.epsl.2004.02.031.

Marriott, C. S., G. M. Henderson, R. Crompton, M. Staubwasser, and S. Shaw (2004b), Effect of mineralogy, salinity, and temperature on Li/Ca and Li isotope composition of calcium carbonate, *Chem. Geol.*, *212*(1-2), 5–15, doi:10.1016/j.chemgeo.2004.08.002.

Martin, J. (1990), Glacial-interglacial CO_2 change: The Iron Hypothesis, *Paleoceanography*, *5*(1), 1–13, doi:10.1029/PA005i001p00001.

Martin, J. M., and A. J. Thomas (1994), The global insignificance of telluric input of dissolved trace metals (Cd, Cu, Ni and Zn) to ocean margins, *Mar, Chem,*, *46*(1-2), 165–178, doi:10.1016/0304-4203(94)90053-1.

McConnaughey, T. (1989), ^{13}C and ^{18}O isotopic disequilibrium in biological carbonates: I. Patterns, *Geochim. Cosmochim. Acta*, *53*(1), 151–162, doi:10.1016/0016-7037(89)90282-2.

Mendoza-Cózatl, D. G., Z. Zhai, T. O. Jobe, G. Z. Akmakjian, W. Y. Song, O. Limbo, M. R. Russell, V. I. Kozlovskyy, E. Martinoia, O. Vatamaniuk, P. Russell, and J. I. Schroeder (2010), Tonoplast-localized Abc2 Transporter Mediates Phytochelatin Accumulation in Vacuoles and Confers Cadmium Tolerance, *J. Biol. Chem.*, *285*(52), 40,416–40,426, doi:10.1074/jbc.M110.155408.

Milliman, J. D., P. J. Troy, W. M. Balch, A. K. Adams, Y. H. Li, and F. Mackenzie (1999), Biologically mediated dissolution of calcium carbonate above the chemical lysocline?, *Deep Sea Res. Part I*, *46*(10), 1653–1669, doi:10.1016/S0967-0637(99)00034-5.

Mitchell, B. G., E. A. Brody, O. Holm-Hansen, C. McClain, and J. Bishop (1991), Light limitation of phytoplankton biomass and macronutrient utilization in the southern ocean, *Limnol. Oceanog.*, *36*(8), 1662–1677, doi:www.jstor.org/stable/2837705.

Mitra, R. S., R. H. Gray, B. Chin, and I. A. Bernstein (1975), Molecular mechanisms of accommodation in *Escherichia coli* to toxic levels of Cd^{2+}, *J. Bacteriol.*, *121*(3), 1180, doi:jb.asm.org/cgi/content/abstract/121/3/1180.

Montaser, A. (Ed.) (1998), *Inductively Coupled Plasma Mass Spectrometry*, 1004 pp., Wiley-VCH, New York, USA.

Morel, F. M. M., and N. M. Price (2003), The biogeochemical cycles of trace metals in the oceans, *Science*, *300*(5621), 944–947, doi:10.1126/science.1083545.

Morel, F. M. M., J. R. Reinfelder, S. B. Roberts, C. P. Chamberlain, J. G. Lee, and D. Yee (1994), Zinc and carbon co-limitation of marine phytoplankton, *Nature*, *369*(6483), 740–742, doi:10.1038/369740a0.

Navarrete, J. U., D. M. Borrok, M. Vivieros, and J. T. Ellzey (2011), Copper isotope fractionation during surface adsorption and intracellular incorporation by bacteria, *Geochim. Cosmochim. Acta*, *75*(3), 784–799, doi:10.1016/j.gca.2010.11.011.

Nies, D. H. (1992), Resistance to cadmium, cobalt, zinc, and nickel in microbes, *Plasmid*, *27*(1), 17–28, doi:10.1016/0147-619X(92)90003-S.

Olivares, J. A., and R. S. Houk (1985), Ion sampling for inductively coupled plasma mass spectrometry, *Anal. Chem.*, *57*(13), 2674–2679, doi:10.1021/ac00290a054.

Ortiz, D. F., T. Ruscitti, K. F. McCue, and D. W. Ow (1995), Transport of Metal-binding Peptides by HMT1, A Fission Yeast ABC-type Vacuolar Membrane Protein, *J. Biol. Chem.*, *270*(9), 4721–4728, doi:10.1074/jbc.270.9.4721.

Park, H., B. Song, and F. M. M. Morel (2007), Diversity of the cadmium-containing carbonic anhydrase in marine diatoms and natural waters, *Environ. Microbiol.*, *9*(2), 403–413, doi:10.1111/j.1462-2920.2006.01151.x.

Parkhurst, D. L., C. A. J. Appelo, and G. S. (U.S.) (1999), *User's guide to PHREEQC: a computer program for speciation, batch-reaction, one-dimensional transport, and inverse geochemical calculations*, xiv, 312 p. pp., U. S. Geological Survey - Earth Science Information Center, Open-File Reports Section, Denver, CO, USA.

Pitchford, J. W., and J. Brindley (1999), Iron limitation, grazing pressure and oceanic high nutrient-low chlorophyll (HNLC) regions , *J. Plankton Res.*, *21*(3), 525–547, doi:10.1093/plankt/21.3.525.

Pokrovsky, O. S., J. Viers, and R. Freydier (2005), Zinc stable isotope fractionation during its adsorption on oxides and hydroxides, *J. Colloid Interface Sci.*, *291*(1), 192–200, doi:10.1016/j.jcis.2005.04.079.

Prévéral, S., L. Gayet, C. Moldes, J. Hoffmann, S. Mounicou, A. Gruet, F. Reynaud, R. Lobinski, J.-M. Verbavatz, A. Vavasseur, and C. Forestier (2009), A Common Highly Conserved Cadmium Detoxification Mechanism from Bacteria to Humans, *J. Biol. Chem.*, *284*(8), 4936–4943, doi:10.1074/jbc.M808130200.

Price, N. M., and F. M. M. Morel (1990), Cadmium and cobalt substitution for zinc in a marine diatom, *Nature*, *344*(6267), 658–660, doi:10.1038/344658a0.

Prieto, M., P. Cubillas, and A. Fernández-Gonzalez (2003), Uptake of dissolved Cd by biogenic and abiogenic aragonite: a comparison with sorption onto calcite, *Geochim. Cosmochim. Acta*, *67*(20), 3859–3869, doi:10.1016/S0016-7037(03)00309-0.

Pritzkow, W., S. Wunderli, J. Vogl, and G. Fortunato (2007), The isotope abundances and the atomic weight of cadmium by a metrological approach, *Int. J. Mass Spectrom.*, *261*(1), 74–85, doi:10.1016/j.ijms.2006.07.026.

Putnis, A. (2010), Effects of kinetics and mechanisms of crystal growth on ion-partitioning in solid solution–aqueous solution (SS-AS) systems, in *Ion partitioning in ambient-temperature aqueous systems*, *EMU Notes in Mineralogy*, vol. 10, edited by M. Prieto and H. M. Stoll, 1st ed., pp. 43–64, European Mineralogical Union, Oviedo.

Quigg, A., Z. V. Finkel, A. J. Irwin, Y. Rosenthal, T. Y. Ho, J. R. Reinfelder, O. Schofield, F. M. M. Morel, and P. G. Falkowski (2003), The evolutionary inheritance of elemental stoichiometry in marine phytoplankton, *Nature*, *425*(6955), 291–294, doi:10.1038/nature01953.

Rayleigh, J. W. S. (1896), Theoretical considerations respecting the separation of gases by diffusion and similar processes, *Philos. Mag.*, *42*(259), 493–498, doi:10.1080/14786449608620944.

Reeder, R. J. (1996), Interaction of divalent cobalt, zinc, cadmium, and barium with the calcite surface during layer growth, *Geochim. Cosmochim. Acta*, *60*(9), 1543–1552, doi:10.1016/0016-7037(96)00034-8.

Rehkämper, M., and A. N. Halliday (1998), Accuracy and long-term reproducibility of lead isotopic measurements by MC-ICP-MS using an external method for correction of mass discrimination, *Int. J. Mass Spec. Ion Proc.*, *181*(1-3), 123–133, doi:10.1016/S1387-3806(98)14170-2.

Rehkämper, M., M. Schönbächler, and C. H. Stirling (2001), Multiple Collector ICP-MS: Introduction to Instrumentation, Measurement Techniques and Analytical Capabilities, *Geostand. Geoanal. Res.*, *25*(1), 23–40, doi:10.1111/j.1751-908X.2001.tb00785.x.

Rehkämper, M., M. Frank, J. R. Hein, D. Porcelli, A. N. Halliday, J. Ingri, and V. Liebetrau (2002), Thallium isotope variations in seawater and hydrogenetic, diagenetic, and hydrothermal ferromanganese deposits, *Earth Planet. Sci. Lett.*, *197*(1-2), 65–81, doi:10.1016/S0012-821X(02)00462-4.

Rehkämper, M., M. Frank, J. R. Hein, and A. N. Halliday (2004), Cenozoic marine geochemistry of thallium deduced from isotopic studies of ferromanganese crusts and pelagic sediments, *Earth Planet. Sci. Lett.*, *219*(1), 77–91, doi:10.1016/S0012-821X(03)00703-9.

Rehkämper, M., Z. Xue, T. van de Flierdt, R. Middag, and H. De Baar (2010), Cd isotope constraints on nutrient cycling in the Southern Ocean, *Geochim. Cosmochim. Acta*, *74*(12, Suppl. 1), A857, doi:10.1016/j.gca.2010.04.044.

Rehkämper, M., F. Wombacher, T. J. Horner, and Z. Xue (2011), Natural and anthropogenic Cd isotope variations, in *Handbook of Environmental Isotope Geochemistry*, *Adv. Isot. Geochem.*, vol. 1, edited by M. M. Baskaran, 1st ed., pp. 125–154, Springer Berlin Heidelberg, Heidelberg, doi:10.1007/978-3-642-10637-8_8.

Reynolds, B. C., M. Frank, and A. N. Halliday (2006), Silicon isotope fractionation during nutrient utilization in the North Pacific, *Earth Planet. Sci.Lett.*, *244*(1-2), 431–443, doi:10.1016/j.epsl.2006.02.002.

Rickaby, R. E. M., and H. Elderfield (1999), Planktonic foraminiferal Cd/Ca: Paleonutrients or paleotemperature?, *Paleoceanography*, *14*(3), 293–303, doi:10.1029/1999PA900007.

Rickaby, R. E. M., and D. P. Schrag (2005), Biogeochemistry of Carbonates: Recorders of Past Oceans and Climate, in *Biogeochemistry, Availability, and Transport of Metals in the Environment*, *Metal ions Biol. Syst.*, vol. 44, edited by H. Sigel and R. Sigel, pp. 241–268, CRC Press, doi:www.crcpress.com/product/isbn/9780849338205.

Rickaby, R. E. M., M. J. Greaves, and H. Elderfield (2000), Cd in planktonic and benthic foraminiferal shells determined by thermal ionisation mass spectrometry, *Geochim. Cosmochim. Acta*, *64*(7), 1229–1236, doi:10.1016/S0016-7037(99)00317-8.

Ripperger, S., and M. Rehkämper (2007), Precise determination of cadmium isotope fractionation in seawater by double spike MC-ICPMS, *Geochim. Cosmochim. Acta*, *71*(3), 631–642, doi:10.1016/j.gca.2006.10.005.

Ripperger, S., M. Rehkämper, D. Porcelli, and A. N. Halliday (2007), Cadmium isotope fractionation in seawater–A signature of biological activity, *Earth Planet. Sci. Lett.*, *261*(3-4), 670–684, doi:10.1016/j.epsl.2007.07.034.

Ripperger, S., R. Schiebel, M. Rehkämper, and A. N. Halliday (2008), Cd/Ca ratios of in situ collected planktonic foraminiferal tests, *Paleoceanography*, *23*(3), PA3209, doi:10.1029/2007PA001524.

Robinson, L. F., J. F. Adkins, D. S. Scheirer, D. P. Fernandez, A. C. Gagnon, and R. G. Waller (2007), Deep-sea scleractinian coral age and depth distributions in the northwest Atlantic for the last 225,000 years, *Bull. Mar. Sci.*, *81*(3), 371–391, doi:www.ingentaconnect.com/content/umrsmas/bullmar/2007/00000081/00000003/art00007.

Robinson, R. S., D. M. Sigman, P. J. DiFiore, M. M. Rohde, T. A. Mashiotta, and D. W. Lea (2005), Diatom-bound $^{15}N/^{14}N$: New support for enhanced nutrient consumption in the ice age subantarctic, *Paleoceanography*, *20*, PA3003, doi:10.1029/2004PA001114.

Rosenthal, Y., E. A. Boyle, L. Labeyrie, and D. Oppo (1995), Glacial enrichments of authigenic Cd and U in Subantarctic sediments: A climatic control on the elements' oceanic budget?, *Paleoceanography*, *10*(3), 395–413, doi:10.1029/95PA00310.

Rosman, K. J. R., and J. R. De Laeter (1975), The isotopic composition of cadmium in terrestrial minerals, *Int. J. Mass Spectrom. Ion Phys.*, *16*(4), 385–394, doi:10.1016/0020-7381(75)85027-3.

Rosman, K. J. R., and J. R. De Laeter (1976), Isotopic fractionation in meteoritic cadmium, *Nature*, *261*(5557), 216–218, doi:10.1038/261216a0.

Rosman, K. J. R., and J. R. De Laeter (1978), A survey of cadmium isotopic abundances, *J. Geophys. Res.*, *83*(B3), 1279–1287, doi:10.1029/JB083iB03p01279.

Rosman, K. J. R., J. R. De Laeter, and M. Gorton (1980), Cadmium isotope fractionation in fractions of two H3 chondrites, *Earth Planet. Sci. Lett.*, *48*(1), 166–170, doi:10.1016/0012-821X(80)90179-X.

Rudge, J. F., B. C. Reynolds, and B. Bourdon (2009), The double spike toolbox, *Chem. Geol.*, *265*(3-4), 420–431, doi:10.1016/j.chemgeo.2009.05.010.

Saito, M. A., D. M. Sigman, and F. M. M. Morel (2003), The bioinorganic chemistry of the ancient ocean: the co-evolution of cyanobacterial metal requirements and biogeochemical cycles at the Archean-Proterozoic boundary?, *Inorg. Chim. Acta*, *356*, 308–318, doi:10.1016/S0020-1693(03)00442-0.

Sambrook, J., and D. W. Russell (2001), *Molecular cloning: a laboratory manual*, 3rd ed., 2344 pp., CSHL press, New York, USA.

Sands, D. G., K. J. R. Rosman, and J. R. De Laeter (2001), A preliminary study of cadmium mass fractionation in lunar soils, *Earth Planet. Sci. Lett.*, *186*(1), 103–111, doi:10.1016/S0012-821X(01)00233-3.

Sarmiento, J. L., and J. R. Toggweiler (1984), A new model for the role of the oceans in determining atmospheric pCO_2, *Nature*, *308*(5960), 621–624, doi:10.1038/308621a0.

Sarmiento, J. L., N. Gruber, M. A. Brzezinski, and J. P. Dunne (2004), High-latitude controls of thermocline nutrients and low latitude biological productivity, *Nature*, *427*(6969), 56–60, doi:10.1038/nature02127.

Schediwy, S., K. J. R. Rosman, and J. R. De Laeter (2006), Isotope fractionation of cadmium in lunar material, *Earth Planet. Sci. Lett.*, *243*(3-4), 326–335, doi:10.1016/j.epsl.2006.01.007.

Schiebel, R. (2002), Planktic foraminiferal sedimentation and the marine calcite budget, *Global Biogeochem. Cycles*, *16*(4), 1065, doi:10.1029/2001GB001459.

Schlitzer, R. (2011), Ocean Data View, http://odv.awi.de/.

Schmitt, A. D., S. J. G. Galer, and W. Abouchami (2009a), High-precision cadmium stable isotope measurements by double spike thermal ionisation mass spectrometry, *J. Anal. At. Spectrom.*, *24*(8), 1079–1088, doi:10.1039/b821576f.

Schmitt, A. D., S. J. G. Galer, and W. Abouchami (2009b), Mass-dependent cadmium isotopic variations in nature with emphasis on the marine environment, *Earth Planet. Sci. Lett.*, *277*(1-2), 262–272, doi:10.1016/j.epsl.2008.10.025.

Siebert, C., T. F. Nägler, and J. D. Kramers (2001), Determination of molybdenum isotope fractionation by double-spike multicollector inductively coupled plasma mass spectrometry, *Geochem. Geophys. Geosyst.*, *2*(7), 1032, doi:10.1029/2000GC000124.

Siebert, C., T. Nägler, F. von Blanckenburg, and J. D. Kramers (2003), Molybdenum isotope records as a potential new proxy for paleoceanography, *Earth Planet. Sci. Lett.*, *211*(1), 159–171, doi:10.1016/S0012-821X(03)00189-4.

Sigman, D. M., and E. A. Boyle (2000), Glacial/interglacial variations in atmospheric carbon dioxide, *Nature*, *407*(6806), 859–869, doi:10.1038/35038000.

Sigman, D. M., M. A. Altabet, D. C. McCorkle, R. François, and G. Fischer (1999), The δ^{15}N of nitrate in the Southern Ocean: Consumption of nitrate in surface waters, *Global Biogeochem. Cycles*, *13*(4), 1149–1166, doi:10.1029/1999GB900038.

Sigman, D. M., P. J. DiFiore, M. P. Hain, C. Deutsch, Y. Wang, D. M. Karl, A. N. Knapp, M. F. Lehmann, and S. Pantoja (2009), The dual isotopes of deep nitrate as a constraint on the cycle and budget of oceanic fixed nitrogen, *Deep Sea Res. Part I*, *56*(9), 1419–1439, doi:10.1016/j.dsr.2009.04.007.

Sigman, D. M., M. P. Hain, and G. H. Haug (2010), The polar ocean and glacial cycles in atmospheric CO_2 concentration, *Nature*, *466*(7302), 47–55, doi:10.1038/nature09149.

Silver, S., and L. T. Phung (2005), A bacterial view of the periodic table: genes and proteins for toxic inorganic ions, *J. Ind. Microbiol. Biotechnol.*, *32*(11), 587–605, doi:10.1007/s10295-005-0019-6.

Sinclair, D. J., and M. J. Risk (2006), A numerical model of trace-element coprecipitation in a physicochemical calcification system: Application to coral biomineralization and trace-element 'vital effects', *Geochim. Cosmochim. Acta*, *70*(15), 3855–3868, doi:10.1016/j.gca.2006.05.019.

Slater, C., T. Preston, and L. T. Weaver (2001), Stable isotopes and the international system of units, *Rapid Commun. Mass Spectrom.*, *15*(15), 1270–1273, doi:10.1002/rcm.328.

Smith, J. E., M. J. Risk, H. P. Schwarcz, and T. A. McConnaughey (1997), Rapid climate change in the North Atlantic during the Younger Dryas recorded by deep-sea corals, *Nature*, *386*, 818–820, doi:10.1038/386818a0.

Strelow, F. W. E. (1978), Improved separation of cadmium from indium, zinc, gallium and other elements by anion-exchange chromatography in hydrobromic nitric acid mixtures, *Anal. Chim. Acta*, *100*, 577–588, doi:10.1016/S0003-2670(01)93352-5.

Stuiver, M., P. D. Quay, and H. G. Ostlund (1983), Abyssal Water Carbon-14 Distribution and the Age of the World Oceans, *Science*, *219*(4586), 849–851, doi:10.1126/science.219.4586.849.

Sverjensky, D. A., E. L. Shock, and H. C. Helgeson (1997), Prediction of the thermodynamic properties of aqueous metal complexes to 1000 °C and 5 kb, *Geochim. Cosmochim. Acta*, *61*(7), 1359–1412, doi:10.1016/S0016-7037(97)00009-4.

Tambutté, E., D. Allemand, D. Zoccola, A. Meibom, S. Lotto, N. Caminiti, and S. Tambutté (2007a), Observations of the tissue-skeleton interface in the scleractinian coral *Stylophora pistillata*, *Coral Reefs*, *26*(3), 517–529, doi:10.1007/s00338-007-0263-5.

Tambutté, E., S. Tambutté, N. Segonds, D. Zoccola, A. Venn, J. Erez, and D. Allemand (2012), Calcein labelling and electrophysiology: insights on coral tissue permeability and calcification, *Proc. R. Soc. London, Ser. B*, *279*(1726), 19–27, doi:10.1098/rspb.2011.0733.

Tambutté, S., E. Tambutté, D. Zoccola, N. Caminiti, S. Lotto, A. Moya, D. Allemand, and J. F. Adkins (2007b), Characterization and role of carbonic anhydrase in the calcification process of the azooxanthellate coral *Tubastrea aurea*, *Mar. Biol.*, *151*(1), 71–83, doi:10.1007/s00227-006-0452-8.

Tang, D., and F. M. M. Morel (2006), Distinguishing between cellular and Fe-oxide-associated trace elements in phytoplankton, *Mar. Chem.*, *98*(1), 18–30, doi:10.1016/j.marchem.2005.06.003.

Tanner, S. (1992), Space charge in ICP-MS: calculation and implications, *Spectrochim. Acta, Part B*, *47*(6), 809–823, doi:10.1016/0584-8547(92)80076-S.

Tesoriero, A. J., and J. F. Pankow (1996), Solid solution partitioning of Sr^{2+}, Ba^{2+}, and Cd^{2+} to calcite, *Geochim. Cosmochim. Acta*, *60*(6), 1053–1063, doi:10.1016/0016-7037(95)00449-1.

van de Flierdt, T., L. F. Robinson, and J. F. Adkins (2010), Deep-sea coral aragonite as a recorder for the neodymium isotopic composition of seawater, *Geochim. Cosmochim. Acta*, *74*(21), 6014–6032, doi:10.1016/j.gca.2010.08.001.

van Geen, A., D. C. McCorkle, and G. P. Klinkhammer (1995), Sensitivity of the phosphate-cadmium-carbon isotope relation in the ocean to cadmium removal by suboxic sediments, *Paleoceanography*, *10*(2), 159–169, doi:10.1029/94PA03352.

Vance, D., and M. Thirlwall (2002), An assessment of mass discrimination in MC-ICPMS using Nd isotopes, *Chem. Geol.*, *185*(3-4), 227–240, doi:10.1016/S0009-2541(01)00402-8.

Von Damm, K. L., J. M. Edmond, B. Grant, C. I. Measures, B. Walden, and R. F. Weiss (1985), Chemistry of submarine hydrothermal solutions at 21 N, East Pacific Rise, *Geochim. Cosmochim. Acta*, *49*(11), 2197–2220, doi:10.1016/0016-7037(85)90222-4.

Waldron, K. J., and N. J. Robinson (2009), How do bacterial cells ensure that metalloproteins get the correct metal?, *Nat. Rev. Microbiol.*, *7*(1), 25–35, doi:10.1038/nrmicro2057.

Waldron, K. J., J. C. Rutherford, D. Ford, and N. J. Robinson (2009), Metalloproteins and metal sensing, *Nature*, *460*(7257), 823–830, doi:10.1038/nature08300.

Wasylenki, L. E., P. M. Dove, and J. J. De Yoreo (2005), Effects of temperature and transport conditions on calcite growth in the presence of Mg^{2+}: Implications for paleothermometry, *Geochim. Cosmochim. Acta*, *69*(17), 4227–4236, doi:10.1016/j.gca.2005.04.006.

Wasylenki, L. E., A. D. Anbar, L. J. Liermann, R. Mathur, G. W. Gordon, and S. L. Brantley (2007), Isotope fractionation during microbial metal uptake measured by MC-ICP-MS, *J. Anal. At. Spectrom.*, *22*(8), 905–910, doi:10.1039/B705476A.

Wedepohl, K. H. (1995), The composition of the continental crust, *Geochim. Cosmochim Acta*, *59*(7), 1217–1232, doi:10.1016/0016-7037(95)00038-2.

Wombacher, F., and M. Rehkämper (2003), Investigation of the mass discrimination of multiple collector ICP-MS using neodymium isotopes and the generalised power law, *J. Anal. At. Spectrom.*, *18*(11), 1371–1375, doi:10.1039/B308403E.

Wombacher, F., and M. Rehkämper (2004), Problems and suggestions concerning the notation of cadmium stable isotope compositions and the use of reference materials, *Geostds. Geoanal. Res.*, *28*(1), 173–178, doi:10.1111/j.1751-908X.2004.tb01054.x.

Wombacher, F., M. Rehkämper, K. Mezger, and C. Münker (2003), Stable isotope compositions of cadmium in geological materials and meteorites determined by multiple-collector ICPMS, *Geochim. Cosmochim. Acta*, *67*(23), 4639–4654, doi:10.1016/S0016-7037(03)00389-2.

Wombacher, F., M. Rehkämper, and K. Mezger (2004), Determination of the mass-dependence of cadmium isotope fractionation during evaporation, *Geochim. Cosmochim. Acta*, *68*(10), 2349–2357, doi:10.1016/j.gca.2003.12.013.

Wombacher, F., M. Rehkämper, K. Mezger, A. Bischoff, and C. Münker (2008), Cadmium stable isotope cosmochemistry, *Geochim. Cosmochim. Acta*, *72*(2), 646–667, doi:10.1016/j.gca.2007.10.024.

Wombacher, F., A. Eisenhauer, F. Böhm, N. Gussone, M. Regenberg, W.-C. Dullo, and A. Rüggeberg (2011), Magnesium stable isotope fractionation in marine biogenic calcite and aragonite, *Geochim. Cosmochim. Acta*, *75*(19), 5797–5818, doi:10.1016/j.gca.2011.07.017.

Woodland, S. J., M. Rehkämper, A. N. Halliday, D.-C. Lee, B. Hattendorf, and D. Günther (2005), Accurate measurement of silver isotopic compositions in geological materials including low pd/ag meteorites, *Geochim. Cosmochim. Acta*, *69*(8), 2153–2163, doi:10.1016/j.gca.2004.10.012.

Wright, M. H. (2004), The interior-point revolution in optimization: history, recent developments, and lasting consequences, *Bull. Am. Math. Soc.*, *42*(1), 39–56, doi:10.1090/S0273-0979-04-01040-7.

Xu, Y., D. Tang, Y. Shaked, and F. M. M. Morel (2007), Zinc, cadmium, and cobalt interreplacement and relative use efficiencies in the coccolithophore *Emiliania huxleyi*, *Limnol. Oceanogr.*, *52*(5), 2294–2305, doi:www.jstor.org/stable/10.2307/4502377.

Xu, Y., L. Feng, P. D. Jeffrey, Y. Shi, and F. M. M. Morel (2008), Structure and metal exchange in the cadmium carbonic anhydrase of marine diatoms, *Nature*, *452*(7183), 56–61, doi:10.1038/nature06636.

Xue, Z., M. Rehkämper, M. Schönbächler, P. J. Statham, and B. J. Coles (2011), A new methodology for precise cadmium isotope analyses of seawater, *Anal. Bioanal. Chem*, *402*, 1–11, doi:10.1007/s00216-011-5487-0.

Yi, W., A. N. Halliday, D.-C. Lee, and J. N. Christensen (1995), Indium and tin in basalts, sulfides, and the mantle, *Geochim. Cosmochim. Acta*, *59*(24), 5081–5090, doi:10.1016/0016-7037(95)00342-8.

Zhu, X. K., R. K. O'nions, Y. Guo, N. S. Belshaw, and D. Rickard (2000), Determination of natural Cu-isotope variation by plasma-source mass spectrometry: implications for use as geochemical tracers, *Chem. Geol.*, *163*(1-4), 139–149, doi:10.1016/S0009-2541(99)00076-5.

Zoccola, D., E. Tambutté, E. Kulhanek, S. Puverel, J. C. Scimeca, D. Allemand, and S. Tambutté (2004), Molecular cloning and localization of a PMCA P-type calcium ATPase from the coral *Stylophora pistillata*, *Biochim. Biophys. Acta, Biomembr.*, *1663*(1), 117–126, doi:10.1016/j.bbamem.2004.02.010.